UCLA
UCLA Electronic Theses and Dissertations

Title
Distribution and Sources of Black Carbon in the Arctic

Permalink
https://escholarship.org/uc/item/3mr3f0gn

Author
Qi, Ling

Publication Date
2016

Peer reviewed|Thesis/dissertation

eScholarship.org Powered by the California Digital Library
University of California

University of California
Los Angeles

Distribution and Sources of Black Carbon in the Arctic

A dissertation submitted in partial satisfaction
of the requirements for the degree
Doctor of Philosophy in Atmospheric and Oceanic Science

by

Ling Qi

2016

© Copyright by
Ling Qi
2016

Abstract of the Dissertation

Distribution and Sources of Black Carbon in the Arctic

by

Ling Qi

Doctor of Philosophy in Atmospheric and Oceanic Science

University of California, Los Angeles, 2016

Professor Qinbin Li, Chair

The Arctic is warming at twice the global rate over recent decades. To slow down this warming trend, there is growing interest in reducing the impact from short-lived climate forcers, such as black carbon (BC), because the benefits of mitigation are seen more quickly relative to CO_2 reduction. To propose efficient mitigation policies, it is imperative to improve our understanding of BC distribution in the Arctic and to identify the sources. In this dissertation, we investigate the sensitivity of BC in the Arctic, including BC concentrations in snow (BC_{snow}) and BC concentrations in air (BC_{air}), to emissions, dry deposition and wet scavenging using a global 3-D chemical transport model (CTM) GEOS-Chem. By including flaring emissions, estimating dry deposition velocity using resistance-in-series method, and including Wegener-Bergeron-Findeisen (WBF) in wet scavenging, simulated BC_{snow} in the eight Arctic sub-regions agree with the observations within a factor of two, and simulated BC_{air} fall within the uncertainty range of observations. Specifically, we find that natural gas flaring emissions in Western Extreme North of Russia (WENR) strongly enhance BC_{snow} (by up to $\sim$50%) and BC_{air} (by 20–32%) during snow season in the so-called 'Arctic front', but has negligible impact on BC in the free troposphere. The updated dry deposition velocity over snow and ice is much larger than those used in most of global CTMs and agrees better with observation. The resulting BC_{snow} changes marginally because of the offsetting of higher dry and lower wet deposition fluxes. In contrast, surface BC_{air} decreases strongly due to the

faster dry deposition (by 27–68%). WBF occurs when the environmental vapor pressure is in between the saturation vapor pressure of ice crystals and water drops in mixed-phase clouds. As a result, water drops evaporate and releases BC particles in them back into the interstitial air. In most CTMs, WBF is either missing or represented by a uniform and low BC scavenging efficiency. In this dissertation, we relate WBF with temperature and ice mass fraction based on long-term observations in mixed-phase clouds. We find that WBF reduces BC scavenging efficiency globally, with larger decrease at higher latitude and altitude (from 8% in the tropics to 76% in the Arctic). WBF slows down and reduces wet deposition of BC and leave more BC in the atmosphere. Higher BC_{air} results in larger dry deposition. The resulting total deposition is lower in mid-latitudes (by 12–34%) and higher in the Arctic (2–29%). Globally, including WBF significantly reduces the discrepancy of BC_{snow} (by ∼50%), BC_{air} (by ∼50%), and washout ratios (by a factor of two to four). The remaining discrepancies in these variables suggest that in-cloud removal is likely still excessive over land. In the last part, we identify sources of surface atmospheric BC in the Arctic in springtime, when radiative forcing is the largest due to the high insolation and surface albedo. We find a large contribution from Asian anthropogenic sources (40–43%) and open biomass burning emissions from forest fires in South Siberia (29–41%). Outside the Arctic front, BC is strongly enhanced by episodic, direct transport events from Asia and Siberia after ∼12 days of transport. In contrast, in the Arctic front, a large fraction of the Asian contribution is in the form of 'chronic' pollution on 1–2 month timescale. As such, it is likely that previous studies using 5- or 10-day trajectory analyses strongly underestimated the contribution from Asia to surface BC in the Arctic. Our results point toward an urgent need for better characterization of flaring emissions of BC (e.g. the emission factors, temporal and spatial distribution), extensive measurements of both the dry deposition of BC over snow and ice, and the scavenging efficiency of BC in mixed-phase clouds, particularly over Ocean. More measurements of ^{14}C are needed to better understand sources of BC (fossil fuel combustion versus biomass burning) and to provide additional constrain on BC simulations.

The dissertation of Ling Qi is approved.

James T. Randerson

Jochen Stutz

Kuo-Nan Liou

Qinbin Li, Committee Chair

University of California, Los Angeles

2016

To my husband Luyi Ma ...

for your love, patience, friendship,

and willingness to cook

To my parents and younger brother ...

for letting me experience the kind of love

that lasts forever with no doubt

Table of Contents

1 Overview **1**

2 Factors Controlling Black Carbon Distribution in the Arctic **7**

2.1 Introduction 8

2.2 BC observations in the Arctic 11

2.2.1 Measurements of BC in snow 11

2.2.2 Measurements of BC in surface air 13

2.3 Model description and simulations 15

2.3.1 GEOS-Chem simulation of BC 15

2.3.2 Gas flaring emissions of BC 16

2.3.3 Dry deposition over snow and ice 17

2.3.4 WBF process in mixed-phase clouds 19

2.3.5 BC concentration in snow 22

2.4 The effects of gas flares, dry deposition, WBF and precipitation 23

2.4.1 Gas flaring emissions 25

2.4.2 Dry deposition velocity 29

2.4.3 WBF in mixed-phase clouds 33

2.4.4 Precipitation 35

2.4.5 BC in snow in Greenland, Tromsø and Canadian sub-Arctic 38

2.5 Discussions 39

2.6 Summary and conclusions 42

3 Effects of Wegener-Bergeron-Findeisen Process on Global Black Carbon Distribution . . . 46

3.1 Introduction . . . 47

3.2 Observations . . . 51

3.2.1 BC Scavenging efficiency measurements . . . 52

3.2.2 BC concentration in surface air . . . 54

3.2.3 BC concentration in snow . . . 55

3.2.4 BC Washout ratio measurements . . . 56

3.3 Model description and simulations . . . 59

3.3.1 Model description . . . 59

3.3.2 Wet scavenging . . . 60

3.4 Results and discussions . . . 62

3.4.1 BC scavenging efficiency . . . 62

3.4.2 BC concentration in air . . . 66

3.4.3 BC wet deposition fluxes . . . 68

3.4.4 BC concentration in snow . . . 70

3.4.5 Washout ratio of BC . . . 74

3.5 Global BC budget . . . 76

3.6 Conclusions and implications . . . 79

4 Sources of Springtime Surface Black Carbon in the Arctic: An Adjoint Analysis . . . 81

4.1 Introduction . . . 82

4.2 Surface BC Observations . . . 86

4.3 GEOS-Chem and its adjoint 86
4.3.1 GEOS-Chem simulation of BC 86
4.3.2 GEOS-Chem adjoint simulation of BC 90
4.4 Results and Discussion 92
4.4.1 Sources of Arctic BC in April 2008 92
4.4.2 Adjoint source attribution of Arctic BC during a pollution episode . . 97
4.4.3 Uncertainty analysis 107
4.5 Summary and conclusions 111

5 Conclusions and Implications 114

List of Figures

2.1 Annual BC emissions (Gg yr^{-1}) in the Arctic in Experiment A (left panel) and Experiments B, C and D (right panel). Also shown are in-situ BC measurement stations (open triangles) and snow sample locations (solid circles). The eight sub-regions of the Arctic as defined in *Doherty et al.* (2010) are color-coded. See text for details. 12

2.2 Probability density function of observed (solid red) and GEOS-Chem simulated (black curves: dotted–Experiment A; dashed–Experiment B; dash dotted–Experiment C; solid–Experiment D, see Table 2.2 and text for details) BC concentration in snow (ng g^{-1}) in the Arctic (left panel), medians (vertical lines, left panel), residual errors (model–observation, right panel) and mean residual errors (vertical lines, right panel). 24

2.3 Observed and GEOS-Chem simulated median BC concentration in snow (ng g^{-1}) in the eight sub-regions in the Arctic (see Fig. 2.1). Solid line is 1:1 ratio line and dashed lines are 1:2 (or 2:1). 26

2.4 Observed (red solid) and GEOS-Chem simulated (dotted–Exp. A, dashed–Exp. B, see Table 2.2 and text for details) daily BC concentrations in air (ng m^{-3}) at Zeppelin from January–March in 2007–09. 29

2.5 Observed (red solid) and GEOS-Chem simulated (black curves: dotted–Exp. A, dashed–Exp. B, dash dotted–Exp. C, solid–Exp. D, see Table 2.2 and text for details) BC concentrations in air (ng m^{-3}) at Denali, Barrow, Alert, Zeppelin, and Summit, averaged for 2007–09. Also shown are standard deviations of observations (error bars). 30

2.6 Monthly precipitation (cm month^{-1}) averaged over sub-regions in the Arctic for 2006–08 (Fig. 2.1). Data are from the Goddard Earth Observing System Model version 5 data assimilation system (GEOS-5 DAS), Global Precipitation Climatology Project (GPCP), and NOAA Climate Prediction Center Merged Analysis of Precipitation (CMAP). 36

2.7 Same as Fig. 2.3, but for Exp. D with standard precipitation (red symbols), 50% precipitation (green symbols), and 200% precipitation (blue symbols). See text for details. 38

2.8 Same as Fig. 2.5, but for Exp. D with standard precipitation (solid black), 50% precipitation (dashed black), and 200% precipitation (dotted black). See text for details. 39

3.1 BC measurements used in this study: scavenging efficiencies (purple squares), concentration in air (red diamonds), concentration in snow (blue circles), washout ratio (black triangles), and average snow depth (cm) for 2006–12 (color contours). 51

3.2 GEOS-Chem simulated monthly mean BC scavenging efficiency in the Arctic (60–90°N), mid-latitudes (20–60°N) and the tropics (0–20°N) in the boundary layer (0–2 km), the lower troposphere (2–5 km) and the middle to upper troposphere (5–10 km). Results are averages for 2007–09. 65

3.3 (Left panel) Probability density function of observed (red line) and GEOS-Chem simulated (dotted: riming; dashed: WBF_T; solid black: WBF_{IMF}) annual mean BC concentration in air (μg m^{-3}) and (right panel) observed and simulated annual BC concentrations (black: riming; blue: WBF_T; red: WBF_{IMF}; the percentage of annual BC concentrations locate outside the 1:2 and 2:1 lines are in parentheses; Solid line – 1:1 ratio line, dashed lines – 1:2 (or 2:1) ratio lines). Data are for 2007–09. See text for details. 66

3.4 GESO-Chem simulated fractional change to BC concentration, relative to riming-only, as a result of WBF, ($[BC]_{WBF}$ - $[BC]_{riming}$) / $[BC]_{riming}$ that varies with (left panel) altitude and (right panel) latitude, averaged for 2007–09. . 68

3.5 IMPROVE observed (red solid line) and GEOS-Chem simulated (dotted: riming-only; dashed: WBF_T; solid black: WBF_{IMF}) seasonal variation of monthly mean BC concentrations (μg m^{-3}) for 2007–09. Also shown are standard deviations of observations (error bars). 69

3.6 (Left panel) Probability density function of observed (solid red line) and GEOS-Chem simulated (dotted: riming-only, dashed: WBF_T, solid black: WBF_{IMF}) BC in snow (ng g^{-1}) and (right panel) medians of observed and simulated BC in snow (ng g^{-1}) in the Arctic, North America (Canada, the Great Plains, the Pacific Northwest, and the Rockies, as defined by Doherty et al. (2014)), Northern China (Inner Mongolia, Northeast Border and Northeast industrial, as defined by Wang et al. (2013)), and Xinjiang, China. The regions are symbol-coded and the simulations are color-coded (see text for details). Solid line – 1:1 ratio line, dashed lines – 1:2 (or 2:1) ratio lines. . . . 73

3.7 Observed and simulated BC washout ratio, BC concentration in surface air and in snow at Cape Hedo in East China Sea, Aveiro and K-puszta (rural sites), and Schauinsland and Sonnblick (elevated sites). 75

4.1 BC emissions (Gg $month^{-1}$) in the Arctic for April. Solid circles are surface sites: Denali, AL (63.7°N, 149.0°W, 0.66 km a.s.l.), Barrow, AL (71.3°N, 156.6°W, 0.01 km a.s.l.), Alert, Canada (82.3°N, 62.3°W, 0.21 km a.s.l.), Summit, Greenland (72.6°N, 38.5°W, 3.22 km a.s.l.), and Zeppelin, Norway (79°N, 12°E, 0.47 km a.s.l.). Data from *Bond et al.* (2007) and natural gas flaring emissions from *Stohl et al.* (2013). 87

4.2 Northern hemispheric BC emissions for April (Gg month^{-1}). BC tracers are tagged by four anthropogenic (blue rectangles) and five biomass burning sources (red rectangles): North America (172.5–17.5°W, 24–88°N) – both anthropogenic and biomass burning, Europe (17.5°W–30°E, 33–88°N and 30–60°E, 33–50°N) – both, Siberia (30–172.5°E, 50–88°N) – both, Asia – anthropogenic (60–152.5°E, 0–50°N), Northern China (60–152.5°E, 30–50°N) – biomass burning sources, South Asia and Southern China (60–152.5°E, 0–30°N) – biomass burning. 88

4.3 GEOS-Chem adjoint versus finite difference gradients of BC concentration for 10 model gridcells with largest anthropogenic BC contributions and 10 gridcells with largest biomass burning BC contributions at Denali, Barrow, Alert, Zeppelin, and Summit (see Fig. 4.1). Values are for March 1–April 25, 2008. Regression lines, slopes and r^2 values are shown. 93

4.4 (left panels) Observed (red lines) and GEOS-Chem simulated (black lines) daily mean BC concentrations at Denali, Barrow, Alert, Zeppelin and Summit (see Fig. 4.1) for April 2008. Bars are standard deviations of observations. Modeled BC concentrations are decomposed into contributions from anthropogenic (purple lines) and biomass burning emissions (blue lines). (right panels) major contributions: Siberian biomass burning (red dashed line), Asian anthropogenic (green solid line), European anthropogenic (blue solid line), North American anthropogenic (orange solid line), and Siberian anthropogenic (purple solid line) sources. 95

4.5 Sensitivity of mean BC concentration (averages for April 20–25, 2008) at Denali, Barrow, Alert, Zeppelin, and Summit (see Fig. 4.1) to Northern Hemispheric BC emissions from during the 5, 10 and 25 days prior to April 25. See text for details. 100

4.6 GEOS-Chem simulated contributions to BC concentrations, averaged over April 20–25, 2008, at (stars, left panels) Denali, AL (63.7°N, 149.0°W, 0.66 km a.s.l.), Barrow, AL (71.3°N, 156.6°W, 0.01 km a.s.l.), Alert, Canada (82.3°N, 62.3°W, 0.21 km a.s.l.), Zeppelin, Norway (79°N, 12°E, 0.47 km a.s.l.), and Summit, Greenland (72.6°N, 38.5°W, 3.22 km a.s.l.) from global emissions as computed from adjoint simulations (see Sect. 4.3.2 for details): (left panels) Cumulative contributions from March 1–April 25 and (right panels) time-dependent contributions from Siberian biomass burning (red dashed line), Asian anthropogenic (solid green line), European anthropogenic (solid blue), North American anthropogenic (solid orange), and Siberian anthropogenic sources (solid purple). Source regions are as defined in Fig. 4.2. 102

4.7 Same as Fig. 4.6 (right panels) but for BC at 750 hPa above Barrow. 106

4.8 (left) Biomass burning BC emission rates (Gg hr^{-1}, red – monthly, black – 3-hourly) in Siberia (see Fig. 4.2) for April 2008 and (right) contributions to BC at the five sites from Siberian biomass burning emissions (red – monthly, black – 3-hourly) during March 1–April 25. Emission data is from the Global Fire Emissions Database version 3 (GFEDv3) inventory (*Randerson et al.*, 2012). Adjoint sensitivities of mean BC during April 20–25, 2008 at the five sites (see Fig. 4.1) to Siberia biomass burning emissions are also shown (left panel, dashed blue). 109

4.9 Reduction of adjoint sensitivities of BC concentration at selected Arctic sites (Fig. 4.1) to global emissions in the absence of WBF relative to standard simulation, averaged for the whole simulation period in March 1–April 25, 2008. 110

List of Tables

2.1 Measurements of BC in surface air in the Arctic. 13

2.2 GEOS-Chem simulations of BC in the Arctic. 16

2.3 Observed and simulated dry deposition velocity (v_d) using resistance-in-series method over snow and ice. 19

2.4 Observed and GEOS-Chem simulated BC concentration in snow in the Arctic (ng g^{-1}, see Fig. 2.1). 25

2.5 GEOS-Chem simulated BC dry deposition velocity (cm s^{-1}), dry deposition flux (ng m^{-2} d^{-1}) and fraction of dry to total deposition (%) in the Arctic.). 32

2.6 Model simulations of BC in the Arctic (60°N to 90°N). 41

3.1 Observed and GEOS-Chem simulated scavenging efficiency of BC (fraction of BC incorporated into cloud droplets and ice crystals). 53

3.2 Observed and GEOS-Chem simulated BC concentration in snow and rain (μg L^{-1}), BC concentration in surface air (μg m^{-3}) and the corresponding washout ratio. 58

3.3 Observed and simulated precipitation (cm) and BC wet deposition fluxes (mg m^{-2} yr^{-1}). 71

3.4 GEOS-Chem simulated BC deposition fluxes (mg m^{-2} mon^{-1}) in the Arctic (Sep.–Apr.), North America (Nov.–Feb.), Northern China (Nov.–Feb.) and Western China (Nov.–Feb.), averaged for 2007–09. 72

3.5 Global annual budget of BC. 77

4.1 Atmospheric lifetimes of Arctic BC (2008) from major sources and source regions (days). 97

4.2 Model simulated relative contributions to surface BC concentration (ng m^{-3}) at selected Arctic sites (Fig. 4.1) for April 20–25*, 2008. 99

Acknowledgments

I would like to express my deepest appreciation to my advisor, Professor Qinbin Li, for the continuous support of my Ph.D study and related research. I would like to thank him for helping me to grow as a research scientist. From him I learnt to think critically and to express ideas logically. I learnt to be problem-oriented and detail-oriented in research. Without his help, I would not be here.

My deepest gratitude also goes to my committee members, Professor Kuo-Nan Liou, Professor Jochen Stutz, and Professor James T. Randerson, for sharing with me their expertise and insights and providing me with constructive comments and help.

I would also like to thank all my collaborators for their contributions to this work. Special thanks to Professor Daven K. Henze and Professor Hongyu Liu for all the stimulating discussions. I would like to extend my appreciation to my fellow group members, Dr. Yuhao Mao, Dr. Li Zhang, Dr. Dan Chen, Dr. Mei Gao, Dr. Bin Zhao, Dr. Hsien-Liang Tseng, and Cenlin He, for all the helpful discussions, and to my fellow colleagues, Yang Cao, Ross Cheung, Kevin Quinn, Chao Yue, Wu Sun, and Xin An for all the help. I want to thank them for their company for the past few years and for sharing all my happiness and sorrows.

Lastly I want to give my special thanks to my family. Words can not express how grateful I am to my father-in-law, mother-in-law, my father, mother and little brother for the patient and love they gave me and the sacrifices they've made on my behalf. At the end, I want to express my appreciation to my beloved husband for his unconditional love and support.

Vita

2004–2008	B.S. ∼(Environmental Science) and B.A. ∼(Pychology) , Peking University, Beijing, China.
2008–2011	M.S. ∼(Environmental Science), Peking University, Beijing, China.
2011–2012	M.S. ∼(Atmospheric Science), UCLA.

CHAPTER 1

Overview

Black carbon (BC) is carbonaceous material of aerosols formed through incomplete combustion of fossil fuel, biofuel and biomass. Unlike other aerosols in the atmosphere, which primarily scatter sunlight and cool the atmosphere, BC absorbs much more sunlight than it reflects and warms the atmosphere. BC also influences clouds (cloud cover, emissivity and brightness) and precipitation through semi-direct and indirect effects. When deposited on snow and ice surfaces, BC reduces the high albedo of snow and ice surface, enhances the surface absorption of sunlight and accelerates snow melting. A recent comprehensive review (*Bond et al.*, 2013) suggests that radiative forcing of BC through all forcing mechanisms is +1.1 W m^{-2} (+0.17 – +2.1 W m^{-2}, with 90% uncertainty bounds) for the industrial-era, suggesting that BC is the second most important climate forcer in terms of its radiative forcing.

The Arctic, the most sensitive region to climate change, is warming at a rate twice as rapid as the global average (*Quinn et al.*, 2011). Surface air temperature in Alaska and Siberia has increased by $2-3$°C annually and by 4°C in winter from 1954 to 2003 (*Quinn et al.*, 2011). In addition to ice-albedo and temperature feedbacks, studies suggest that BC is probably a large contributor to the fast warming rate (*Shindell and Faluvegi*, 2009; *Flanner*, 2013; *Sand et al.*, 2013, 2015). It is estimated that about $0.48-1.09$°C of the warming is from BC both in the Arctic and at lower latitudes (*Shindell and Faluvegi*, 2009; *Sand et al.*, 2013, 2015). BC in the upper tropospheric Arctic slightly cools the Arctic surface (-0.03 ± 0.02 K (Gg yr)$^{-1}$, -0.2 ± 0.1 K W^{-1} m^2), but BC in the middle and lower troposphere and BC in snow and ice strongly warm the Arctic surface (0.11 ± 0.02 K (Gg yr)$^{-1}$, 1.4–2.8 K

W^{-1} m^2, *Flanner*, 2013). BC at lower latitudes warms the Arctic (0.7–0.8 K W^{-1} m^2) due to increased transport of heat absorbed by BC (*Shindell and Faluvegi*, 2009; *Sand et al.*, 2013, 2015). To improve our understanding of climate response in the Arctic to global BC, it is thus imperative to improve the understanding of BC distribution in the atmosphere and in snow and ice in the Arctic.

Simulation of Arctic BC distribution in the atmosphere and in snow is associated with large uncertainties. A recent assessment of BC in Arctic snow and sea ice using Aerosol Comparisons between Observations and Models (AeroCom) found that the discrepancy between model simulations and observations is a factor of 5–6 (*Jiao et al.*, 2014). In addition, the disagreement among the AeroCom models is also a factor of 5–6, resulting from the disagreement of deposition fluxes in the models (*Jiao et al.*, 2014). However, the reason for the large disagreement is unclear. BC concentration at surface is underestimated by more than a factor of two for the mean over 11 models and by up to a factor of 27 for individual models (*Eckhardt et al.*, 2015).

In Chapter 2, we investigate the sensitivity of BC concentration in snow (BC_{snow}, ng g^{-1}) and in surface atmosphere (BC_{air}, ng m^{-3}) to gas flaring emissions, dry deposition, wet scavenging and precipitation using a 3D global chemical transport (CTM) model GEOS-Chem. We find that the model underestimates BC_{snow} in the Arctic by 40% on average (median = 11.8 ng g^{-1}). It is estimated that gas flaring emissions account for a rather small fraction of global emissions (∼3%) and have been ignored in earlier global studies (*Stohl et al.*, 2013). However, it is a significant source of BC in the Arctic (> 40%, *Stohl et al.*, 2013). We find that flaring emissions increase BC_{snow} in the eight Arctic sub-regions (by 0.1–8.5 ng g^{-1}), reducing the model discrepancy substantially (by up to ∼50% close to the gas flares). At Zeppelin, the closest in-situ measurement site to gas flares in Russia, including flaring emissions captures large spikes of BC_{air} observed in winter. However, the estimate of gas flaring emissions is associated with large uncertainties because of the lack of field measurements of flaring emission factors. The emission factor used in this study was derived

from emission factor of particulate matter from gas flares (*Stohl et al.*, 2013), which is a factor of three larger than that measured in a lab experiment (*McEwen and Johnson*, 2012). Recent field measurements of gas flaring emission factor in North Dakota suggest a much lower value (*Schwarz et al.*, 2015; *Weyant et al.*, 2016). We call for extensive measurements of gas flaring emission factor in Russia to better constrain flaring emissions and the resulting effects on BC distribution in the Arctic.

Ample observations suggest that BC dry deposition velocities over snow and ice in current CTMs (0.03 cm s^{-1} in GEOS-Chem) are exceedingly small. We apply a resistance-in-series method to compute dry deposition velocity that varies with local meteorological and surface conditions. The resulting velocity is significantly larger and varies by a factor of eight in the Arctic (0.03–0.24 cm s^{-1}). However, this method still underestimates BC dry deposition velocity derived from measurements on Mt. Changbai by a factor of ten, because coarse horizontal resolution of global models does not capture the complex terrain. In the Arctic, updated dry deposition velocity increases the fraction of dry to total BC deposition (16% to 25%), yet leaves the total BC deposition and BC_{snow} unchanged. This is largely explained by the offsetting higher dry and lower wet deposition fluxes. Larger fraction of dry to total deposition means less internally mixed BC and snow/ice composite and thereby less absorption of sunlight (*Flanner et al.*, 2012). Unlike BC_{snow}, updated dry deposition velocity strongly decreases surface BC_{air} in winter ($\sim$50%) and fails to reproduce the seasonal variation. This dramatic decrease of BC_{air} in winter and the resulting missing of winter and spring Arctic haze is one of the major reasons of using low dry deposition velocity in earlier studies. However, this does not justify the use of a low dry deposition velocity over snow and ice, because BC_{air} is also affected by a lot of other factors, such as emissions, transport and wet deposition.

In mixed-phase clouds, when the environmental vapor pressure is above the saturation vapor pressure of ice crystals and below the saturation vapor pressure of water, ice crystals grow at the expense of water drops, releasing BC particles in the water drops back into the

interstitial air. This Wegener-Bergeron-Findeisen (WBF) process substantially reduces BC scavenging efficiency and slows down the subsequent wet scavenging. Rimming (snowflakes fall and collect cloud water drops and the BC in them along their pathways), in contrast, results in more efficient wet scavenging of BC than WBF-dominated conditions in mixed-phase clouds. Measurements showed that effects of WBF strongly depends on cloud microphysics, such as temperature and ice mass fraction. However, in most current global models, WBF is missing or treated as a uniform and constant value of BC scavenging efficiency. We differentiate riming- versus WBF-dominated in-cloud scavenging based on liquid water content (LWC) and temperature. Specifically, we relate WBF to either temperature or ice mass fraction (IMF) in mixed-phase clouds. We find that in the Arctic with WBF, BC scavenging efficiency is strongly reduced (by 43–76%), BC_{snow} is up to 80% higher, BC loading is considerably larger (from 0.25 to 0.43 mg m^{-2}), and BC lifetime is markedly prolonged (from 9 to 16 days). BC_{snow} in the North American sector increases by up to ∼50%, consistent with observations which showed that WBF dominates the in-cloud scavenging in mixed-phase clouds in this region. Surface BC_{air} in winter increases substantially and agrees much better with observations. The enhancement of both BC_{snow} and BC_{air} in the Arctic is resulted from the increased transport of BC from mid-latitudes.

In Chapter 3, as an extension, we systematically evaluate the effects of WBF on global BC scavenging efficiency, surface BC_{air}, deposition flux, BC_{snow}, and washout ratio. We find the reduction resulting from WBF to global BC scavenging efficiency varies substantially, from 8% in the tropics to 76% in the Arctic. The resulting annual mean BC_{air} increases by up to 156% at high altitudes and latitudes because of lower temperature and higher IMF. At Jungfraujoch, Switzerland and Abisko, Sweden, where WBF dominates, the discrepancies of simulated BC scavenging efficiency and washout ratio are significantly reduced (from a factor of three to 10% for BC scavenging efficiency and from a factor of 4–5 to a factor of two for BC washout ratio). However, at Zeppelin, Norway, where riming dominates, simulation of BC scavenging efficiency, BC_{air}, and washout ratio become worse (relative to

observations) when WBF is included. There is thus an urgent need for extensive observations to distinguish riming- versus WBF-dominated in-cloud scavenging in mixed-phase clouds and to characterize the associated BC scavenging efficiency. In addition, BC scavenging efficiency also strongly depends on its size and hygroscopicity (*Hallberg et al.*, 1992, 1994; *Sellegri et al.*, 2003). Thus the treatment of BC size and aging process in global models might also affect the simulation of BC scavenging efficiency.

WBF halves the model-observation discrepancy of BC_{air} (from -65% to -30%) across North America, Europe, China and the Arctic. Globally WBF increases BC burden from 0.22 to 0.29–0.35 mg m^{-2} yr^{-1}, which partially explains the gap between observed and previous model simulated BC burdens over land (*Bond et al.*, 2013). In addition, WBF significantly increases BC lifetime from 5.7 days to ∼8 days. Additionally, WBF results in a significant redistribution of BC deposition in source and remote regions. Specifically, it lowers BC wet deposition (by 37–63% at northern mid-latitudes and by 21–29% in the Arctic) while increases dry deposition (by 3–16% at mid-latitudes and by 81–159% in the Arctic). The resulting total BC deposition is lower at mid-latitudes (by 12–34%) but higher in the Arctic (by 2–29%). We find that WBF decreases BC_{snow} at mid-latitudes (by ∼15%) but increases it in the Arctic (by 26%) while improving model comparisons with observations. In addition, WBF dramatically reduces the model-observation discrepancy of washout ratios in winter (from a factor of 16 to 4). The remaining discrepancies in BC_{air}, BC_{snow} and BC washout ratios suggest that BC removal is likely still excessive over land.

In Chapter 4, we quantify source contributions to springtime (April 2008) surface BC in the Arctic by interpreting surface observations of BC at five receptor sites (Denali, Barrow, Alert, Zeppelin, and Summit) using GEOS-Chem and its adjoint. Contributions to BC at Barrow, Alert, and Zeppelin are dominated by Asian anthropogenic sources (40–43%) before April 18 and by Siberian open biomass burning emissions (29–41%) afterward. In contrast, Summit, a mostly free tropospheric site, has predominantly an Asian anthropogenic source contribution (24–68% with an average of 45%). We compute the adjoint sensitivity of BC

concentrations at the five sites during a pollution episode (April 20–25) to global emissions from March 1 to April 25. The associated contributions are the combined results of these sensitivities and BC emissions. Local and regional anthropogenic sources in Alaska are the largest anthropogenic sources of BC at Denali (63%), and natural gas flaring emissions in the Western Extreme North of Russia are the largest anthropogenic sources of BC at Zeppelin (26%) and Alert (13%). We find that long-range transport of emissions from Beijing-Tianjin-Hebei (also known as Jing-Jin-Ji), the biggest urbanized region in Northern China, contribute significantly (∼10%) to surface BC across the Arctic. On average it takes ∼12 days for Asian anthropogenic emissions and Siberian biomass burning emissions to reach Arctic lower troposphere, supporting earlier studies. Natural gas flaring emissions from the Western Extreme North of Russia reach Zeppelin in about a week. We find that episodic, direct transport events dominate BC at Denali (87%), a site outside Arctic front, a strong transport barrier. The relative contribution of direct transport to surface BC within the Arctic front is much smaller (∼50% at Barrow and Zeppelin and ∼10% at Alert). The large contributions from Asian anthropogenic sources are predominately in the form of 'chronic' pollution (∼40% at Barrow and 65% at Alert and 57% at Zeppelin) on 1–2 month timescales. As such, it is likely that previous studies using 5- or 10-day trajectory analyses strongly underestimated the contribution from Asia to surface BC in the Arctic.

CHAPTER 2

Factors Controlling Black Carbon Distribution in the Arctic

Abstract

We investigate the sensitivity of black carbon (BC) in the Arctic, including BC concentration in snow (BC_{snow}, ng g^{-1}) and surface air (BC_{air}, ng m^{-3}), to emissions, dry deposition and wet scavenging using a global 3-D chemical transport model (CTM) GEOS-Chem. We find that the model underestimates BC_{snow} in the Arctic by 40% on average (median = 11.8 ng g^{-1}). Natural gas flaring substantially increases total BC emissions in the Arctic (by ∼70%). The flaring emissions lead to up to 49% increases (0.1–8.5 ng g^{-1}) in Arctic BC_{snow}, dramatically improving model comparison with observations (50% reduction in discrepancy) near flaring source regions (Western Extreme North of Russia). Ample observations suggest that BC dry deposition velocities over snow and ice in current CTMs (0.03 cm s^{-1} in GEOS-Chem) are exceedingly small. We apply the resistance-in-series method to compute the dry deposition velocity that varies with local meteorological and surface conditions. The resulting velocity is significantly larger and varies by a factor of eight in the Arctic (0.03–0.24 cm s^{-1}), increases the fraction of dry to total BC deposition (16% to 25%), yet leaves the total BC deposition and BC_{snow} in the Arctic unchanged. This is largely explained by the offsetting higher dry and lower wet deposition fluxes. Additionally, we account for the effect of the Wegener-Bergeron-Findeisen (WBF) process in mixed-phase clouds, which releases BC particles from condensed phases (water drops and ice crystals) back to the interstitial air and thereby substantially reduces the scavenging efficiency of BC (by 43–76% in the Arctic).

The resulting BC_{snow} is up to 80% higher, BC loading is considerably larger (from 0.25 to 0.43 mg m^{-2}), and BC lifetime is markedly prolonged (from 9 to 16 days) in the Arctic. Over all, flaring emissions increase BC_{air} in the Arctic (by ∼20 ng m^{-3}), the updated dry deposition velocity more than halves BC_{air} (by ∼20 ng m^{-3}), and the WBF effect increases BC_{air} by 25–70% during winter and early spring. The resulting model simulation of BC_{snow} is substantially improved (within 10% of the observations) and the discrepancies of BC_{air} are much smaller during snow season at Barrow, Alert and Summit (from -67%– -47% to -46%–3%). In addition, we find that poorly constrained precipitation in the Arctic may introduce large uncertainties in estimating BC_{snow}. Doubling (halving) precipitation introduces a positive (negative) bias similar as the magnitude of the overall effects of flaring emissions and the WBF effect. Our results point toward an urgent need for better characterization of flaring emissions of BC (e.g. the emission factors, temporal and spatial distribution), extensive measurements of both the dry deposition of BC over snow and ice, the scavenging efficiency of BC in mixed-phase clouds, and more observations of precipitation in the Arctic.

2.1 Introduction

Black carbon (BC, loosely also known as soot), light absorbing refractory carbonaceous aerosols, influence climate through direct absorption of solar radiation, semi-direct cloud effects, indirect cloud effects, and snow-albedo effect (*Bond et al.*, 2013) (IPCC, 2014). BC deposited on surfaces with high albedo, such as snow and ice, reduces surface albedo (the so-called snow albedo effect), increases surface solar heating, and accelerates snow and ice melting (*Flanner et al.*, 2007, 2012; *He et al.*, 2014a; *Liou et al.*, 2014). This snow albedo feedback leads to enhanced BC radiative forcing (*Bond et al.*, 2013, and references therein). *Clarke and Noone* (1985) highlighted the climate effect of fallen soot from 'smokes' for a nuclear war scenario, which reduced the surface reflectivity of snow and sea ice in the Arctic. Measurements by (*Clarke and Noone*, 1985) showed that there was ample amount of BC in the Arctic snow to exert climate impact in the region. Using observations of BC_{snow},

Hansen and Nazarenko (2004) quantified, for the first time, the albedo reduction due to BC deposition on snow and ice (2.5% on average) across the Arctic. Snow albedo effect of BC in the Arctic has since received wide attention. Numerous studies have examined the snow albedo change in this region due to BC deposition (*Jacobson*, 2004; *Marks and King*, 2013; *Namazi et al.*, 2015; *Tedesco et al.*, 2016) and estimated the associated surface BC snow albedo radiative forcing to be substantial (0.024–0.39 W m^{-2}) in the Arctic (*Bond et al.*, 2013; *Flanner*, 2013; *Jiao et al.*, 2014; *Namazi et al.*, 2015), comparable to the forcing of tropospheric ozone in springtime Arctic (0.34 W m^{-2}, *Quinn et al.*, 2008). BC deposited on snow and ice is likely to be an important reason for unexpected rapid sea ice shrinkage in the Arctic (*Koch et al.*, 2009; *Goldenson et al.*, 2012; *Stroeve et al.*, 2012). Widespread surface melting of the Greenland ice sheet was attributed to rising temperatures and reductions in surface albedo resulting from deposition of BC from northern hemispheric forest fires (*Keegan et al.*, 2014; *Tedesco et al.*, 2016).

To better constrain the radiative forcing and the associated uncertainty of BC snow albedo effect in the Arctic, it is imperative to improve the prediction of BC_{snow} in the region. Previous studies found large discrepancies between modeled and observed BC_{snow} (up to a factor of six) in the Arctic (e.g. *Flanner et al.*, 2007; *Koch et al.*, 2009). A comprehensive survey of BC_{snow} observations across the Arctic (1000 snow samples) by *Doherty et al.* (2010) provides a unique opportunity to constrain BC_{snow} in the region. *Bond et al.* (2013) compared results of BC_{snow} from the Community Atmospheric Model (CAM version 3.1) (*Flanner et al.*, 2009) and the Goddard Institute of Space Studies (GISS) model (*Koch et al.*, 2009) with the observations from *Doherty et al.* (2010), averaged over the eight Arctic sub-regions (Fig. 2.1) as defined by *Doherty et al.* (2010). The resulting ratio of modeled to observed BC_{snow} (sub-regional means) were 0.6–3.4 for CAM3.1 and 0.3–1.6 for GISS. *Jiao et al.* (2014) found large discrepancies in BC_{snow} (up to a factor of six) between results from the Aerosol Comparisons between Observations and Models (AeroCom, http://aerocom.met.no/) and the *Doherty et al.* (2010) observations. They also found large variations in BC deposition fluxes amongst

the AeroCom models. *Jiao et al.* (2014) further pointed out that BC transport and deposition processes are more important for differences in simulated BC_{snow} than differences in snow meltwater scavenging rates or emissions in models.

Studies have shown that Arctic atmospheric BC on average cools the surface due to surface dimming, while BC in the lower troposphere warms the surface with a climate sensitivity (surface temperature change per unit forcing) of 2.8 ± 0.5 K W^{-1} m^2 due to low clouds and sea-ice feedbacks that amplify the warming (e.g. *Flanner*, 2013). This sensitivity is a factor of two larger than that of BC snow albedo feedback (1.4 ± 0.7 K W^{-1} m^2, *Flanner*, 2013), a factor of four larger than that of CO_2 (0.69 K W^{-1} m^2, *Bond et al.*, 2013) and much larger than that of tropospheric ozone (0.2 K W^{-1} m^2, *Shindell and Faluvegi*, 2009). However, estimates of BC in surface air (hereafter referred to as BC_{air}) in the Arctic are associated with large uncertainties (*Textor et al.*, 2006, 2007; *Koch et al.*, 2009; *Liu et al.*, 2011; *Browse et al.*, 2012; *Sharma et al.*, 2013). Observations have shown decreasing trends of BC_{air} since 1990 at Barrow, Alert and Zeppelin (*Sharma et al.*, 2004, 2006; *Eleftheriadis et al.*, 2009). The modeling studies by *Sharma et al.* (2006, 2013) reproduced the declining trends and have associated these trends with declining emissions in Russia. In general, current models failed to reproduce the seasonal cycles of BC_{air} observed at the aforementioned sites, with large underestimates during Arctic haze and overestimates in summer (*Textor et al.*, 2006, 2007; *Koch et al.*, 2009; *Liu et al.*, 2011; *Browse et al.*, 2012; *Sharma et al.*, 2013). The low biases are likely due to uncertainties associated with treatments of BC aging in the models (*Liu et al.*, 2011; *He et al.*, 2015), excessive dry deposition of BC (*Huang et al.*, 2010a; *Liu et al.*, 2011) and wet scavenging of BC (*Koch et al.*, 2009; *Huang et al.*, 2010a; *Bourgeois and Bey*, 2011; *Liu et al.*, 2011), and overly efficient vertical mixing (*Koch et al.*, 2009). *Liu et al.* (2011) used an OH dependent aging scheme, constrained a low dry deposition velocity and suppressed scavenging efficiency in ice clouds. They found that with all these improvements, the discrepancy of modeled and simulated BC_{air} during Arctic haze reduced from orders of magnitude to within a factor of two. *Browse et al.* (2012) suppressed the scavenging of BC

in ice clouds and included low level cloud scavenging and found an improved simulation of BC seasonal cycles in the Arctic. Recently, *Huang et al.* (2015) pointed out that the low biases are partly due to uncertainties in the estimates of BC emissions in Russia, which likely resulted in biases in both BC emission rates and spatial distributions. *Eckhardt et al.* (2015) evaluated the capabilities for simulating seasonal variations of BC_{air} at surface Arctic by 11 models and found much better agreements with observations. Specifically, mean BC_{air} during January to March was underestimated by about a factor of 2 for the mean of all models, although the discrepancy is up to a factor of 27 for individual models.

In this study, we systematically investigate the controlling factors of BC distribution in snow and surface air in the Arctic using a 3-D chemical transport model GEOS-Chem. We first examine and incorporate gas flaring emissions of BC around the Arctic circle (Sect. 2.4.1). We then discuss and improve dry deposition velocity of BC in the Arctic (Sect. 2.4.2). Finally, we analyze BC wet scavenging efficiency (Sect. 2.4.3) and the sensitivity of BC_{snow} and BC_{air} to precipitation (Sect. 2.4.4).

2.2 BC observations in the Arctic

2.2.1 Measurements of BC in snow

The most comprehensive measurements of BC_{snow} were in eight sectors in the Arctic: Alaska, Arctic Ocean, Canadian Arctic, Canadian sub-Arctic, Greenland, Russia, Ny-Ålesund and Tromsø, mostly from March to May during 2005–2009 (*Doherty et al.*, 2010, data available at http://www.atmos.washington.edu/sootinsnow/). Samples were for full snowpack depth and the sampling sites are shown in Fig. 2.1 (color coded by the sub-regions). These observations provide a reasonable constraint on Arctic-wide annual mean radiative effect from BC deposited in snow (*Jiao et al.*, 2014).

Doherty et al. (2010) measured the light absorption of impurity in snow samples using the Integrating Sphere/Integrating Sandwich optical method and derived equivalent, maxi-

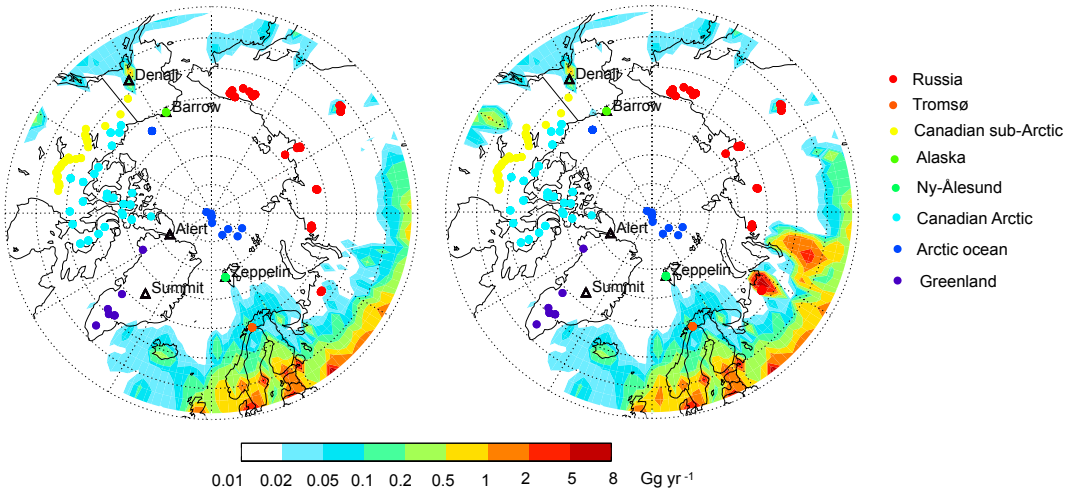

Figure 2.1: Annual BC emissions (Gg yr^{-1}) in the Arctic in Experiment A (left panel) and Experiments B, C and D (right panel). Also shown are in-situ BC measurement stations (open triangles) and snow sample locations (solid circles). The eight sub-regions of the Arctic as defined in *Doherty et al.* (2010) are color-coded. See text for details.

mum, and estimated BC_{snow} using the wavelength-dependent absorption of BC and non-BC fractions (*Doherty et al.*, 2010). We use here the estimated BC_{snow}. The largest sources of uncertainty stem from uncertainties of BC mass absorption cross-section (MAC), BC absorption Ångstrom exponent ($Å_{BC}$), and non-BC absorption Ångstrom exponent ($Å_{non\text{-}BC}$) constituents. *Doherty et al.* (2010) used MAC = 6.0 mg^2 g^{-1} (at 500 nm), the MAC of their calibration filters. Using MAC = 7.5 mg^2 g^{-1} (at 500 nm) as recommended by *Bond and Bergstrom* (2006) would increase the estimated BC_{snow} by ∼25%. *Doherty et al.* (2010) used $Å_{BC}$ = 1.0 (range: 0.8–1.9) and $Å_{non\text{-}BC}$ = 5.0 (range: 3.5–7.0) in their derivation and estimated a 50% error in the estimated BC_{snow}. Additional uncertainties include instrumental uncertainty ($\leq$ 11%), under-catch correction ($\pm$15%), and loss of aerosol to plastic flakes in the collection bags ($\pm$20%) for samples from West Russia and the Canadian sub-Arctic. The overall uncertainty of the estimated BC_{snow} is $<$ 60%.

2.2.2 Measurements of BC in surface air

In-situ measurements of BC_{air} from 2007 to 2009 are available at five stations within the Arctic Circle (Fig. 2.1): Denali, AL (63.7°N, 149.0°W, 0.66 km a.s.l.), Barrow, AL (71.3°N, 156.6°W, 0.01 km a.s.l.), Alert, Canada (82.3°N, 62.3°W, 0.21 km a.s.l.), Summit, Greenland (72.6°N, 38.5°W, 3.22 km a.s.l.), and Zeppelin, Norway (79°N, 12°E, 0.47 km a.s.l.). Data descriptions are shown in Table 2.1. Denali is part of the Interagency Monitoring of PROtected Visual Environment (IMPROVE) network (*Malm et al.*, 1994, data available at http://vista.cira.colostate.edu/improve/). IMPROVE measurements are made every three days and 24-hour averages are reported. Thermal Optical Reflectance (TOR) combustion method is used based on the preferential oxidation of organic carbon (OC) and BC at different temperatures (*Chow et al.*, 2004). BC-like products of OC pyrolysis can lead to an overestimate of the BC mass. The uncertainties of the TOR method are difficult to quantify (*Park et al.*, 2003; *Chow et al.*, 1993).

Table 2.1: Measurements of BC in surface air in the Arctic.

Station	Temporal frequency	Data availability	References
Denali (63.7°N, 149.0°W, 0.66 km)	24-h average every 3 days	91%	Malm *et al.* (1994)
Barrow (71.3°N, 156.6°W, 0.01 km)	1 h	46%	Bodhaine (1989)
Alert (82.3°N, 62.3°W, 0.21 km)	1 h	84%	Sharma *et al.* (2004)
Zeppelin (79°N, 12°E, 0.47 km)	30 min	79%	Eleftheriadis *et al.* (2009)
Summit (72.6°N, 38.5°W, 3.22 km)	5 min	95%	Delene and Ogren (2002)

Barrow is part of the NOAA Global Monitoring Division (GMD) network, where BC light absorption coefficients are measured from a particle soot absorption photometer (PSAP) since 1997 (*Bond et al.*, 1999; *Delene and Ogren*, 2002). PSAP measures the change in light transmission at three wavelengths (467, 530 and 660 nm) through a filter on which particles

are collected. We used the measurements at 530 nm in this study. Site Barrow is about 8 km northeast of the village of Barrow and is less than 3 km southeast of the Arctic Ocean. Given that the site has a prevailing east-northeast wind off the Beaufort Sea, it receives minimal influence from local anthropogenic emissions and is strongly affected by weather in the Central Arctic.

BC_{air} at Alert were measured using an aethalometer model AE-6 with 1-wavelength operated by Environment Canada (*Sharma et al.*, 2004, 2006, 2013, data available at http://www.ec.gc.ca/). The instruments measure the attenuation of light transmitted through particles that accumulate on a quartz fiber filter at 880nm. Alert, located the furthest north of the five sites on the north-eastern tip of Ellesmere Island, is most isolated from continental sources (*Hirdman et al.*, 2010a)

The Zeppelin observatory is part of the European Supersites for Atmospheric Aerosol Research, where BC mass concentrations are also measured by an aethalometer and reported for seven wavelengths (370, 470, 520, 590, 660, 880 and 950 nm) (*Eleftheriadis et al.*, 2009, data available at http://ebas.nilu.no/). We use the 520 nm data. Measurements at site Zeppelin, on mountain Zeppelin in island archipelago of Svalbard, were generally considered to represent the free troposphere conditions (*Eleftheriadis et al.*, 2009).

BC mass concentrations were also measured by an aethalometer at Summit (*von Schneidemesser et al.*, 2009, data available at http://www.esrl.noaa.gov/gmd/aero/net/), on the center of the Greenland glacial ice sheet. Due to the high elevation (3.2 km) and the flat and homogeneous terrain around (*Hirdman et al.*, 2010a), measurements at Summit are representative for the Arctic free troposphere.

The uncertainty of filter-based absorption measurements of BC (PSAP and aethalometer) lies in empirical corrections of the overestimated absorption if light transmission is also affected by particulate light scattering (*Bond et al.*, 1999). Accuracy of this correction is 20–30% (*Delene and Ogren*, 2002; *Weingartner et al.*, 2003; *Virkkula et al.*, 2005). Additional uncertainty results from the empirical conversion from optical response to BC mass using

an assumed mass absorption cross-section (MAC), which depends on the composition and morphology of the particles used in the calibration of the instrument and on the specific technique used to quantify the BC mass (*Clarke et al.*, 1987; *Slowik et al.*, 2007). The MAC of BC varies by up to a factor of four, from 5 m^2 g^{-1} in remote areas to 20 m^2 g^{-1} near source regions (*Weingartner et al.*, 2003). We use 9.5 m^2 g^{-1} for station Barrow at wavelength 530 nm as recommended for the ARCTAS period (*McNaughton et al.*, 2011; *Wang et al.*, 2011). The MAC used at station Alert (*Sharma et al.*, 2013), Zeppelin (*Eleftheriadis et al.*, 2009) and Summit (*Hagler et al.*, 2007) are 19 m^2 g^{-1}, 15.9 m^2 g^{-1}, and 20 m^2 g^{-1}. The uncertainty of absorption enhancement by non-BC absorbers (organic carbon and mineral dust) is generally difficult to quantify unless the non-BC absorbers contribute more than 40% of absorption (*Petzold et al.*, 2013).

2.3 Model description and simulations

2.3.1 GEOS-Chem simulation of BC

GEOS-Chem is a global 3-D chemical transport model driven with assimilated meteorology from the Goddard Earth Observing System (GEOS) of the NASA Global Modeling and Assimilation Office (GMAO). GEOS-5 meteorological data set are used to drive model simulation at 2° latitude × 2.5° longitude resolution and 47 vertical layers from the surface to 0.01 hPa. Tracer advection is computed every 15 min with a flux-form semi-Lagrangian method (*Lin and Rood*, 1996). Tracer moist convection is computed using GEOS convective, entrainment, and detrainment mass fluxes as described by (*Allen et al.*, 1996a,b). Deep convection is parameterized using the relaxed Arakawa-Schubert scheme (*Moorthi and Suarez*, 1992; *Arakawa and Schubert*, 1974), and the shallow convection treatment follows (*Hack*, 1994). BC aerosols are emitted by incomplete fossil fuel and biofuel combustion and biomass burning. We use global BC emissions from *Bond et al.* (2007) with updated emissions in Asia from *Zhang et al.* (2009b). Biomass burning emissions are from the Global Fire Emissions

Database version 3 (GFEDv3) (*Van der Werf et al.*, 2010) with updates for small fires in *Randerson et al.* (2012). It is assumed that 80% of the freshly emitted BC aerosols are hydrophobic (*Park et al.*, 2003) and are converted to hydrophilic with an e-folding time of 1.15 days, which yields a good simulation of BC export efficiency in continental outflow (*Park et al.*, 2005). Dry deposition in the model is computed using a resistance-in-series method (*Wesely*, 1989; *Zhang et al.*, 2001), whereas it assumes a constant aerosol dry deposition velocity of 0.03 cm s^{-1} over snow and ice (see Sect. 2.3.3). Wet deposition follows *Liu et al.* (2001), with updates as described in *Wang et al.* (2011).

Table 2.2: GEOS-Chem simulations of BC in the Arctic.

<table>
<tr><th colspan="2">Experiments</th><th>A</th><th>B</th><th>C</th><th>D</th></tr>
<tr><td rowspan="3">Anthropogenic emissions</td><td>Arctic</td><td>Bond et al. (2007)</td><td colspan="3">Bond et al. (2007) and flaring emissions from Stohl et al. (2013)</td></tr>
<tr><td>Asia</td><td colspan="4">Zhang et al. (2009)</td></tr>
<tr><td>Rest of world</td><td colspan="4">Bond et al. (2007)</td></tr>
<tr><td colspan="2">Biomass burning</td><td colspan="4">GFEDv3 (van der Werf et al., 2010), with updates from Randerson et al. (2012)</td></tr>
<tr><td colspan="2">BC aging</td><td colspan="4">e-folding time 1.15 days</td></tr>
<tr><td rowspan="3">Deposition</td><td>Dry</td><td colspan="2">0.03 cm s^{-1} over snow/ice and resistance-in-series over other surfaces (Wang et al., 2011)</td><td colspan="2">Resistance-in-series over all surfaces (Wesely, 1989; Zhang et al., 2001)</td></tr>
<tr><td rowspan="2">Wet</td><td colspan="4">Liu et al. (2001) with updates from Wang et al. (2011)</td></tr>
<tr><td colspan="3">Riming: scavenging efficiency for hydrophilic BC is 100% in warm and mixed phase clouds</td><td>Account for both riming and WBF in mixed phase clouds (Fukuta et al., 1999; Verheggen et al., 2007; Cozic et al., 2007)</td></tr>
</table>

2.3.2 Gas flaring emissions of BC

Gas flaring is the controlled burning of natural gas in petroleum producing areas, particularly in areas lacking gas transportation infrastructure (*Elvidge et al.*, 2009, 2011). It is estimated that 3.5% of world's natural gas is flared (*Elvidge et al.*, 2015) and results in a large amount of green house gas emissions (13,662.6 Gg of CO_2, *Bradbury et al.*, 2015). *Stohl et al.* (2013) derived BC emissions from from gas flares by multiplying gas flaring volumes by

emission factors. The flaring volumes were estimated using low light imaging data acquired by the Defense Meteorological Satellite Program (DMSP) (*Elvidge et al.*, 2011). The DMSP estimates of flared gas volume are based on a calibration developed with a pooled set of reported national gas flaring volumes and data from individual flares. *Stohl et al.* (2013) derived BC emission factor based upon emission factors of particulate matter from flared gases. The resulting gas flaring emissions (228 Gg yr^{-1}) accounts for ∼5% of global anthropogenic emissions (4.8 Tg yr^{-1}, *Bond et al.*, 2007) and ∼3% of global total emissions (8.5 Tg yr^{-1}, including anthropogenic emissions from Bond et al., 2007 and Zhang et al., 2009 and biomass burning emissions from Randerson et al., 2012). However, the largest contributor Russia, contributing ∼30% to the global flaring volume, locates in the clean Arctic Circle. About 40% of BC emissions in the Arctic (115 Gg yr^{-1}) are from gas flaring (48 Gg yr^{-1}), shown in Fig. 2.1. It is estimated that flaring emissions contribute 42% to the annual mean BC_{air} at surface in the Arctic (*Stohl et al.*, 2013). However, to our knowledge, no study so far has investigated the contribution of flaring emissions to BC_{snow} in the Arctic. Thus, we included flaring emissions from *Stohl et al.* (2013) (data on flaring emissions is available at http://eclipse.nilu.no upon request) and investigated the contribution of flaring emissions to BC_{snow} and BC_{air} in the Arctic in Experiment B (Table 2.2).

2.3.3 Dry deposition over snow and ice

Rannik (2001) conducted eddy-covariance flux measurements of aerosol number dry deposition in the Arctic Ocean and found a mean dry deposition velocity (v_d) of 0.19 cm s^{-1} over open sea, 0.03 cm s^{-1} over ice floes and 0.03–0.09 cm s^{-1} over leads (Table 2.3). Following *Rannik* (2001), *Fisher et al.* (2011) imposed $v_d = 0.03$ cm s^{-1} for aerosols over snow and ice. They found improved agreements of simulated sulfate with in-situ observations in spring and winter in the Arctic. *Wang et al.* (2011), also imposing $v_d = 0.03$ cm s^{-1} for aerosols over snow and ice, found better agreements for BC at the same stations as used by *Fisher et al.* (2011). They thus recommended a uniform $v_d =$ cm s^{-1} for sulfate and BC over snow

and ice. To capture the winter and spring haze, other studies also used relatively low v_d = 0.01–0.07 cm s^{-1} (*Liu et al.*, 2011; *Sharma et al.*, 2013). These low values, however, are likely too small for snow-covered land surface, where larger roughness lengths reduce the aerodynamic resistance thereby increase v_d (*Gallagher et al.*, 2002). The roughness length is 0.005 m for sea ice and 0.03–0.25 m for snow-covered land surface with grass and scattered obstacles (*Wieringa*, 1980). As a result, v_d is larger over snow-covered land surface than over sea ice. Observed values over snow and ice are 0.01–2.4 cm s^{-1} for aerosol particles in general and 0.01–1.52 cm s^{-1} for BC in particular (Table 2.3). Again, this suggests that a uniform value of v_d = 0.03 cm s^{-1} is problematic. We apply the resistance-in-series method to calculate dry deposition velocity of BC over snow and ice, as a function of aerodynamic resistance, particle density and size and surface types (Experiment C, Table 2.2).

We would like to note that most of these observations (*Held et al.*, 2011; *Rannik*, 2001; *Bergin et al.*, 1995) were from summertime Arctic (June–August) and clean regions (e.g., the Arctic and Greenland) far from anthropogenic pollutions. In addition, most of the dry deposition velocity measurements are for general aerosol particles. The only available dry deposition velocities specific to BC particles are derived from the strong surface enhancement of BC_{snow} between two snow events at Mt. Changbai (42.5°N, 128.5°E, 0.74 km) in Northern China (Table 2.3). *Wang et al.* (2014e) derived v_d = 0.16–1.52 cm s^{-1}. They then calculated dry deposition fluxes of 2.65 ± 1.93 μg cm^{-2} $month^{-1}$, a factor of five higher than the corresponding wet deposition fluxes. Despite these uncertainties, these measurements suggest that the low dry deposition velocity used in previous studies (*Fisher et al.*, 2011; *Liu et al.*, 2011; *Wang et al.*, 2011; *Sharma et al.*, 2013) might underestimate the role of dry deposition during snow season, particularly near source regions. *Wang et al.* (2014e) concluded that dry deposition in the boundary layer may dominate over wet deposition during dry season in some regions, particularly near source regions with high BC_{air}. It is thus imperative to obtain measurements of BC dry deposition velocities in polluted regions in Russia and Northern Europe in spring, when radiative forcing associated with BC snow-albedo effect is maximum

(*Flanner et al.*, 2009, 2012).

Table 2.3: Observed and simulated dry deposition velocity (v_{d}) using resistance-in-series method over snow and ice.

Region	Sample	Observed v_d (cm s^{-1})	Simulated v_d (cm s^{-1})	References	Particle diameter
Arctic Ocean	Open water leads, ice ridges, snow and ice surfaces	0.027-0.068[a]	0.006-0.070[a]	Held *et al.* (2011)	< 50 nm
Arctic Ocean	Open sea	0.19[b]		Nilsson and Rannik (2001)	
Arctic Ocean	Frozen, partly snow-covered ice	0.03[b]	0.013-0.22[b]	Nilsson and Rannik (2001)	Mostly ultrafine and Aitken mode
Arctic Ocean	Summer lead	0.034[b]		Nilsson and Rannik (2001)	
Arctic Ocean	Freeze-up lead	0.091[b]		Nilsson and Rannik (2001)	
Greenland	Snow (sulfate)	0.023-0.062[c]	0.007-0.16[c]	Bergin *et al.* (1995)	< 10 μm
Greenland	Snow (sulfate)	0.01-0.18[d]	0.007-0.20[d]	Hillamo *et al.* (1993)	0.6 μm
Greenland	Snow	0.2-0.7		Hillamo *et al.* (1993)	2 μm
Antarctic	Snow grass	0.02-0.1		Wesely *et al.* (1979)	0.05-1.0 μm
Antarctic	Smooth snow surface	0.33 (0.08-1.89)		Grönlund *et al.* (2002)	14 nm
Antarctic	Rocky surface interrupted by snow	0.8 (0.2-2.4)		Grönlund *et al.* (2002)	42 nm
Norway	Snow	0.06-0.38		Dovland and Elliassen (1976)	
Pennsylvania	Snow covered farm land in December	0.034±0.014		Duan *et al.* (1988)	0.15-0.3 μm
Mt. Changbai	Snow covered mountain (BC)	0.16-1.52[e]	0.09-0.14[e]	Wang *et al.* (2014)	

[a] This range of measurements are medians of dry deposition velocities derived from aerosol number fluxes measured by an eddy covariance system over different surface types (open water leads, ice ridges, snow and ice surfaces) in the Arctic Ocean between 2°−10° W longitude and 87°−87.5° N latitude in late August 2008 (Held et al., 2011). The simulated dry deposition velocities are sampled at the same region during the same time period as observations for BC particles.
[b] Observations are medians of dry deposition velocities derived from aerosol number fluxes measured by an eddy covariance system over different surface types in late July and early August in 1996 in the Arctic Ocean for ultra fine and Aitken mode aerosol particles (Nilsson and Rannik, 2001). Simulations are sampled in the same region during the same months as observations in 2008 for BC particles.
[c] Sulpate dry deposition velocities were derived based on particle mass using surrogate surfaces and impactor data at site Summit, Greenland in July 1993 (Bergin et al., 1995). Simulations are sampled at the same site during July 2008 for BC particles.
[d] Sulpate dry deposition velocities were derived based on particle mass from Cascade impactor at Dye 3 on the south-central Greenland Ice Sheet in March 1989 (Hillamo et al., 1993). Simulations are sampled at the same site during March 2008 for BC particles.
e The dry deposition velocities specific to BC particles were derived from measured surface enhancement of BC in snow between two snow events at Changbai Mountain in Northern China in winter (December, January, and February) in 2009-2012 (Wang et al., 2014). Simulations are sampled at the same site during the same time period for BC particles.

2.3.4 WBF process in mixed-phase clouds

Most AeroCom models (*Textor et al.*, 2006) parameterize rainout rate following *Giorgi and Chameides* (1986). The rainout ratio is proportional to precipitation formation rate and mass mixing ratio of BC in condensed phase in clouds, which is determined by the scavenging efficiency of BC ($r_{\mathrm{scav.}}$),

$$r_{\text{scav.}} = \frac{[BC]_{\text{condensed}}}{[BC]_{\text{condensed}} + [BC]_{\text{interstitial}}}$$

where $r_{\text{scav.}}$ is the scavenging efficiency and quantifies the partition of BC aerosols between condensed phase and the interstitial air; $[\text{BC}]_{\text{condensed}}$ is the mass mixing ratio of BC in condensed phase, including water drops and ice crystals in clouds, $[\text{BC}]_{\text{interstitial}}$ is the mass mixing ratio of BC in the interstitial air.

Hygroscopicity and size of BC-containing particles are determining factors for BC scavenging efficiency (*Sellegri et al.*, 2003; *Hallberg et al.*, 1992, 1994). Internal mixing with soluble inorganic species enhances the scavenging efficiency for aged BC particles (*Sellegri et al.*, 2003). The scavenging efficiency is 0.39±0.16 for BC-containing particles with diameter smaller than 0.3 μm and a small fraction (38%) of soluble inorganic material. The scavenging efficiency increases to 0.97±0.02 for particles with diameter larger than 0.3 μm and a larger fraction (57%) of soluble inorganic material (*Sellegri et al.*, 2003). In addition to particle properties, cloud microphysics and dynamics play a significant role in determining the scavenging efficiency of BC in mixed-phase clouds (*Hitzenberger et al.*, 2000, 2001; *Cozic et al.*, 2007; *Hegg et al.*, 2011). Measured BC scavenging efficiency decreased from 0.60 in liquid only clouds to 0.05–0.10 in mixed-phase clouds, a reduction of more than a factor of five (*Cozic et al.*, 2007; *Henning et al.*, 2004; *Verheggen et al.*, 2007). Such reduction was attributed to the effect of the WBF process (*Cozic et al.*, 2007). In mixed-phase clouds, ice crystals grow at the expense of water drops when the environmental vapor pressure is higher than the saturation vapor pressure of ice crystals but lower than the saturation vapor pressure of water droplets (Wegener, 1911; Bergeron, 1935; Findeisen, 1938). As such, BC-containing particles in the water drops are released back to the interstitial air and consequently the scavenging efficiencies are reduced. Another process, riming (*Hegg et al.*, 2011), in mixed-phase clouds has an opposite effect to BC scavenging. When ice particles fall and collect the water drops along the pathway, the snow particles show rimed structure and the

scavenging efficiency remains the same. Riming rate is determined by the terminal velocity of snowflakes, ice crystals and liquid water contents in clouds (*Fukuta and Takahashi*, 1999).

Previously, only the hygroscopicity of BC containing particles is considered in BC scavenging efficiency in models (*Wang et al.*, 2011, and references therein). It is typically assumed that 100% of hydrophilic BC particles are readily incorporated into cloud drops and all hydrophobic BC particles remain in the interstitial air in warm and mixed-phase clouds. This treatment of mixed-phase clouds as liquid phase is likely to overestimate the scavenging rate in mixed-phase clouds. In models that include mixed-phase clouds, assumptions still need to be made about scavenging efficiency. A uniform scavenging efficiency (0.4 or 0.06) for all mixed-phase clouds has been imposed (*Stier et al.*, 2005; *Bourgeois and Bey*, 2011), while observations show that scavenging efficiency varies dramatically with temperature and ice mass fraction (*Cozic et al.*, 2007; *Henning et al.*, 2004; *Verheggen et al.*, 2007).

In Experiment D (Table 2.2), we discriminate WBF-dominated and riming-dominated conditions and parameterize BC scavenging efficiency under the two conditions separately in mixed-phase clouds (248 K $<$ T $<$ 273 K, Garrett et al., 2010). We assume that riming dominates when temperature is around -10°C (261 K $<$ T $<$ 265 K) and liquid water content is above 1.0 g m^{-3}, following *Fukuta and Takahashi* (1999). The WBF process dominates otherwise. Our parameterization of the effect of the WBF process on BC scavenging efficiency is based on the measurements at Mt. Jungfraujoch (46.4°N, 8°E, 3850 m), an elevated mountainous site far from pollution sources and regularly engulfed in clouds (30% of the time) (*Cozic et al.*, 2007). These characteristics make the site well suited for investigating continental background aerosols and clouds from a ground based platform. We evaluated the effect of WBF on global BC simulation and tested the sensitivity of the simulation to the switch temperature from warm clouds to mixed-phase clouds and from mixed-phase clouds to ice clouds in Chapter 3. In this chapter, we focus on the effect to BC distribution in the Arctic.

2.3.5 BC concentration in snow

In snow models, such as SNICAR, the initial surface BC_{snow} is defined as the ratio of BC deposition to snow precipitation (*Flanner et al.*, 2007). Here we approximate BC_{air} using BC deposition flux and snow precipitation rate, following *Kopacz et al.* (2011) and *He et al.* (2014b):

$$[BC]_{\text{snow}} = \frac{F_{\text{dep}}}{F_{\text{snow}}} = \frac{F_{\text{wet_dep}} + F_{\text{dry_dep}}}{F_{\text{snow}}}$$

where F_{dep}, $F_{\text{wet_dep}}$, and $F_{\text{dry_dep}}$ are total, dry and wet deposition flux of BC and F_{snow} the snow precipitation. The top and bottom snow depth of each sample are provided in the observation dataset (*Doherty et al.*, 2010). We calculate the dates of the snow fall of the top and bottom depth of the snow sample first and then use the average BC deposition fluxes and snow precipitation between the two dates to estimate the BC snow concentration for the sample. Snow depth is accumulated from the observation date backward until it reaches the top or bottom snow depth of the sample, then the dates are stored. The accumulation rate is estimated as snow precipitation flux (kg m^{-2} s^{-1}) over snow density (kg m^{-3}). The annual average snow density is 300 kg m^{-3} over the Arctic basin, increasing from 250 kg m^{-3} in September to 320 kg m^{-3} in May with little geographical variation across the Arctic (*Warren et al.*, 1999; *Forsström et al.*, 2013). We use the annual average snow density in the estimate.

The above estimate of BC_{snow} ignores many processes that may alter the BC snow concentrations, such as wind-redistribution of surface snow, sublimation, and melt water flushing (*Doherty et al.*, 2010, 2013; *Wang et al.*, 2014e). Wind-redistribution of surface snow is a sub-grid scale phenomenon. Except for turbulent scale wind direction and strength, small-scale topography also plays an important role in surface snow redistribution. So this process is really difficult to simulate by global models. Precipitation rate and relative humidity in much of the Arctic are low, so in some areas appreciable (up to 30–50%) surface snow is lost

to sublimations (*Liston and Sturm*, 2004). BC_{snow} at surface can thus be underestimated by our method. We filtered snow samples collected during melting season, so the melt water flushing has little effect to our estimate.

To reduce the biases in comparison of model results and observations, we organize the observations as follows: (1) Observations from March to May in 2007-09 are used while those from June to August are excluded, because our estimate of BC_{snow} does not resolve snow melting; (2) We exclude observations with obvious dust or local wood-burning contaminations as described in *Doherty et al.* (2010); (3) We average the observations in the same model grid and snow layer and collected on the same day.

Table 2.2 summarizes various model simulations in the present study. Experiment A is the standard case. We include gas flaring emissions in Experiment B (Sect. 2.3.2). Contrasting Experiments B and A thus offer insights to the contribution of gas flaring emissions on BC in the Arctic. Experiment C includes the updated dry deposition velocity (Sect. 2.3.3). The difference of Experiment B and C denote the effects of updated dry deposition velocity to BC distribution. Experiment D includes temperature-based WBF parameterization (Sect. 2.3.4). The effects of WBF to BC in the Arctic are shown by the difference of Experiment C and D. Additional simulations are described where appropriate.

2.4 The effects of gas flares, dry deposition, WBF and precipitation

We discuss the effect of gas flaring emissions, dry deposition, WBF in mixed-phase clouds, and precipitation to BC distribution in the Arctic in this section. The probability density function (PDF) of observed and GEOS-Chem simulated BC_{snow} in the Arctic is approximately lognormal (Fig. 2.2(a)). The arithmetic mean of observations is 17.4 ng g^{-1}, larger than the geometric mean of 12.7 ng g^{-1} and the median of 11.8 ng g^{-1} (see the vertical lines in Fig. 2.2 and Table 2.1). The model reproduces the observed distribution, but underestimates

BC_{snow} by 40% (Experiment A). By including flaring emissions (Sect. 2.4.1), updating dry deposition velocity (Sect. 2.4.2) and including WBF in mixed-phase clouds (Sect. 2.4.3), the discrepancy is reduced to -10%. Gas flaring emissions lower the discrepancy from -40% to -20% (Experiment B). The updated dry deposition velocity (Experiment C) makes insignificant changes to BC_{snow} in the Arctic. WBF (Experiment D) further reduces the discrepancy from -20% to -10%. The resulting BC_{snow} in the eight sub-regions agree with observations within a factor of two. This discrepancy is acceptable for global models because it has been suggested that the error due to different spatial sampling of global models (∼200 km) and point observations was up to 160% (*Schutgens et al.*, 2016). In addition, BC_{air} at surface and in the free troposphere is sensitive to the above three processes in the Arctic, particularly during winter and spring (see Sects. 2.4.1–2.4.3).

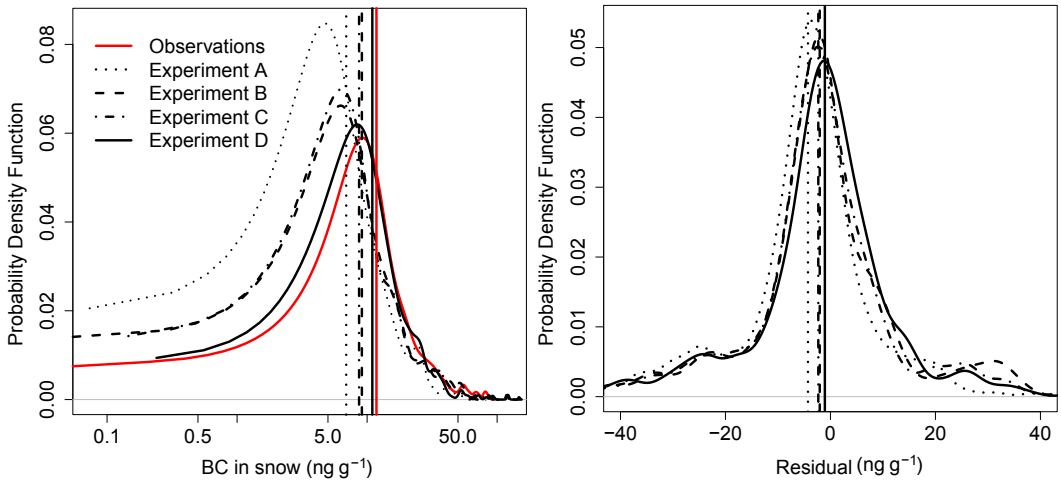

Figure 2.2: Probability density function of observed (solid red) and GEOS-Chem simulated (black curves: dotted–Experiment A; dashed–Experiment B; dash dotted–Experiment C; solid–Experiment D, see Table 2.2 and text for details) BC concentration in snow (ng g^{-1}) in the Arctic (left panel), medians (vertical lines, left panel), residual errors (model–observation, right panel) and mean residual errors (vertical lines, right panel).

Table 2.4: Observed and GEOS-Chem simulated BC concentration in snow in the Arctic (ng g^{-1}, see Fig. 2.1).

			Arctic	Alaska	Arctic Ocean	Canadian Sub-Arctic	Canadian Arctic	Greenland	Ny_Ålesund	Russia	Tromsø
Sample size			334	3	23	34	86	8	39	118	23
Arithmetic mean	Obs.		19.8	12.4	8.0	14.8	8.8	3.2	13.7	28.3	19.3
	Experiment	A	10.9 (0.6[+])	6.0 (0.5)	8.5 (1.1)	7.7 (0.5)	5.7 (0.7)	3.6 (1.1)	10.9 (0.8)	12.3 (0.4)	35.6 (1.8)
		B	15.0 (0.8)	7.7 (0.6)	10.8 (1.4)	9.3 (0.6)	6.7 (0.8)	3.6 (1.1)	14.9 (1.1)	19.6 (0.7)	41.8 (2.2)
		C	15.1 (0.8)	8.0 (0.6)	10.3 (1.3)	9.1 (0.6)	7.0 (0.8)	4.3 (1.3)	12.8 (0.9)	20.7 (0.7)	38.4 (2.0)
		D	16.0 (0.8)	12.2 (1.0)	12.4 (1.6)	8.5 (0.6)	8.8 (1.0)	5.1 (1.6)	14.9 (1.1)	19.4 (0.7)	45.8 (2.4)
Geometric Mean	Obs.		12.9	11.4	6.8	13.2	8.2	2.7	11.2	21.2	18.8
	Experiment	A	7.6 (0.6)	5.9 (0.5)	7.3 (1.1)	5.9 (0.5)	4.9 (0.6)	2.3 (0.9)	8.4 (0.8)	9.3 (0.4)	28.3 (1.5)
		B	10.4 (0.8)	7.6 (0.7)	9.6 (1.4)	7.6 (0.6)	6.1 (0.7)	2.4 (0.9)	11.4 (1.0)	14.3 (0.7)	35.1 (1.9)
		C	10.1 (0.8)	7.9 (0.7)	9.3 (1.4)	7.3 (0.6)	6.3 (0.8)	2.8 (1.0)	9.7 (0.9)	13.9 (0.7)	31.6 (1.7)
		D	11.5 (0.9)	11.6 (1.0)	11.6 (1.7)	7.6 (0.6)	8.1 (1.0)	3.8 (1.4)	11.9 (1.0)	14.2 (0.7)	37.2 (2.0)
Median	Obs.		11.8	11.0	7.6	12.8	8.9	2.5	11.9	22.1	19.1
	Experiment	A	6.9 (0.6)	6.3 (0.6)	6.4 (0.8)	5.5 (0.4)	4.1 (0.5)	2.3 (0.9)	8.4 (0.7)	10.8 (0.5)	25.2 (1.3)
		B	9.5 (0.8)	7.6 (0.7)	7.7 (1.0)	7.3 (0.6)	5.7 (0.6)	2.3 (0.9)	11.1 (0.9)	16.1 (0.7)	33.7 (1.8)
		C	8.7 (0.7)	7.8 (0.7)	8.5 (1.1)	7.3 (0.6)	6.0 (0.7)	3.2 (1.3)	9.2 (0.8)	16.1 (0.7)	29.2 (1.5)
		D	11.0 (0.9)	12.1 (1.1)	10.9 (1.4)	6.8 (0.5)	8.6 (1.0)	5.7 (2.3)	11.3 (1.0)	16.9 (0.8)	38.2 (2.0)

[+]Ratio of model to observation

2.4.1 Gas flaring emissions

Gas flaring emissions increase total BC emissions by 67% (from 0.068 to 0.115 Tg yr^{-1}) in the Arctic Circle (60°N and higher latitudes), resulting in a 19% increase of the total BC deposition (from 0.32 to 0.38 Tg yr^{-1}). Flaring emissions increase BC_{snow} (by 0.1–8.5 ng g^{-1}) in the eight Arctic sub-regions. The higher BC_{snow} leads to significant reduction in the negative biases (by 20–100%), except in the Arctic Ocean and in Troms, where BC_{snow} is already overestimated without flaring emissions (Fig. 2.3). BC_{snow} in Greenland is not affected by gas flaring emissions. The reason is two-folded: first, snow samples in Greenland are far from the flares in Western Russia; second, the vertical transport of BC from surface

to the upper troposphere is suppressed by the stable atmosphere in the Arctic (*Stohl*, 2006), resulting in negligible effect of flaring emissions to BC_{snow} over Greenland (above 1.5 km).

The largest enhancement of BC_{snow} from flaring emissions is in the Western Extreme North of Russia within the Arctic Circle (by 5.0 ng g^{-1} on average, or, 50%), which reduces model discrepancy substantially across Russia (from -50% to -30%). However, simulated BC_{snow} is now too high by a factor of two near the flares (observed value 19.3 ng g^{-1}). The overestimate is likely because of excessively large flaring emission estimates. Yet BC_{snow} is too low by a factor of two in far fields (observed value 30.7 ng g^{-1}), despite a large increase (by 50%, from 10.5 to 15.5 ng g^{-1}) as a result of flaring emissions.

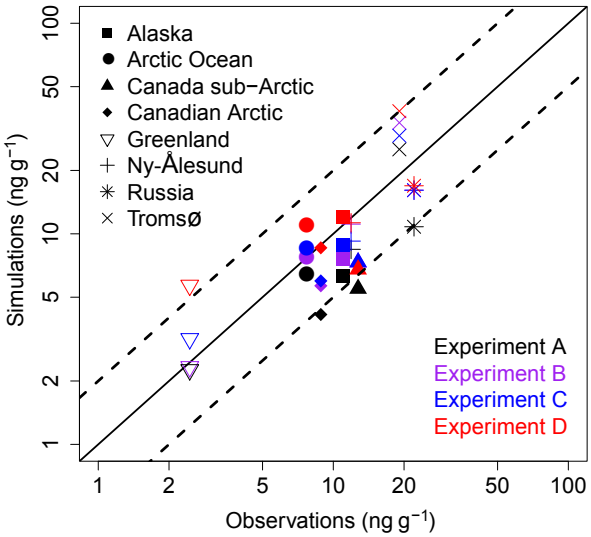

Figure 2.3: Observed and GEOS-Chem simulated median BC concentration in snow (ng g^{-1}) in the eight sub-regions in the Arctic (see Fig. 2.1). Solid line is 1:1 ratio line and dashed lines are 1:2 (or 2:1).

Flaring emissions are assumed to be proportional to flared gas volumes and emission factors. Errors in estimates of flared volumes in Russia is small (within ±5%, *Elvidge et al.*, 2009). Estimates of emission factors, on the other hand, are known to have several orders of magnitude uncertainties (*Schwarz et al.*, 2015; *Weyant et al.*, 2016). Given limited observations of BC emission factors from actual flares, *Stohl et al.* (2013) derived BC emission

factor based upon emission factors of particulate matter from flared gases. They used a BC emission factor of 1.6 g m^{-3}, which is more than a factor of three higher than that (0.5 g m^{-3}) from a lab experiment on fuel mixtures typical in the oil and gas industry (*McEwen and Johnson*, 2012). Recent field measurements have suggested an even lower emission factor (0.13±0.36 g m^{-3}) from ∼30 individual flares in North Dakota, with an upper bound of 0.57 g m^{-3} (*Schwarz et al.*, 2015; *Weyant et al.*, 2016). These studies found that average BC emission factors for individual flares varied by two orders of magnitude, and furthermore, two flares from the same flare stack that were resampled on different days showed different BC emission factors (*Weyant et al.*, 2016). They also pointed out that emission factors are not correlated with ambient temperature, pressure, humidity, flared gas volumes or gas composition. It is thus imperative that extensive measurements of BC emission factors be made in the flare regions.

Yet another source of uncertainty is flare stack height, which is not accounted for in current flaring emission estimates. Typical stack heights vary from 15 to 250 m, sometimes above the nighttime boundary layer eight of 150–300 m in the Arctic (*Di Liberto et al.*, 2012). The stack height affects the ventilation, dispersion, deposition, and long-range transport of the emissions. For example, local deposition of BC may be suppressed and downwind long-range transport enhanced when the stacks emit BC in the free troposphere (*Chen et al.*, 2009). The lack of proper treatment of flare stack height in the model may partially explain the aforementioned discrepancies of modeled BC_{snow} (biased high in Western Russian and low in Eastern Russia). Another factor for the underestimate of BC_{snow} in Eastern Russia is likely local sources, such as domestic wood burning in nearby villages and fishing camps, diesel trucks on highway and coal burning in a power plant, that are unaccounted for in the emission inventory (*Doherty et al.*, 2010, Fig. 2.1). Although we filter out samples with strong local contamination, it is conceivable that local emissions still add to the background BC_{snow} in Eastern Russia.

Jiao et al. (2014) have shown that most AeroCom models underestimated BC_{snow} in

Russia and pointed to the flaring emissions as a likely cause. Our model results show that even with flaring emissions, which are likely on the high side, BC_{snow} is still too low (by 50%) in Eastern Russia. Therefore, there are likely other factors such as the lack of local emissions in Eastern Russia, weak dry deposition fluxes (Sect. 2.4.2), and excessively low rate of sublimation of surface snow, that contribute to the large model discrepancy in BC_{snow}.

Fig. 2.4 shows observed and GEOS-Chem simulated daily BC_{air} from January to March at Zeppelin, a site that is closest to the gas flares in the Western Extreme North of Russia. The inclusion of flaring emissions captures some of the large spikes in the observed BC_{air}, such as those from late February to March in 2008 and in January 2009. *Stohl et al.* (2013) found that flaring emissions captured observed large spikes at Zeppelin during a transport event in February 2010 with a high BC/CO ratio, a signature of gas flaring emissions (CAPP, 2007). The inclusion of flaring emissions results in enhanced BC_{air}, for instance, in February 2007 and in January 2008, that are not seen in the observations. This is largely from the lack of temporal variation of flaring emissions (*Weyant et al.*, 2016). The temporal variation is, however, difficult to characterize based on the current knowledge of flaring emissions in the Western Extreme North of Russia (*Stohl et al.*, 2013). Flaring emissions also increase BC_{air} during snow season (Sep. to Apr.) (by 16–19 ng m^{-3}) at Barrow and Alert, resulting in substantial reductions of discrepancies (from -47% to -15% at Barrow and -67% to -46% at Alert) (Fig. 2.5). Flaring emissions are transported to the high Arctic within the Arctic dome by efficient circumpolar transport (*Stohl*, 2006). The effect of flaring emissions at Denali in low Arctic is negligible, because the site is outside of the cold Arctic front (around 65–70°N in Alaska) (*Barrie*, 1986; *Ladd and Gajewski*, 2010). The front is a strong barrier for the meridional transport of BC (*Stohl*, 2006). BC_{air} at Summit (3.22 km a.s.l.), which is mostly in the free troposphere, is not affected by flaring emissions, either. This is because the vertical transport of BC is suppressed by the stable atmosphere during snow season in the Arctic (*Stohl*, 2006).

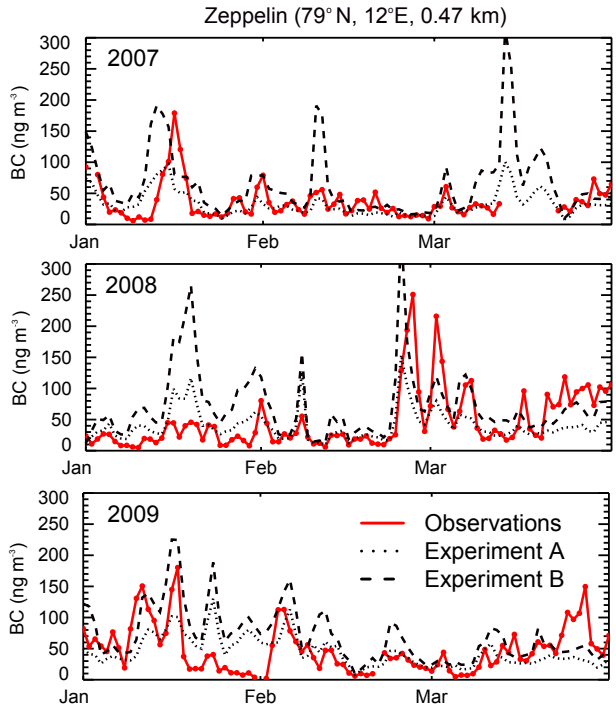

Figure 2.4: Observed (red solid) and GEOS-Chem simulated (dotted–Exp. A, dashed–Exp. B, see Table 2.2 and text for details) daily BC concentrations in air (ng m^{-3}) at Zeppelin from January–March in 2007–09.

2.4.2 Dry deposition velocity

It is known that v_d of aerosol particles over snow and ice surfaces strongly depend on particle size, surface types and meteorological conditions and vary by orders of magnitude (Table 2.3). We estimate v_d of BC particles as a function of particle properties, aerodynamic resistance and surface types (Sect. 2.3.3). The results over the Arctic Ocean and Greenland are shown in Table 2.3, generally within the observed range. At Mt. Changbai, model result of BC v_d (0.09–0.14 cm s^{-1}) is an order of magnitude lower than that derived by *Wang et al.* (2014e) (0.16–1.52 cm s^{-1}). The resulting dry deposition fluxes are lower than observations by a factor of five. We attribute the large discrepancies to two factors. First, the point measurements were at a mountainous site with complex terrain and micro-meteorological

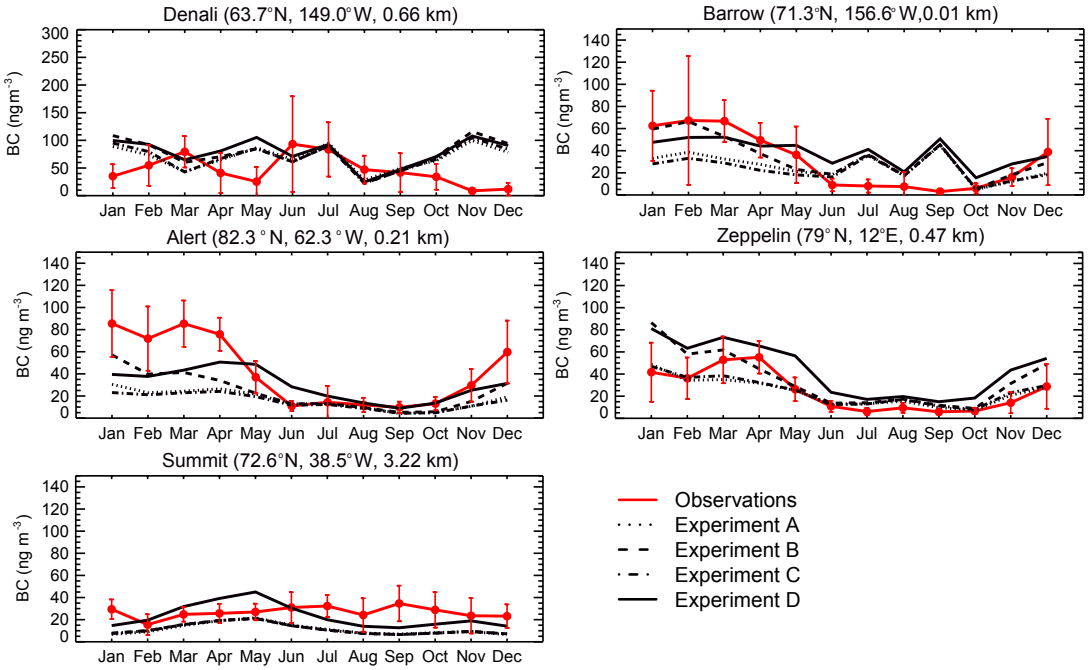

Figure 2.5: Observed (red solid) and GEOS-Chem simulated (black curves: dotted–Exp. A, dashed–Exp. B, dash dotted–Exp. C, solid–Exp. D, see Table 2.2 and text for details) BC concentrations in air (ng m^{-3}) at Denali, Barrow, Alert, Zeppelin, and Summit, averaged for 2007–09. Also shown are standard deviations of observations (error bars).

conditions. Neither can be resolved in a global model (*He et al.*, 2014b). Second, the values reported by *Wang et al.* (2014e) were estimated from relative enhancements of surface BC_{snow} between two snow events. These estimates are known to have large uncertainties (a factor of two) from the measured sublimation fluxes and the assumption of snow density (*Wang et al.*, 2014e).

Compared to the results of uniform v_d of 0.03 cm s^{-1} over snow and ice, the updated v_d leads to larger dry deposition fluxes, a larger fraction of dry over total deposition, and relatively unchanged total deposition fluxes. Simulated mean BC v_d in the eight Arctic sub-regions (Fig. 2.1) are 0.03–0.14 cm s^{-1}, considerably larger that the uniform value of 0.03 cm s^{-1} over snow and ice (Table 2.5). Correspondingly, the v_d are 19–195% larger in most sub-regions, with the largest increase in Greenland (by 195%) and over Russia (by 87%)

(Table 2.5). We find that BC dry deposition flux is more sensitive to v_d in source regions (e.g., Russia) than in remote regions, reflecting the high BCair in the former. A comparable increase in v_d of BC (from 0.03 cm s^{-1} to 0.08 cm s^{-1}) in Russia and Alaska results in vastly different increases in BC dry deposition flux (87% in Russia versus 30% in Alaska). As expected, larger dry deposition flux depletes BC_{air} thereby reducing wet deposition flux but offsets the reduction in wet deposition. As a result, both total deposition flux and BC_{snow} remain relatively unchanged ($< 5\%$) in the eight sub-regions, except in Ny-Ålesund and Tromsø. In these last two regions, the total deposition fluxes are 10–15% smaller. The lower deposition fluxes reflect efficient removal of BC aerosols over source regions. BC in Ny-Ålesund and Troms are primarily from Europe and Russia, transported isentropically in cold season (*Stohl*, 2006; *Eleftheriadis et al.*, 2009) . Rapid dry deposition in these source regions results in enhances boundary layer removal hence lower BC loadings in air and a reduced boundary layer outflow (*Liu et al.*, 2011).

The change in the fraction of dry to total deposition has important implications for BC radiative forcing before melting season in the Arctic. The fraction increases from 19% (7–33%) to 26% (14–41%), by 14–73%, with the largest increase in Russia (from 23% to 40%) where BC deposition flux and BC_{snow} are the largest in the Arctic (Tables 2.4 and 2.5). Typically, BC particles removed by dry deposition are externally mixed with snow particles, while those removed by wet deposition are internally mixed with snow particles (*Flanner et al.*, 2009, 2012). Internal mixing of BC with snow/ice particles increases the absorption cross-section of BC/snow composites by about a factor of two (*Flanner et al.*, 2012). The enhanced absorption further increases the snow albedo radiative forcing citephe2014black. It is thus conceivable that the larger dry deposition fraction will lead to less internally mixed BC/snow composite and lower snow albedo radiative forcing.

Unlike BC_{snow}, BC_{air} is a strong function of dry deposition velocity, particularly during snow season. With updated v_d, model results fail to capture the seasonal cycle of BC_{air} with dramatic decreases during snow season (by 20–23 ng m^{-3}, 27–68%) at Barrow, Alert, and

Table 2.5: GEOS-Chem simulated BC dry deposition velocity (cm s^{-1}), dry deposition flux (ng m^{-2} d^{-1}) and fraction of dry to total deposition (%) in the Arctic.).

Region	Dry deposition velocity (cm s^{-1})		Dry deposition flux (ng m^{-2} d^{-1})			Total deposition flux (ng m^{-2} d^{-1})			Dry deposition fraction (%)		
	Exp. B	Exps. C & D	Exp. B	Exp. C	Exp. D	Exp. B	Exp. C	Exp. D	Exp. B	Exp. C	Exp. D
Alaska	0.03	0.08	787	1018	1906	2393	2469	3665	33	41	52
Arctic Ocean	0.03	0.07	662	789	1520	4480	4227	4733	15	19	32
Canadian sub-Arctic	0.04	0.08	841	1192	2297	5669	5596	5013	15	21	46
Canadian Arctic	0.03	0.07	661	988	1948	3194	3289	3343	20	30	58
Greenland	0.03	0.10	262	772	1804	3887	4245	4481	7	18	40
Ny_Ålesund	0.12	0.14	2654	2322	4861	19528	16713	19536	14	14	25
Russia	0.03	0.08	3092	5782	7288	13647	14465	12336	23	40	59
Tromsø	0.12	0.13	5826	5110	9339	46382	42085	49598	13	12	19

Zeppelin (Fig. 2.5). The decreases at Barrow and Alert are a direct result of larger dry deposition in the boundary layer because of substantially larger v_d (0.07 cm s^{-1}, Table 2.5). At Zeppelin (in Ny-Ålesund), where v_d is only marginally higher (17%), the large reduction of BC_{air} (∼40%) is largely attributed to the suppressed transport from proximate source regions in Europe and Russia. This dramatic decrease of BC_{air} in winter with larger v_d and the lack of winter and spring Arctic haze is one of the major reasons of using low v_d in previous studies (*Wang et al.*, 2011; *Sharma et al.*, 2013; *Liu et al.*, 2011). However, this does not justify the use of a low v_d over snow and ice. First, observations have shown very large variations of v_d (Table 2.3), which suggest that a uniform representation might involve large uncertainties. Second, observations of v_d over snow and ice show very large values in certain region, which is still underestimated by the resistance-in-series method. Third, besides dry deposition in boundary layer, BC_{air} is affected by a lot of other factors, such as emissions, transport and wet deposition (Sect. 2.4.3).

2.4.3 WBF in mixed-phase clouds

In mixed-phase clouds, when environmental vapor pressure is between the saturation vapor pressures of water and ice, ice crystals grow at the expense of water drops and release BC particles in cloud water drops back to the interstitial air, now commonly referred to as the WBF effect (Wegener, 1911; Bergeron, 1935; Findeisen, 1938). Our model results show that WBF increases BC_{snow} by 20–80% in the eight Arctic sub-regions, except Canadian sub-Arctic, and increases BC_{air} during snow season by 25–70% (Figs. 2.2 and 2.7). Clearly WBF suppresses the scavenging of BC in mixed-phase clouds and consequently enhances poleward transport. We report this in Chapter 3.

WBF not only increases BC_{snow} in the Arctic but also changes the partition of dry and wet deposition of BC_{snow}. Intuitively WBF slows down wet scavenging, thus allowing more BC particles available for dry deposition. Our results show that the fraction of dry to total deposition increases from 26% (12–41%) to 35% (19–59%) on average in the eight Arctic sub-regions, thereby lowering the absorption of solar radiation due to less internally mixed BC-snow composite (Sect. 2.4.2). In Alaska, Canadian Arctic and Russia, BC removed by dry deposition increases to more than 50%. However, averaged globally, this fraction increases only slightly (from 19% to 20%), indicating that the fraction in the Arctic is more sensitive to the WBF effect.

The scavenging efficiency of BC, heretofore defined as the fraction of BC incorporated in cloud water drops or ice crystals in mixed-phase clouds, is strongly affected by WBF and as a result varies temporally and spatially in response to varying temperature (Sect. 2.3.3). Thus, improved treatment of mixed-phase cloud processes, such as WBF and riming, is essential to improve the simulation of spatial and temporal distribution of BC. BC in Alaska and the Canadian Arctic are most sensitive to the WBF effect in the Arctic. WBF increases BC_{snow} by 55% in Alaska and 43% in the Canadian Arctic and reduces the model discrepancies to within 10% (Table 2.3 and Fig. 2.3). BC_{air} at Barrow in Alaska and at Alert in Canadian Arctic are higher by 20–30 ng m^{-3} in winter, reducing the model discrepancies significantly

(from -54% to -18% at Barrow and from -72% to -46% at Alert) and enhancing the seasonal variation (Fig. 2.5). Similar improvements are also seen at Summit in Greenland, where BC_{air} increases by 12 ng m^{-3} and the model discrepancy lowers significantly (from -48% to 3%). This is consistent with recent observations, which showed that high riming rate was rare (12%) in the North American sector of the Arctic and that WBF dominated in-cloud scavenging in mixed-phase clouds (*Fan et al.*, 2011).

At Zeppelin where snow samples show rimed structures (*Hegg et al.*, 2011), model discrepancy of BC_{air} increases to 63% from -10% with the WBF effect included. Model results do not capture the magnitude of BC_{air} in winter at Barrow, Alert and Zeppelin (Fig. 2.5). BC_{air} is well simulated at Zeppelin but underestimated at Barrow and Alert in Experiment A. BC_{air} is well simulated at Barrow and Alert but overestimated at Zeppelin in Experiment D (Fig. 2.5) – similar results were shown in *Sharma et al.* (2013). Such apparent discrepancy can be partly attributed to the fact that models do not properly distinguish WBF-dominated in-cloud scavenging at Barrow (*Fan et al.*, 2011) and riming-dominated scavenging at Zeppelin (*Hegg et al.*, 2011). Here we separate WBF- and riming-dominated conditions based on temperature and liquid water content (LWC) (Sect. 2.3.3, and *Fukuta and Takahashi*, 1999) in Experiment D. However, model results still fail to capture the difference among the three sites. There are a number of reasons. First, LWC from GEOS-5 biased high compared to CloudSat observations (*Barahona et al.*, 2014). In addition, the spatial distribution of LWC from GEOS-5 also has large discrepancy (*Li et al.*, 2012; *Barahona et al.*, 2014). Second, this separation is based on a laboratory experiment, while conditions in the real atmosphere are much more complex. Therefore, more field measurements are required to better separate the two conditions and better parameterize BC scavenging efficiency.

Our results show that WBF exaggerates the positive bias of BC_{air} in summer and delays the transition from the late-spring haze to the clean summer boundary layer (Experiment D). Previous studies found that the dominant process controlling low summertime aerosol at Barrow is the onset of local wet scavenging by warmer clouds (*Garrett et al.*, 2010, 2011).

WBF suppresses scavenging in mixed-phase clouds and thus slows down the onset of strong scavenging by warmer clouds during the transition from winter to summer. However, the strong scavenging of warm drizzling clouds in late spring and summer boundary (*Browse et al.*, 2012), which enhances the winter-summer transition, is not considered in the present study. At high latitudes in summer, the relatively high humidity allows the formation of low stratocumulus cloud decks in the boundary layer and lower troposphere (*Browse et al.*, 2012). These low clouds and fogs produce frequent drizzle and can be present for as much as 90% of the time and remove aerosols effectively (*Browse et al.*, 2012).

2.4.4 Precipitation

We compute BC_{snow} as the ratio of BC deposition flux to precipitation rate (Sect. 2.3.5). It has been pointed out that this estimate is very sensitive to uncertainties in precipitation (*He et al.*, 2014b). Climatological precipitation across the Arctic is 14.3 g cm^{-2} yr^{-1} for 1965–89 (*Overland and Turet*, 1994) and is 16.3 g cm^{-2} yr^{-1} for 1971–91 (*Serreze et al.*, 1995) as constrained from observed hydrologic budget (*Warren et al.*, 1999). The annual precipitation, averaged for 2007–09, is 15.5 g cm^{-2} yr^{-1} in GEOS-5, within the range of the observations. There are considerable uncertainties, spatially and temporally, in precipitation in the Arctic (*Warren et al.*, 1999; *Serreze and Hurst*, 2000). Fig. 2.6 compares monthly precipitation from the Global Precipitation Climatology Project (GPCP, *Huffman et al.*, 2001), NOAA Climate Prediction Center Merged Analysis of Precipitation (CMAP, *Xie and Arkin*, 1997), and GEOS-5. The discrepancies can be as large as a factor of 10 and the seasonal cycles are largely out of phase between the three datasets. Specifically, GPCP precipitation is much stronger than CMAP, particularly during summer. GEOS-5 precipitation is within the range of GPCP and CMAP data. The exception is Greenland, Ny-Ålesund, and Tromsø, where GEOS-5 precipitation is substantially (a factor of 2–10) larger than GPCP and CMAP data during the snow season. Snow in the Arctic is difficult to constrain for two reasons. First, accurate measurements of snowfall in the Arctic have proven nearly impossible, because snow

gauges strongly under-catch snowfall (by 55–75%) depending on the gauge type and wind condition (*Liston and Sturm*, 2004). Second, a more fundamental problem is that the sparse observational network in the Arctic is vastly inadequate to accurately estimate the monthly mean precipitation (*Serreze and Hurst*, 2000) – 10–40 stations are required in a 2.5° grid cell (WCRP, 1997).

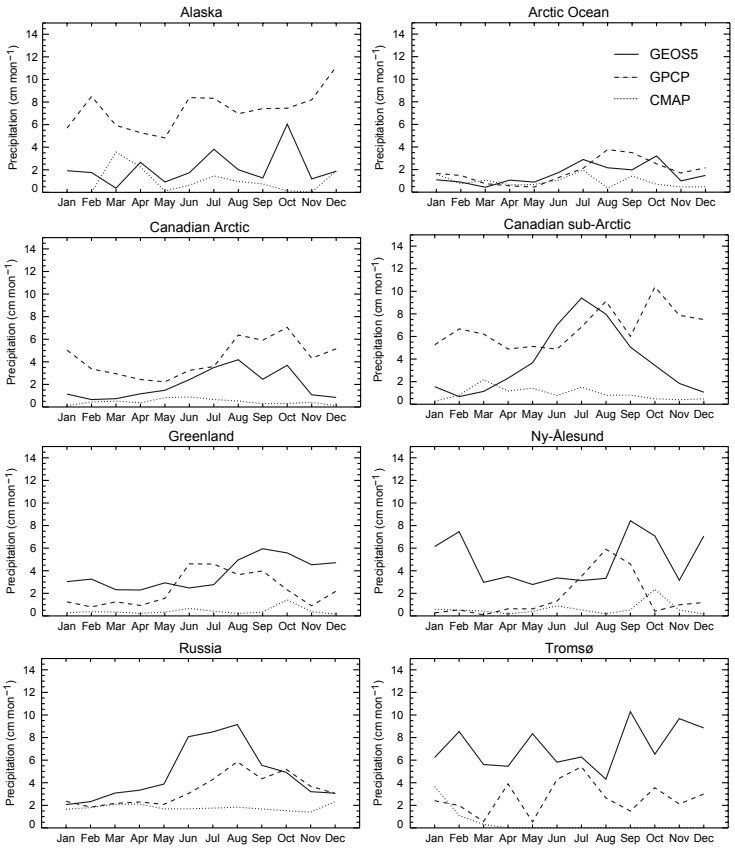

Figure 2.6: Monthly precipitation (cm month^{-1}) averaged over sub-regions in the Arctic for 2006–08 (Fig. 2.1). Data are from the Goddard Earth Observing System Model version 5 data assimilation system (GEOS-5 DAS), Global Precipitation Climatology Project (GPCP), and NOAA Climate Prediction Center Merged Analysis of Precipitation (CMAP).

To probe the sensitivity of BC deposition and BC_{snow} to precipitation, we conduct two additional model simulations, where we halve and double precipitation in the Arctic, with other processes configured as in Experiment D. We find that, in GEOS-5, during the snow

season, nearly all precipitation is in the form of snow in the Arctic. Halving precipitation leads to increases in BC_{snow} by 15–136%, with largest enhancements in Greenland (136%) and Ny-Ålesund (92%) (Fig. 2.7). With precipitation halved, it takes a longer accumulation time for a given snow depth, which results in larger dry deposition (up to 153% increases). As such, the ratio of BC dry deposition to snow precipitation increases as well. On the other hand, the ratio of BC wet deposition to snow precipitation, determined mainly by in-cloud scavenging of BC, remains largely unchanged. Overall, BC_{snow} increases with halved precipitation. It is conceivable that doubled precipitation has the opposite effect. Indeed, BC_{snow} decreases by 14–43% in the eight Arctic sub-regions. In addition, dry deposition decreases by 35–62% and the fraction of dry to total deposition decreases by 23–43%. Although BC_{snow} as computed here is sensitive to precipitation, the resulting medians of BC_{snow} in the eight sub-regions are in agreement with observations within a factor of two, except over Greenland (a factor of five too high) and Tromsø (a factor of three too high). Further analysis of the results at Greenland and Troms is in Sect. 2.4.5. The strong sensitivity of BC_{snow} calls for better constraining of precipitation in the Arctic.

In contrast, annual BC burden and deposition are much less sensitive to precipitation. Halving Arctic precipitation increases annual BC burden by 12% and decreases annual BC deposition by 16% in the Arctic. This is because less precipitation removes fewer BC particles. BC lifetime in the Arctic, as determined by the BC burden and deposition, increases by 27%. When precipitation is doubled, annual BC burden decreases by 14%, while BC deposition increases by 8%, resulting in a 23% reduction of BC lifetime in the Arctic.

BC_{air} is more sensitive to precipitation at Barrow, Alert and Zeppelin than at Denali and Summit (Fig. 2.8). When precipitation is halved, annual BC_{air} increases by 20–70% at Alert, by 10–40% at Barrow and Zeppelin, and by 1–20% at Denali and Summit. When precipitation is doubled, annual BC_{air} decreases by 20–50% at Alert, by 10–40% at Barrow and Zeppelin, and by 2–20% at Denali and Summit. Additionally, BC_{air} is more sensitive to precipitation in summer than in winter. This is because the summer clean boundary layer in

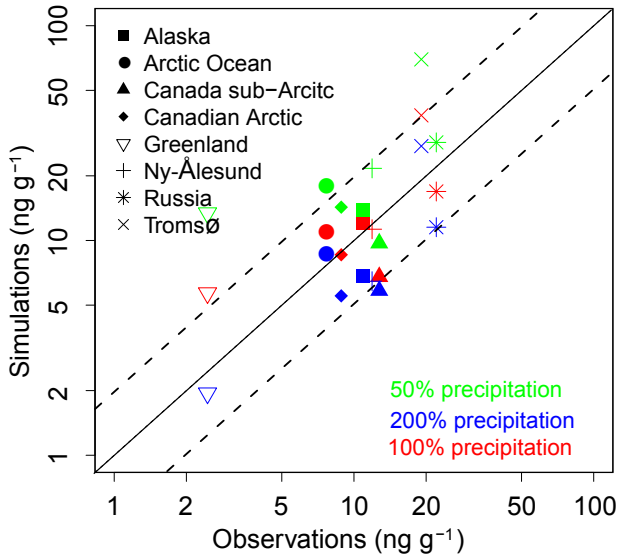

Figure 2.7: Same as Fig. 2.3, but for Exp. D with standard precipitation (red symbols), 50% precipitation (green symbols), and 200% precipitation (blue symbols). See text for details.

the Arctic is controlled by strong local scavenging (*Garrett et al.*, 2010, 2011; *Browse et al.*, 2012).

2.4.5 BC in snow in Greenland, Tromsø and Canadian sub-Arctic

BC_{snow} is associated with much larger uncertainties over short (hence shallower snow depth) than longer (hence larger snow depth) time periods. Because snow samples over Greenland were collected at the very surface (∼0 cm), the computed BC_{snow} thus represents BC deposition only through the duration of a day for direct comparisons. The short time duration thus largely explains the larger uncertainties in the estimated BC_{snow}. In Tromsø, observed BC_{snow} were considerably lower (19.1 ng g^{-1}) from samples collected over a clean mountain plateau upwind of town Tromsø(*Doherty et al.*, 2010) and much higher (53.3 ng g^{-1}) from samples collected in town (*Forsström et al.*, 2013). We use the former for comparisons. Thus, the factor of two overestimate of BC_{snow} in this region is because that GEOS-Chem does not

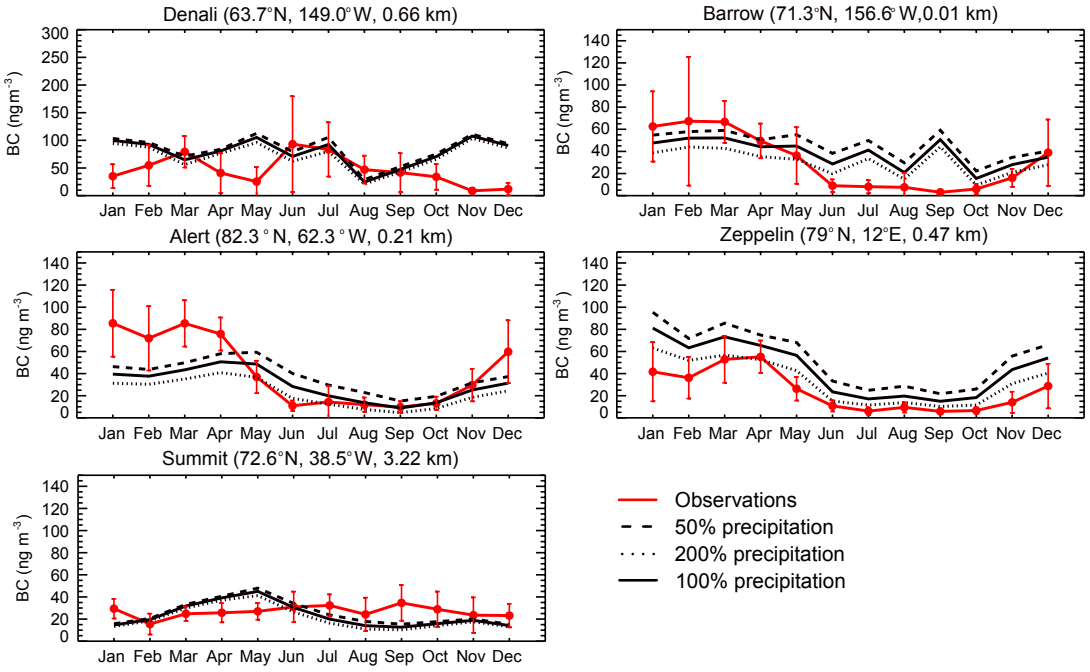

Figure 2.8: Same as Fig. 2.5, but for Exp. D with standard precipitation (solid black), 50% precipitation (dashed black), and 200% precipitation (dotted black). See text for details.

resolve sub-grid variability.

In the Canadian sub-Arctic, BC_{snow} is underestimated by 50% with all the improvements discussed above (Experiment D). This large low bias is mainly from the low BC_{snow} in the subsurface samples (1–20 cm, 11.7 ng g^{-1}, ~60% of all samples), accumulated through the snow season. BC_{snow} in this region increases by 33% from flaring emissions and by 43% from halving precipitation. Yet the resulting BC_{snow} is still 25% lower than observations (12.8 ng g^{-1}). However, GEOS-5 precipitation is at the lower end among the three precipitation datasets (Fig. 2.6). The large discrepancy in BC_{snow} warrants further studies.

2.5 Discussions

Global BC emissions in this study are within the range of previous studies, but emissions in the Arctic (0.115 Tg yr^{-1}) exceed the higher end of those used in previous studies (0.037–

0.077 Tg yr^{-1}, Table 2.6). The large Arctic emissions in this study result from gas flares, which have been missing in previous estimates. It has been suggested that gas flares are a dominant BC source in the Arctic – it is 41% of the total BC emissions in the Arctic, but a rather small fraction (3%) of the global BC emissions (*Stohl et al.*, 2013). Although this estimate is probably biased high because of the large emission factor (Sect. 2.4.1), it does not justify that we should exclude these emissions in modelling BC.

BC deposition in the Arctic (0.38 Tg yr^{-1}) exceeds the higher end of those used in previous studies (0.13–0.34 Tg yr^{-1}) with flaring emissions included (Table 2.6). Annual BC deposition is more sensitive to BC emissions and precipitation rate in the Arctic than v_d and WBF. Flaring emissions increases BC deposition flux in the Arctic by 19%. Doubling (halving) precipitation in the Arctic increases (decreases) BC deposition by 8% (18%). Total BC emissions in the Arctic is a factor of two to five lower than the total BC deposition, suggesting that a large fraction of BC deposited in the Arctic is from long-range transport.

Simulation of BC_{snow} in this study is much better than most of the AeroCom models in the perspective of mean model bias across the Arctic (Experiment D in this study: -0.8 ng g^{-1}; AeroCom models: -13.2 – +21.4 ng g^{-1}, Table 2.6) and the biases for the eight sub-regions (Experiment D in this study: a factor of 2; AeroCom estimates: a factor of 5–6, Jiao et al., 2014). In addition, the correlation coefficient of modelled and simulated BC_{snow} in this study (0.21) locates at the higher end of previous AeroCom estimates (0.12–0.24). We find that flaring emissions improve the agreement of BC_{snow} with observations significantly, with a 50% reduction to the negative bias of modeled BC_{snow} across the Arctic and a substantially stronger correlation (0.15 to 0.24) between simulated and observed BC_{snow} in the region (Table 2.6). WBF further reduces the average bias across the Arctic by 70%. Overall, modeled BC_{snow} is poorly correlated with observations (r = 0.15 to 0.24) for all AeroCom models and GEOS-Chem. This disagreement is probably resulted from a common problem in the Arctic, which is the poorly constrained meteorological fields including precipitation in the Arctic due to the scarcity of observations in the region (Sect. 2.4.4). Our model results

show that doubling (halving) precipitation introduces a much larger positive (negative) bias, similar as the magnitude of the overall effects of flaring emissions and the WBF effect (Sect. 2.4.4).

Table 2.6: Model simulations of BC in the Arctic (60°N to 90°N).

	Model	Global Emission[b] ($Tg\ yr^{-1}$)	Arctic Emission[b] ($Tg\ yr^{-1}$)	Arctic Deposition[b] ($Tg\ yr^{-1}$)	Arctic Loading[c] ($mg\ m^{-2}$)	Arctic Lifetime[d] (d)	BC_{snow} Bias[e] ($ng\ g^{-1}$)	BC_{snow} r [e]	Year of deposition field[b]
GEOS-Chem[a]	Experiment A	8.3	0.068	0.32	0.24	9.9	- 5.3	0.15*	2006-2009
	Experiment B	8.5	0.115	0.38	0.27	9.5	- 2.5	0.24*	2006-2009
	Experiment C	8.5	0.115	0.37	0.25	9.2	- 2.9	0.23*	2006-2009
	Experiment D	8.5	0.115	0.37	0.43	16.3	- 0.8	0.21*	2006-2009
	Exp. D_ 50% precip.	8.5	0.115	0.31	0.48	20.7	+5.8	0.22*	2006-2009
	Exp. D_200% precip.	8.5	0.115	0.40	0.37	12.6	-4.4	0.20*	2006-2009
AeroCom Phase I[f]		7.8	0.069	0.11-0.22	-	-	-13.2~-0.5[g]	0.11-0.28	-
AeroCom Phase II	HADGEM2	6.6	0.063	0.34	0.34	22.6	+ 18.7	0.18*	2006-2008
	GOCART	10.3	0.058	0.29	0.14	16.0	+ 7.3	0.04	2006
	OsloCTM2	7.8	0.068	0.28	0.07	6.9	+ 21.4	0.10*	2006
	GISS-modelE	7.6	0.077	0.22	0.16	11.6	+ 7.8	0.21*	2004-2008
	SPRINTARS	8.1	0.037	0.22	0.08	6.9	+ 5.3	0.06	2006
	CAM4-Oslo	10.6	0.056	0.21	0.20	22.7	- 0.2	0.12*	Present-day
	GMI	7.8	0.059	0.20	0.08	7.7	+ 1.9	0.10*	2006
	IMPACT	10.6	0.039	0.16	0.05	-	+ 3.8	0.18*	Present-day
	CAM5.1	7.8	0.056	0.13	0.02	-	- 13.0	0.23*	2006

[a]This study
[b]AeroCom model results are from Jiao *et al.* (2014).
[c]AeroCom models simulated Arctic Burdens are for year 2000 using only anthropogenic emissions from Samset *et al.* (2013)
[d]Lifetime is approximated by dividing the annual Arctic BC column burden by the annual Arctic deposition flux.
[e]BC snow concentrations were calculated using CLM4 and CICE4 models with monthly deposition field from AeroCom models (Jiao *et al.*, 2014).
[f]Paticipating models are DlR, GISS, LOA, LSCE, MATCH, MPI-HAM, TM5, UIO-CTM, UIO-GCM,UIO-GCM-V2, ULAQ, UMI, CAM-Oslo (Jiao *et al.*, 2014)
[g]This range is for the AeroCom Phase I models except for ULAQ, which is the only one produce a positive bias of +10.7 ng g^{-1}.
*The regression is significant at α=0.05

BC loading in the Arctic in this study exceeds the high end of the previous AeroCom estimates (0.02–0.34 mg m^{-2}) by including the WBF effect (Table 2.6). Previous studies attributed the large range of BC loading in the Arctic to differences in the aerosol processing and removal and atmospheric transport (*Eckhardt et al.*, 2015). We find that BC scavenging efficiency play a more important role on determining BC loading in the Arctic than emissions, v_d , and precipitation. BC loading in this region increases by 13% from flaring emissions, which represents a ∼70% enhancement to previous emission estimates, and by

7% from updated v_d , which in some cases are a factor of two to three larger. In addition, Arctic BC loading increases by 12% when precipitation is halved and decreases by 14% when precipitation is doubled. WBF reduces BC scavenging efficiency in mixed-phase clouds by 20–80% and increases annual BC loading by 70% in the Arctic. This large sensitivity of BC loading in the Arctic to treatments of BC scavenging efficiency in mixed-phase clouds and in ice clouds is also shown by previous studies. For example, *Bourgeois and Bey* (2011) reduced the scavenging efficiency in mixed-phase clouds from 0.10–0.75 to a uniform value of 0.06 in the ECHAM5-HAMMOZ model (*Pozzoli et al.*, 2008) and found that the resulting BC_{air} in the Arctic increased by up to a factor of ten and were in improved agreement with aircraft observations. In addition, their model results of BC burden in the Arctic were five times higher. We note here that a scavenging efficiency of 0.06 is on the low end of observed values in mixed-phase clouds (*Cozic et al.*, 2007; *Verheggen et al.*, 2007), which leads to a considerably larger WBF effect. *Liu et al.* (2011) found that lowering BC scavenging efficiency in ice clouds (from 0.2 to 0.01) in the AM3 model (*Anderson et al.*, 2004) dramatically enhanced BC transport to the Arctic (nearly 10 times higher) and improved model comparison with aircraft observations. *Browse et al.* (2012) suppressed the scavenging of soluble BC in ice clouds in the GLOMAP model (*Mann et al.*, 2010) and found that the resulting BC_{air} in the Arctic were six times higher. Better characterization of scavenging efficiency in all could types globally is thus critical for accurately reproducing BC distribution and the associated climatic effects in the Arctic.

2.6 Summary and conclusions

This study sought to understand the capability of GEOS-Chem in simulating BC distribution in the Arctic and the controlling factors of BC distribution. We evaluated the model simulation against BC_{snow} measurements across the Arctic and in-situ measurements of surface BC_{air} at Denali in lower Arctic, Barrow, Alert and Zeppelin in higher Arctic, and Summit in the free troposphere. We also examined the role of gas flaring emissions, dry deposition

velocity, the WBF effect, and precipitation on BC distribution in the Arctic.

We estimated the date of snow accumulation to the top and bottom depth of a snow sample and BC_{snow} was estimated as the ratio of mean BC deposition flux to precipitation flux between the two dates. The model underestimated BC_{snow} in the Arctic by ∼40%. Flaring emissions increased BC_{snow} by 0.1–8.5 ng g^{-1} in the eight Arctic sub-regions and decreased the discrepancy to -20% on average. Among the eight Arctic sub-regions, BC_{snow} over Greenland was not affected by flaring emissions, because the stable atmosphere during snow season in the Arctic strongly suppressed the vertical transport of BC to the upper troposphere (Stohl, 2006). With flaring emissions, BC_{snow} in Western Russia biased high by a factor of two, while BC_{snow} in Eastern Russia biased low by a factor of two. This discrepancy is likely due to excessive emission factors or missing of flare stack height. We call for extensive measurements of flaring emission factors in the Arctic.

Our analysis suggested that resistance-in-series method captures the large variations of dry deposition velocity over snow and ice surfaces from observations. The updated v_d (increases from 0.03–0.12 cm s^{-1} to 0.03–0.24 cm s^{-1} in the eight sub-regions) did not affect BC_{snow}, because higher dry deposition flux was compensated by lower wet deposition flux. The fraction of dry to total deposition increased from 15% to 26%. Thus, the radiative forcing induced by BC deposition in snow could decrease because of fewer internally mixed BC/snow composite. BC deposition in Ny-Ålesund decreased by ∼10% due to the reduced boundary layer transport from the proximate BC sources in Russia and Troms with updated v_d, which strongly increased the boundary layer deposition of BC in the two source regions. WBF enhanced BC_{snow} by 0.3–5.6 ng g^{-1} and further decreased the model discrepancy to -10% for the whole Arctic. In addition, WBF increased the fraction of dry to total deposition from 26% to 35%. BC_{snow} in Alaska and Canadian Arctic was most sensitive to the WBF effect, which increased BC_{snow} in the two regions by ∼50% and reduced the discrepancy to within 10%. With all above improvements, median BC_{snow} in the Arctic agreed with observations within 10%. In the eight sub-regions, BC_{snow} agreed with observations within a

factor of two. In addition, BC_{snow} was sensitive to precipitation as well. Halving (doubling) precipitation in the Arctic increased (decreased) BC_{snow} by 72–92% (15-36%).

BC_{air} in the Arctic was sensitive to flaring emissions, dry deposition velocity and the WBF effect in mixed-phase clouds. Gas flaring emissions increased BC_{air} in winter and spring by about ∼20 ng m^{-3} in the lower troposphere (Barrow, Alert and Zeppelin), while BC_{air} in the free troposphere (Summit) was not affected by flaring emissions. BC_{air} decreased by about ∼20 ng m^{-3} during snow season in high Arctic. WBF increased BC_{air} by ∼20 ng m^{-3} during snow season and offseted the decrease cause by increasing vd. However, WBF also increased BC_{air} during the transition period from winter haze to clean summer boundary layer and slows down the transition. This can be attributed to the missing of scavenging by boundary layer drizzle in late spring and summer in the Arctic (Browse et al., 2012). In addition, our scheme with the WBF effect did not capture the magnitude of BC_{air} at Barrow, Alert and Zeppelin, because it did not resolve the WBF-dominated (Barrow and Alert) and riming-dominated in-cloud scavenging (Zeppelin) properly.

BC loading and lifetime in the Arctic was very sensitive to the WBF effect. WBF reduced scavenging efficiency by up to 80% globally and increased BC loading in the Arctic from 0.25 mg m^{-2} to 0.43 mg m^{-2} and increased BC lifetime in the Arctic from ∼9 days to ∼16 days. However, the parameterization of the WBF effect in this study was based on observations at one single site in Europe in mid-latitudes, we need more observations of BC scavenging efficiency in the Arctic and in other mid-latitude regions to understand the BC-cloud interaction and constrain BC distribution.

Acknowledgements. This study was funded by NASA grant NNX14AF11G from the Atmospheric Chemistry Modeling and Analysis Program (ACMAP). The authors thank Y. Kondo, J. P. Schwarz, S. G. Warren, and H. Liu for helpful discussions. We would also like to thank the Global Monitoring Division at NOAA Earth System Research Laboratory, the Atmospheric Science and Technology Directorate at Environment Canada and SFT Norway for providing data. The Swedish Environmental Protection Agency and the Swedish Research

Council have sponsored BC measurements at Zeppelin. We would also like to thank 'Soot In Arctic Snow' group from University of Washington for providing measurements of BC concentration in snow in the Arctic.

CHAPTER 3

Effects of Wegener-Bergeron-Findeisen Process on Global Black Carbon Distribution

Abstract

In mixed-phase clouds, the Wegener-Bergeron-Findeisen (WBF) process (ice crystals may grow while water drops evaporate, thereby releasing black carbon (BC) particles into the interstitial air) slows down wet scavenging of BC and enhances BC_{air} (μg m^{-3}). Rimming (snowflakes fall and collect cloud water drops and the BC in them along their pathways), in contrast, results in more efficient wet scavenging of BC than WBF-dominated conditions in mixed-phase clouds. We systematically investigate the effects of WBF on BC scavenging efficiency, surface BC_{air}, deposition flux, concentration in snow (BC_{snow}, ng g^{-1}), and washout ratio using a global 3D chemical transport model (GEOS-Chem). We differentiate riming- versus WBF-dominated in-cloud scavenging based on liquid water content (LWC) and temperature. Specifically, we relate WBF to either temperature or ice mass fraction (IMF) in mixed-phase clouds. We find that at Jungfraujoch, Switzerland (46.5°N, 8°E, 3.85 km) and Abisko, Sweden (68.3°N, 18.8°E, 0.35 km), where WBF dominates, the discrepancies of simulated BC scavenging efficiency and washout ratio are significantly reduced (from a factor of 3 to 10% and from a factor of 4–5 to a factor of two). However, at Zeppelin, Norway (79.0°N, 12.0°E, 0.47 km), where riming dominates, simulation of BC scavenging efficiency, BCair, and washout ratio become worse (relative to observations) when WBF is included. There is thus an urgent need for extensive observations to distinguish and characterize riming- versus WBF-dominated aerosol scavenging in mixed-phase clouds and the

associated BC scavenging efficiency. We find the reduction resulting from WBF to global BC scavenging efficiency varies substantially, from 8% in the tropics to 76% in the Arctic. The resulting annual mean BC_{air} increases by up to 156% at high altitudes and at northern high latitudes because of lower temperature and higher IMF. Overall, WBF halves the model-observation discrepancy (from -65% to -30%) of BC_{air} across North America, Europe, China and the Arctic. Globally WBF increases BC burden from 0.22 to 0.29–0.35 mg m^{-2} yr^{-1}, which partially explains the gap between observed and previous model simulated BC burdens over land (*Bond et al.*, 2013). In addition, WBF significantly increases BC lifetime from 5.7 days to ∼8 days. Additionally, WBF results in a significant redistribution of BC deposition in source and remote regions. Specifically, it lowers BC wet deposition (by 37–63% at northern mid-latitudes and by 21–29% in the Arctic) while increases dry deposition (by 3–16% at mid-latitudes and by 81–159% in the Arctic). The resulting total BC deposition is lower at mid-latitudes (by 12–34%) but higher in the Arctic (by 2–29%). We find that WBF decreases BC_{snow} at mid-latitudes (by ∼15%) but increases it in the Arctic (by 26%) while improving model comparisons with observations. In addition, WBF dramatically reduces the model-observation discrepancy of washout ratios in winter (from a factor of 16 to 4). The remaining discrepancies in BC_{air}, BC_{snow} and BC washout ratios suggest that in-cloud removal in mixed-phased clouds is likely still excessive over land.

3.1 Introduction

BC effectively heats the atmosphere by absorbing solar radiation and has been regarded as the second largest warming agent after CO_2 (*Ramanathan and Carmichael*, 2008; *Bond et al.*, 2013) . Moreover, BC deposited on snow and ice reduces surface albedo and accelerates melting (*Flanner et al.*, 2007; *He et al.*, 2014a; *Liou et al.*, 2014). However, there are large uncertainties in estimating direct radiative forcing of BC, mainly arising from the uncertainties in predicting BC distribution (*Bond et al.*, 2013). Current Aerosol Comparisons between Observations and Models (AeroCom) underestimate aerosol absorption optical

depth (AAOD) of BC observed by AErosol RObotic NETwork (AERONET) and satellite by a factor of 1.6–4 (*Bond et al.*, 2013), but overestimates BC_{air} observed in remote Pacific by a factor of 2–5 (*Schwarz et al.*, 2010; *Wang et al.*, 2014b,c). Moreover, inter-model disagreement of BC loadings simulated by AeroCom models is up to two to three orders of magnitude (*Koch et al.*, 2009; *Bond et al.*, 2013). The large discrepancy with observations and large disagreement among models are primarily attributed to wet deposition, which is the dominant mechanism to remove BC from the atmosphere (*Textor et al.*, 2006; *Koch et al.*, 2009; *Bond et al.*, 2013) and consequently determines its lifetime and atmospheric burden. The major process of wet scavenging is in-cloud scavenging (*Taylor et al.*, 2014), which occurs in two stages: aerosol activation to form cloud droplets, and removal of droplets by precipitation. The ability of a particle to be activated as a cloud condensation nucleus (CCN) and thereby be scavenged by in-cloud scavenging depends on its hygroscopicity, size, and super-saturation in the cloud (*Ghan et al.*, 2011). The partition of BC particles between condensed phase and interstitial air in clouds is quantified by scavenging efficiency, which is defined as the ratio of aerosol mass mixing ratio in cloud drops and ice crystals to total aerosol mass mixing ratio in clouds (including aerosols in interstitial air and in cloud drops).

The determining factors controlling BC scavenging efficiency in clouds are the properties of BC particles, including their hygroscopicity, size, and chemical composition (*Sellegri et al.*, 2003; *Hallberg et al.*, 1992, 1994). Freshly emitted BC particles are small and generally hydrophobic (*Lammel and Novakov*, 1995; *Dusek et al.*, 2006; *Koehler et al.*, 2009; *McMeeking et al.*, 2011), which are less likely to serve as CCN and the scavenging efficiency is low (*Sellegri et al.*, 2003). When BC particles are aged (e.g., coated by hydrophilic species), both their hygroscopicity and size increase. These aged particles are more likely to become activated and serve as CCNs (*Wyslouzil et al.*, 1994; *Weingartner et al.*, 1997; *Zhang et al.*, 2008a), and the scavenging efficiency is considerably higher than freshly emitted particles. *Sellegri et al.* (2003) reported scavenging efficiencies of 0.39 ± 0.16 for BC aerosols with diameters less than 0.3 μm and hydrophilic material fractions less than 38%. The scavenging efficiency increased

to 0.97 ± 0.02 for particles with diameter larger than 0.3 μm and the fraction of hydrophilic material at 57% or higher. Previous studies have shown that scavenged BC fraction decreases with increasing BC content (*Hallberg et al.*, 1992, 1994; *Gieray et al.*, 1997). A large number of available CCNs may deplete the available water vapor more rapidly and decrease the super-saturation to below critical levels. As a result, the relative increase of the number of activated particles is smaller than that of the total number of particles, resulting in a lower scavenged fraction. However, other studies reported no such dependence (*Hitzenberger et al.*, 2000, 2001; *Kasper-Giebl et al.*, 2000). Additionally, LWC in clouds is another important factor that determines BC scavenging efficiency. That scavenged BC fraction increases with increasing LWC has been observed at several mountainous sites such as Mt. Jungfraujoch (*Cozic et al.*, 2007), Mt. Sonnblick (*Hitzenberger et al.*, 2000; *Kasper-Giebl et al.*, 2000) , and Mt. Rax (*Hitzenberger et al.*, 2001). Observations from Rax, Sonnblick, and Jungfraujoch showed an increase of BC scavenging efficiency up to a plateau of 0.6–0.8 for LWC at 0.3–0.4 g m^{-3}.

Local changes of updraft velocity and critical super-saturation significantly affect local BC scavenging efficiency. Such effects are also observed at long-time averages. In mixed-phase clouds, the effect of cloud microphysics on BC scavenging is considerably more complex. One complicating factor is the so-called WBF process (Wegener 1911; Bergeron 1935; Findeisen 1938), where water vapor transfers from liquid to ice phases when vapor pressure is between the saturation vapor pressure over ice and water droplets. WBF leads to evaporation of liquid cloud droplets and subsequent release of the aerosol materials in the droplets back into interstitial air, thus reducing the scavenging efficiency of aerosol particles in mixed-phase clouds. Measurements at Jungfraujoch confirmed such effects and showed that BC scavenging efficiency decreased with decreasing temperature and increasing IMF (*Cozic et al.*, 2007; *Verheggen et al.*, 2007). On average, BC scavenging efficiency decreased from 0.60 in warm clouds to 0.05–0.10 in mixed-phase clouds (*Cozic et al.*, 2007). Another process that affects BC scavenging in mixed-phase clouds is riming (*Hegg et al.*, 2011). Riming occurs

when LWC is high and gravitationally settling of snowflakes and ice crystals collect the water drops along their pathways thereby scavenge BC particles in the water drops. At Zeppelin, where snow particles show predominantly rimed structures, the scavenging efficiencies in summer (0.77) and in winter (0.81) agree within 5% (*Heintzenberg and Leck*, 1994).

BC scavenging efficiency is typically prescribed as a constant (between 0 and 1) in global chemical transport models (CTMs) for computational efficiency consideration and the limited understanding of the processes controlling the partition of BC between interstitial air and condensed phases in mixed-phase clouds (*Textor et al.*, 2006) . *Textor et al.* (2006) and *Wang et al.* (2011) treated BC scavenging in mixed-phase the same as in warm liquid clouds. *Stier et al.* (2005) used a scavenging efficiency of 0.40 for soluble Aitken mode aerosols and 0.75 for accumulation mode aerosols in mixed-phase clouds, lower (by 0.10) than their corresponding values in liquid-only clouds. *Bourgeois and Bey* (2011) used a substantially lower scavenging efficiency (0.06) for both Aitken and accumulation mode aerosols in mixed-phase clouds based on measurements from *Henning et al.* (2004). They found that the resulting BC burden in the Arctic increased by fivefold (from 0.75 Gg to 3.7 Gg) and BC lifetime increased by threefold (from 1.8 to 5.8 days). *Liu et al.* (2011) and *Browse et al.* (2012) also showed that BC loading and lifetime are both very sensitive to scavenging efficiency. It is clear that a systematic examination of BC scavenging efficiency and wet deposition is warranted. To that end, recent comprehensive large-scale measurements of BC_{snow} in North America (*Doherty et al.*, 2014a), China (*Huang et al.*, 2011; *Ye et al.*, 2012; *Wang et al.*, 2013, 2014d; *Zhang et al.*, 2013), and the Arctic (*Doherty et al.*, 2010) provide a unique opportunity. Concurrent measurements of BC in fresh snow and rain ($BC_{snow/rain}$) and BC_{air} (*Cerqueira et al.*, 2010; *Mori et al.*, 2014) provide better constraints on BC wet deposition.

BC scavenging efficiency varies as a function of BC aging in GEOS-Chem (*Park et al.*, 2005; *Wang et al.*, 2011). Specifically, in warm and mixed-phase clouds, hydrophilic BC particles are completely (100%) incorporated in cloud drops and serve as CCNs, while hydrophobic BC particles remain in interstitial air. In ice clouds, hydrophobic BC particles

serve as ice condensation nuclei while hydrophilic BC particles are not scavenged. In this study we investigate the effect of WBF on BC scavenging, its distribution in air and snow and budget using GEOS-Chem. Specifically, we distinguish riming- and WBF-dominated in-cloud scavenging in mixed-phase clouds and parameterize BC scavenging efficiency accordingly. We evaluate model results of BC scavenging efficiency (Sect. 3.4.1), BC_{air} (Sect. 3.4.2), BC wet deposition fluxes (Sect. 3.4.3), BCsnow (Sect. 3.4.4), and BC washout ratio (Sect. 3.4.5). We further discuss the WBF effects on global BC budget (Sect. 3.5), followed by conclusions and implications (Sect. 3.6).

3.2 Observations

Fig. 3.1 shows sites with measurements of BC scavenging efficiency, BC_{air}, BC_{snow}, and BC washout ratio in the Northern Hemisphere.

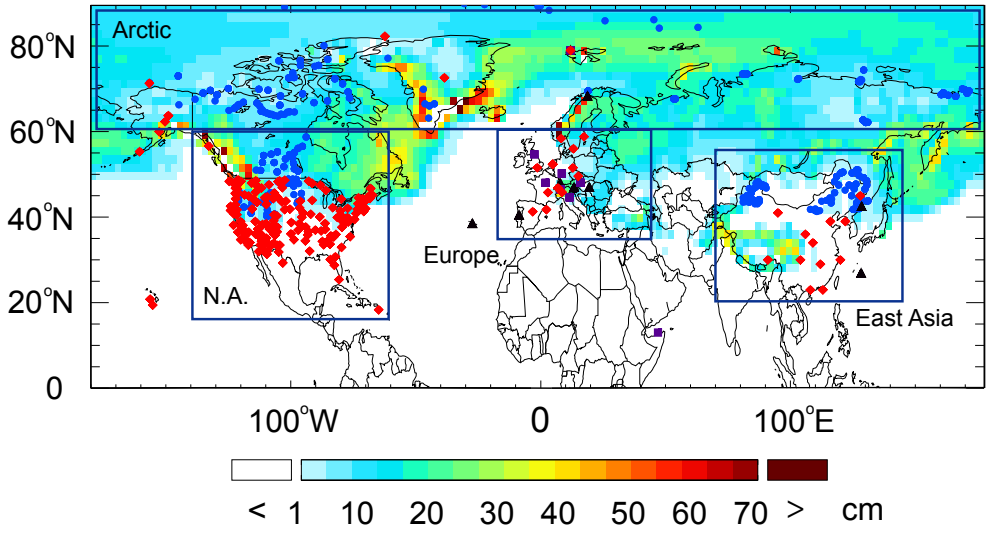

Figure 3.1: BC measurements used in this study: scavenging efficiencies (purple squares), concentration in air (red diamonds), concentration in snow (blue circles), washout ratio (black triangles), and average snow depth (cm) for 2006–12 (color contours).

3.2.1 BC Scavenging efficiency measurements

BC scavenging efficiencies in mixed-phase clouds are not well understood. In mixed-phase clouds, BC is partitioned between condensed phase (water drops and ice crystals) and interstitial air, which is crucial for accurate estimates of the in-cloud scavenging of BC. Following (*Hallberg et al.*, 1992) and references thereafter, the scavenging efficiency is defined as

$$r_{\text{scav.}} = \frac{[BC]_{\text{condensed}}}{[BC]_{\text{condensed}} + [BC]_{\text{interstitial}}}$$

where $r_{\text{scav.}}$ is BC scavenging efficiency, $[\text{BC}]_{\text{condensed}}$ the mass mixing ratio of BC in condensed phase, and $[\text{BC}]_{\text{interstitial}}$ the mass mixing ratio of BC in the interstitial air.

There are eight surface sites that reported measurements of BC scavenging efficiencies (Table 3.1 and Fig. 3.1). Cloud droplets and interstitial air were collected through different inlets. Cloud droplets were collected by a counterflow virtual impactor (CVI) (*Ogren et al.*, 1985). Interstitial air was sampled by impator-type collectors such as annular-slit impactor, round jet impactor, and mini-cascade impactor. Field calibration of the two inlets as well as theoretical consideration and laboratory calibration showed that the overall uncertainty of mass concentration of particles of the two phases in clouds was close to 15% (*Sellegri et al.*, 2003). The scavenged fraction was then computed from the comparison between cloud impactor samples and interstitial aerosols (*Hallberg et al.*, 1992, 1994; *Heintzenberg and Leck*, 1994; *Gieray et al.*, 1997; *Hitzenberger et al.*, 2000, 2001).

The observed BC scavenging efficiencies increase with increasing distance from source regions, from 0.06 in heavily polluted fog in Po Valley, Italy (44.6°N, 11.6°E, sea level) (*Hallberg et al.*, 1992) to 0.81 at Zepplin (79°N, 12°E, 0.47 km) in the Arctic (*Heintzenberg and Leck*, 1994) (Table 3.1). The observed scavenging efficiencies were vastly different at Po Valley, 0.06 from *Hallberg et al.* (1992) and 0.39 from *Gilardoni et al.* (2014). Reasons of

Table 3.1: Observed and GEOS-Chem simulated scavenging efficiency of BC (fraction of BC incorporated into cloud droplets and ice crystals).

Site	Observations	Model			Time	References
		Riming -only[a]	WBF_T[b]	WBF_{IMF}[c]		
Jungfraujoch (46.5°N, 8°E, 3.85 km)	0.60	0.90	0.59	0.48	Jul.-Aug. 2004	Cozic *et al.* (2007)
Jungfraujoch	0.05–0.10	0.29	0.11	0.10	Feb.-Mar. 2004	Cozic *et al.* (2007)
Puy de Dôme (48°N, 2°E, 1.46 km)	0.43±0.17	0.71	0.63	0.48	Feb.-Mar. 2001	Sellegri *et al.* (2003)
Zeppelin (79°N, 12°E, 0.47 km)	0.81	0.89	0.53	0.14	May.-Oct. 1990-1992	Heintzenberg and Leck (1994)
Zeppelin	0.77	0.41	0.11	0.03	Oct.-May. 1990-1992	Heintzenberg and Leck (1994)
Mt. Sonnblick (47°N, 13.4°E, 3.11 km)	0.74±0.19	0.67	0.26	0.10	Apr.-May. 1997	Hitzenberger *et al.* (2000)
Po Valley[*] (44.6°N, 11.6°E, 0 km)	0.06 (0.01–0.30)	–	–	–	Nov. 1989	Hallberg *et al.* (1992)
Po Valley[*]	0.39 (0.31–0.57)	0.55	0.53	0.46	Nov. 2011	Gilardoni *et al.* (2014)
Great Dun Fell (54.7°N, 2.5°W, 0.85 km)	0.50±0.20	0.61	0.59	0.46	Apr.-May. 1993	Gieray *et al.* (1997)
Rax (48°N, 16°E, 1.64 km)	0.54±0.25	0.70	0.64	0.35	Mar. 1999-Apr. 2000	Hitzenberger *et al.* (2001)

[*]Observations in urban fog.
[a]Simulation with riming only in-cloud scavenging of BC in mixed-phase clouds. See text for details.
[b]Simulation with in-cloud scavenging of BC by WBF, parameterized by temperature, in mixed-phase clouds. See text for details.
[c]Simulation with in-cloud scavenging of BC by WBF, parameterized by ice mass fraction, in mixed-phase clouds. See text for details.

the difference are unclear. Freshly emitted BC particles are mostly hydrophobic and cannot serve as CCN (*Weingartner et al.*, 1997). Hydrophobic BC particles mix with hydrophilic materials (e.g. sulfate, nitrate or soluble organics) during transit and become hydrophilic and larger in size (*Sellegri et al.*, 2003). The incorporation of BC particles into cloud droplets via nucleation scavenging is thus enhanced (*Moteki et al.*, 2012; *Taylor et al.*, 2014) . Both cloud dynamics (e.g. updraft velocity) and microphysics (nucleation, condensation and coagulation) complicate and determine the partition of BC particles between condensed phase and interstitial air in mixed-phase clouds (*Cozic et al.*, 2007). When riming occurs, large snow crystals collect cloud water drops along their pathways and BC particles in these cloud water drops are likewise removed (*Heintzenberg and Leck*, 1994; *Hegg et al.*, 2011). BC

scavenging efficiency due to riming is thus similar to that in warm clouds. For example, at Zeppelin, where the riming process was typically dominant, BC scavenging efficiencies in winter (0.77) (mostly mixed-phase clouds and ice clouds) and in summer (0.81) (mostly warm liquid clouds) were within 5% (*Heintzenberg and Leck*, 1994). In contrast, when the WBF process occurs, ice crystals grow at the expense of water droplets and hence BC particles inside the water droplets are released back into the interstitial air, thereby lowering in-cloud BC scavenging efficiency. The scavenging efficiency at Jungfraujoch (46.5°N, 8°E, 3.85 km), where the WBF process dominates in mixed-phase clouds, were higher in warm clouds (0.6) in summer and substantially lower in mixed-phase clouds (0.05–0.10) in spring.

Cozic et al. (2007) reported comprehensive observations of BC scavenging efficiency at Jungfraujoch, a site regularly engulfed by clouds (30% of the time) and far away from pollution sources. The site is well suited for investigating continental background aerosols and clouds from a ground based platform. *Cozic et al.* (2007) examined the partitioning of BC in mixed-phase clouds by sampling through two inlets, with one heated inlet collecting aerosols in cloud drops, ice crystals and the interstitial air and the other collecting only aerosols in the interstitial air. They found that the scavenging efficiency of BC was influenced by LWC, BC content, temperature and IMF. We use their results to parameterize the effect of WBF on BC scavenging efficiency in this study (See Sect. 3.3.2).

3.2.2 BC concentration in surface air

Surface BC_{air} have been widely measured across the Arctic, North America, Europe and Asia (Fig. 3.1). Observations in the Arctic are available at Denali, AK, Barrow, AK, Alert, Canada, Zeppelin, Norway, and Summit, Greenland (see details in Qi et al., 2016). We also use here measurements of BC_{air} at 178 sites as part of the Interagency Monitoring of PROtected Visual Environment (IMPROVE, Malm et al., 1994; http://vista.cira.colostate.edu/improve/) network in North America. IMPROVE measurements were made every three days and 24-hour averages were reported. Additionally, we use BC_{air} observations from East Asia in 2006

(*Zhang et al.*, 2008b). Observations of BC_{air} in Europe are from the European Monitoring and Evaluation Programme (EMEP) network (EMEP Status Report, 2014; http://ebas.nilu.no). We use here daily EMEP measurements.

Thermal Optical Reflectance (TOR) combustion method is used to measure BC concentrations by IMPROVE and EMEP network based on the preferential oxidation of organic carbon (OC) and elemental carbon (EC) at different temperatures (*Chow et al.*, 1993, 2004). Heating protocols used by IMPROVE network are as follows: The sample filter is heated stepwise at temperatures of 120°C (OC1), 250°C (OC2), 450°C (OC3), and 550°C (OC4) in a non-oxidizing (He) atmosphere, and at 550°C (EC1), 700°C (EC2), and 800°C (EC3) in an oxidizing atmosphere of 2% oxygen and 98% He. Evolved carbon is oxidized to CO_2, and then reduced to CH_4 for detection. The pyrolyzed or charred OC is monitored by reflectance at wavelength $\lambda = 633$ nm. The portion of EC1 until the laser signal returns to its initial value is assigned to pyrolyzed organic carbon (OP). EC is defined by EC1+EC2+EC3-OP. We use EC here to approximate the concentration of BC. EMEP use different protocols. Samples were heated either up to 850C (NIOSH), hence a fraction of EC may be combusted, or 650°C (EUSAAR˙2, Putaud, 2014). BC-like products of OC pyrolysis can lead to uncertainty in measuring BC mass. The uncertainty is estimated to be ∼20% (EMEP Status Report, 2014).

3.2.3 BC concentration in snow

We use BC_{snow} (ng g^{-1}) to constrain BC deposition on snow-covered surfaces. There is now a comprehensive set of BC_{snow} measurements, from sampling the full snowpack depth, in the Northern Hemisphere (Fig. 3.1): the Arctic (*Doherty et al.*, 2010), North America (*Doherty et al.*, 2014b), Northern China (*Wang et al.*, 2013), and Xinjiang, China (*Ye et al.*, 2012). For direct comparison with model results, we merge the observations in the same model grid cell. We exclude samples with obvious contamination from dust, soil, or local emissions as indicated in the observations. This leaves out a sample number of 334 from the Arctic,

158 from North America, 97 from Northern China, and 47 from Xinjiang, China. *Doherty et al.* (2014b) grouped samples in North America into four geographic regions based on land surface type and seasonal average snow water equivalent: Canada, the Great Plains, the Pacific Northwest, and the Intra-Mountain Northwest. Here we follow the same definitions. *Wang et al.* (2013) defined three sub-regions of Northern China: Inner Mongolia, Northeast Border, and Northeast industrial. We use the same definitions in this study. The overall uncertainty of the observed BC_{snow} is $< 60\%$ (see details in Chapter 2 Sect. **??**).

3.2.4 BC Washout ratio measurements

Washout ratio is a more easily measured parameter (compared to scavenging efficiency) that characterizes wet scavenging of BC. It is defined as the ratio of BC mass mixing ratio in fresh rain and snow to that in surface air following *Hegg et al.* (2011),

$$r_{\text{washout}} = \frac{[BC]_{\text{rain/snow}}}{[BC]_{\text{air}}}$$

where r_{washout} is the washout ratio, $[\text{BC}]_{\text{rain/snow}}$ the BC mass mixing ratio in fresh rain or snow, and $[\text{BC}]_{\text{air}}$ the BC mass mixing ratio in surface air. Washout ratio is an ambiguous metric for scavenging because it is rare that surface BC_{air} is representative of those at the altitude where BC aerosols are scavenged. On the other hand, washout ratio does subsume a number of individual processes such as in-cloud scavenging and below-cloud scavenging to give an estimate of an overall assignment (*Hegg et al.*, 2011). During snow season, washout ratio characterizes the riming- versus WBF-dominated snow process and BC scavenging in mixed-phase clouds. Washout ratio at Zeppelin, where snow particles show rimed structures, was $\sim$770 (*Hegg et al.*, 2011), indicating that BC particles are scavenged efficiently. While at Abisko and Changbai Mt., where pristine crystal snow particles formed mainly from the

WBF effect, washout ratio was ∼150, much less efficient than riming-dominated scavenging (*Noone and Clarke*, 1988; *Wang et al.*, 2014e). This is because BC particles in cloud drops were released back to the interstitial air and not subject to scavenging.

Fig. 3.1 shows nine remote sites (black triangles) with concurrent measurements of $BC_{rain/snow}$ and BC_{air} to estimate washout ratio. BC_{air} and $BC_{rain/snow}$ were measured at Cape Hedo (26.9°N, 128.3°E, 0.06 m) in East China Sea during 2011–13. BC_{air} was measured with an integration time of 1 min using a filter-based absorption photometer. The accuracy of this measurement has been estimated to be about 10% (*Mori et al.*, 2014). $BC_{rain/snow}$ was measured with a system based on an ultrasonic nebulizer, with an overall accuracy of about 25% (*Mori et al.*, 2014). BC_{air} and $BC_{rain/snow}$ were measured concurrently in Europe at two rural background sites Aveiro (40.5°N, 8.6°W, 0.05 km) and K-puszta, Hungary (47°N, 19.5°E, 0.2 km), and two Mt. sites Schauinsland, German (47.9°N, 7.9°E, 1.2 km) and Sonnblick, Austria (47°N, 13.4°E, 3.1 km) in 2002–04 (*Cerqueira et al.*, 2010). Sampling of rain and snow mainly focused on major precipitation events in order to collect large volumes over short-time periods. Samples were collected on an event basis with a stainless steel funnel connected to a pre-cleaned glass bottle. In order to minimize dry deposition of particles, the collector was deployed when rain started to fall and was removed immediately after filling or at the end of the event. $BC_{rain/snow}$ was measured by thermal-optical method described by *Castro et al.* (1999). Weekly air samples corresponding to the precipitation period were taken and BC_{air} were determined by thermal-optical method with the NIOSH protocol (*Pio et al.*, 2007).

At Mt. Changbai, China (42.5°N, 128.5°E, 0.74 km), LAVO, CA (40.5°N, 121°W, 1.73 km), Abisko, Sweden (68.3°N, 18.8°E, 0.35 km), and Zeppelin, Norway (79.0°N, 12.0°E, 0.47 km), observations were taken only in spring or winter (Table 3.2). At Mt. Changbai, snow samples were collected once per week during three winters in 2009–12 (*Wang et al.*, 2014e). BC_{snow} was measured using thermal-optical method with IMPROVE protocol and BC_{air} was determined using a particle soot absorption photometer (PSAP). At LAVO, seven

Table 3.2: Observed and GEOS-Chem simulated BC concentration in snow and rain (μg L^{-1}), BC concentration in surface air (μg m^{-3}) and the corresponding washout ratio.

Site		BC concentration		Washout ratio	Time	Reference
		Snow or rain ($\mu g\ L^{-1}$)	Surface air ($\mu g\ m^{-3}$)			
Mt. Changbai (42.5°N, 128.5°E, 0.74 km)	**Observations**			145	Nov.–Dec., Mar., 2009-12	Wang *et al.* (2012)
	Riming-only[a]	281	0.574	501		
	WBF_T[b]	232	0.603	403		
	WBF_{IMF}[c]	178	0.643	336		
LAVO (40.5°N, 121°W, 1.73 km)	**Observations**	4.2	0.024	229	Mar. 2006	Hadley *et al.* (2010)
	Riming-only	13.7	0.021	719		
	WBF_T	18.7	0.034	523		
	WBF_{IMF}	18.3	0.048	400		
Abisko (68.3°N, 18.8°E, 0.35 km)	**Observations**	2.4–77.1	0.03–0.93	94	Mar.–Apr. 1984	Noone and Clark (1988)
	Riming-only	13.3	0.031	482		
	WBF_T	10.0	0.051	203		
	WBF_{IMF}	7.5	0.072	96		
Zeppelin (79.0°N, 12.0°E, 0.47 km)	**Observations**	13.9	0.030	769	Mar.–Apr. 2007	Hegg *et al.* (2011)
	Riming-only	6.1	0.019	444		
	WBF_T	4.9	0.041	109		
	WBF_{IMF}	4.4	0.063	62		

precipitation samples were collected in March 2006 using an automated rain sampler EcoTech with up to 95% capture efficiency (*Hadley et al.*, 2010). BC_{rain} was measured by a modified version of thermo-optical analysis described in detail in (*Hadley et al.*, 2008). BC_{air} was measured by 7-wavelength aethalometer with an overall uncertainty of about $\pm$30%.

At Abisko, snow samples were taken in March and April in 1984 (*Noone and Clarke*, 1988). Snow samples were taken using a plastic spatula to crape fresh snow into pylyethylene jars and transport back to the laboratory. The snow was transferred to a filtration apparatus where it was melted and filtered. The amount of BC on the filters was determined by optical analysis. The air samples were measured using the integrating sandwich

technique. At Zeppelin, BC_{snow} and BC_{air} was measured concurrently in April and May 2007. BC_{snow} was concentrated by nuclepore filters and then determined using a multiwavelength spectrophotometer. Aerosol absorption is measured by PSAP and BC_{air} is computed using a mass absorption cross-section of 11 m^2 g^{-1} at 550 nm (*Hegg et al.*, 2011).

3.3 Model description and simulations

3.3.1 Model description

GEOS-Chem is a 3D global chemical transport model driven with assimilated meteorology from the Goddard Earth Observing System (GEOS) of the NASA Global Modeling and Assimilation Office (GMAO). GEOS-5 meteorological dataset are used to drive model simulation at 2° latitude × 2.5° longitude resolution with 47 vertical layers. BC aerosols are emitted by incomplete combustion of fossil fuel, biofuel and biomass. Global anthropogenic emissions from *Bond et al.* (2007) are used with Asian emissions from *Zhang et al.* (2009b). Previously missed gas flaring emissions are also included in this study (*Stohl et al.*, 2013, The flaring emission inventory is available at: http://eclipse.nilu.no/). Biomass burning emissions are from GFED3 emission inventory with small fire contribution included (*Randerson et al.*, 2012). About 80% of the freshly emitted BC aerosols are assumed to be hydrophobic (*Park et al.*, 2003) and are converted to hydrophilic with an e-folding time of 1.15 days which yields a good simulation of BC export efficiency in continental outflow (*Park et al.*, 2005). Dry deposition of BC is computed using a resistance-in-series method over all surface types (*Wesely*, 1989; *Zhang et al.*, 2001). Due to the lack of land surface module in GEOS-Chem, we approximate BCsnow using BC deposition flux and snow precipitation rate, following *He et al.* (2014b). More details are provided in Qi et al. (2016).

3.3.2 Wet scavenging

Aerosol wet deposition in GEOS-Chem was first described by *Liu et al.* (2001). It includes rainout (in-cloud) and washout (below-cloud) scavenging in large-scale and convective precipitation. Rainout rate is parameterized following *Giorgi and Chameides* (1986),

$$\phi = -\lambda [BC]_{\text{condensed}}$$

where ϕ is rainout rate, λ the removal frequency determined by precipitation forming rate, and $[\text{BC}]_{\text{condensed}}$ BC mass mixing ratio in condensed phase, including cloud water drops and ice crystals. $[\text{BC}]_{\text{condensed}}$ is estimated as

$$[BC]_{\text{condensed}} = [BC]_{\text{total}} \times r_{\text{scav.}}$$

where $[\text{BC}]_{\text{total}}$ is BC mass mixing ratio in clouds, including BC in interstitial air and in condensed phase, and $r_{\text{scav.}}$ the BC scavenging efficiency. We assume hydrophilic BC particles are 100% incorporated in condensed phases, while hydrophobic BC particles remain in interstitial air in both warm and mixed-phase clouds (*Wang et al.*, 2011). The scavenging efficiency is thus the fraction of hydrophilic BC to total BC, which is determined by the initial fraction when aerosols are emitted and the following aging process during transport. We assume that 80% of BC are emitted as hydrophobic (*Cooke et al.*, 1999; *Park et al.*, 2003) and converted to hydrophilic with an e-folding time of 1.15 day (*Park et al.*, 2005). In ice clouds, only hydrophobic BC can serve as ice nuclei (*Andreae and Rosenfeld*, 2008), and the resulting scavenging efficiency is the fraction of hydrophobic BC to total BC. In this wet scavenging scheme, BC scavenging in mixed-phase clouds are treated as that in warm liquid clouds. The underlying assumption is that riming is the dominant process in mixed-phase clouds. We use this setting in Experiment Riming-only.

In convective clouds, rapid updrafts bring water vapor to the middle and upper parts of the clouds and subsequently suppress the WBF process (*Liu et al.*, 2011). In large-scale mixed-phase clouds, cloud microphysics, which determines the rates of riming versus WBF, play a very important role in determining BC scavenging efficiency. Here we distinguish riming- versus WBF-dominated conditions and parameterize BC scavenging efficiencies under these two conditions. Following *Fukuta and Takahashi* (1999), we assume riming dominates when temperature is between 261–265 K and LWC > 1.0 g m^{-3}. *Fukuta and Takahashi* (1999) found that the terminal velocity of snow particles was largest at 263 K and that large LWC provided more water drops for the falling snow particles to collect along their pathways. In this condition, 100% hydrophilic BC particles are incorporated in condensed phase and hydrophobic BC aerosols stay in the interstitial air. The BC scavenging efficiency is simply the fraction of hydrophilic BC to total BC. We assume that WBF dominates under other conditions (258–261 K and 265–273 K), following *Cozic et al.* (2007). Under WBF-dominated conditions at Jungfraujoch, BC scavenging efficiency was found to decrease with decreasing temperature and increasing IMF (*Cozic et al.*, 2007). In Experiment WBFT, BC scavenging efficiency is exponentially related to temperature (*Cozic et al.*, 2007).

$$r_{\text{scav.}} = 0.03 + \frac{0.066}{1 + \frac{exp(-T+9.32)}{6.77}}$$

In Experiment WBF$_{\text{IMF}}$, BC scavenging efficiency is computed using IMF (*Cozic et al.*, 2007).

$$r_{\text{scav.}} = 0.05 + 0.92exp(-8.95\sqrt{IMF})$$

3.4 Results and discussions

The primary goal of this study is to assess the impact of WBF on global BC distribution. In this section, we compare BC distribution from GEOS-Chem with and without WBF (Sect. 3.3.2). The differences can then be attributed to the WBF effect. We present the comparison of BC scavenging efficiency in Sect. 3.4.1. In Sect. 3.4.2, we show how WBF affects BC_{air}. Following this, we present the comparison of BC wet deposition fluxes (Sect. 3.4.3) and BC_{snow} (Sect. 3.4.4). Finally, we show the effect of WBF on BC washout ratio.

3.4.1 BC scavenging efficiency

3.4.1.1 Comparison to observations

WBF improves the simulation of BC scavenging efficiency at sites where mixed-phase clouds are frequent and WBF dominates in-cloud scavenging, for example, Jungfraujoch and Puy de *Dôme* (*Cozic et al.*, 2007) (Table 3.1). At Jungfraujoch, WBF reduces BC scavenging efficiency both in summer (July–August, from 0.90 to 0.48–0.59) and in late winter and early spring (Feburary–March, from 0.29 to 0.10–0.11) and significantly reduces model-observation discrepancies (50% to -20–0% in summer and from a factor of three to 10% in late winter and early spring). At Puy de *Dôme*, WBF brings the simulated BC scavenging efficiency (0.48 for WBF_{IMF} and 0.63 for WBF_{T}) within the uncertainty range of observations (0.43 $\pm$0.17).

However, at sites where riming dominates in-cloud scavenging in mixed-phase clouds, for instance, Zeppelin (*Hegg et al.*, 2011), accounting for WBF leads to scavenging efficiencies considerably lower than observations (Table 3.1). Riming-only reproduces the observed high scavenging efficiencies (0.81 in summer and 0.77 in winter) at Zeppelin to within 50%. Similarly, at Mt. Sonnblick, an elevated site (3.10 km), the simulated scavenging efficiency with rimming-only (0.67) agrees with the observed values (0.74 $\pm$ 0.19) within 10% in April and May. WBF strongly reduces BC scavenging efficiency (0.09–0.26) at the site.

At lower altitudes, where temperature is higher and mixed-phase clouds are less frequent, WBF has relatively weak effect, for example, at Po Valley and Great Dun Fell (Table 3.1). At Po Valley, the measurements were in fog. We use BC scavenging efficiency of the lowest clouds in GEOS-Chem for comparison. All three model results, riming-only, $\mathrm{WBF_T}$, and $\mathrm{WBF_{IMF}}$, agree with the observations (0.39) to within 20–60%. At Mt. Great Dun Fell, WBF reduces BC scavenging efficiency by less than 25%.

To sum up, differentiating riming- versus WBF-dominated in-cloud scavenging in mixed-phase clouds improves the comparison at sites where WBF dominates but degrades the comparison at sites where riming dominates. We attribute the discrepancy to several reasons. First, WBF is parameterized based on observations at a single site (Sect. 3.3.2). Extrapolating it to global scale may introduce large uncertainties. Second, LWC, a key parameter that separates the two conditions (Sect. 3.3.2), is biased high and associated with large spatial discrepancies in GEOS-5 reanalysis (*Li et al.*, 2012; *Barahona et al.*, 2014). Third, this separation is based on a lab experiment (*Fukuta and Takahashi*, 1999), while conditions in the real atmosphere are certainly more complex. This calls for more extensive measurements of BC scavenging efficiency in mixed-phase clouds to better understand the scavenging processes.

In addition to the uncertainties in differentiating riming- versus WBF-dominated in-cloud scavenging in mixed-phase clouds, uncertainties associated with other processes that determine the hygroscopicity of BC particles also affect scavenging efficiency. Hygroscopicity of BC particles is determined by the mixing state of hydrophobic BC particles with other hydrophilic materials (*Sellegri et al.*, 2003). In this study, we assume 80% of freshly emitted BC particles are hydrophobic and externally mixed with co-emitted hydrophilic particles (*Cooke et al.*, 1999). However, field observations show that the fraction systematically differs among urban plumes (∼10%) and biomass burning plumes (∼70%) (*Schwarz et al.*, 2008). The simple assumption of 80% hydrophobic BC for all sources thus carries uncertainties for BC scavenging efficiency. Moreover, we assume hydrophobic BC particles are converted to

hydrophilic with an e-folding time of 1.15 days (*Park et al.*, 2005). However, the conversion is much faster (a few hours) in source regions where the concentration of hydrophilic materials is high, while the conversion is much slower in remote regions (a few days) (*He et al.*, 2015). So the uniform conversion rate used in this study might underestimate the scavenging efficiency near source regions. In addition, faster conversion from hydrophobic to hydrophilic near sources might cause more hydrophilic BC particles to be scavenged near sources and thus alter the scavenging efficiency at remote regions.

3.4.1.2 Seasonal variations of BC scavenging efficiency

Fig. 3.2 shows model simulated monthly mean BC scavenging efficiencies in the Arctic, the northern mid-latitudes, and the tropics at 0–2 km, 2–5 km, and 5–10 km altitudes. The values are averaged for 2007–09. BC scavenging efficiencies in the Arctic show strong seasonal cycle below 5 km. If only riming process in mixed-phase clouds is considered (Experiment Riming-only), BC scavenging efficiency is determined exclusively by its hygroscopicity (*Wang et al.*, 2011). We find that more than 90% of BC particles in the Arctic are hydrophilic. In warm and mixed-phase clouds, hydrophilic BC particles serve as CCNs and are incorporated in cloud water drops, while hydrophobic BC particles remain in the atmosphere (*Wang et al.*, 2011). Fig. 3.2 shows that in the middle and lower troposphere (< 5 km), where most clouds are warm and mixed-phase in summer, BC scavenging efficiency is approximately the ratio of hydrophilic to total BC (0.80–0.90). In ice clouds, hydrophobic BC particles serve as ice nuclei and are removed with the falling snowflakes, while scavenging of hydrophilic BC particles are suppressed completely (*Wang et al.*, 2011). Consequently, when ice clouds dominate in most of the wintertime, BC scavenging efficiency is around the ratio of hydrophobic to total BC ($\sim$0.10). WBF reduces BC scavenging efficiency by 22–69% in summer and by 63–85% in winter. In the upper troposphere (> 5 km), where ice clouds dominate year round, BC scavenging efficiency likewise is around the ratio of hydrophobic to total BC ($\sim$0.1) and shows little to no seasonal variation.

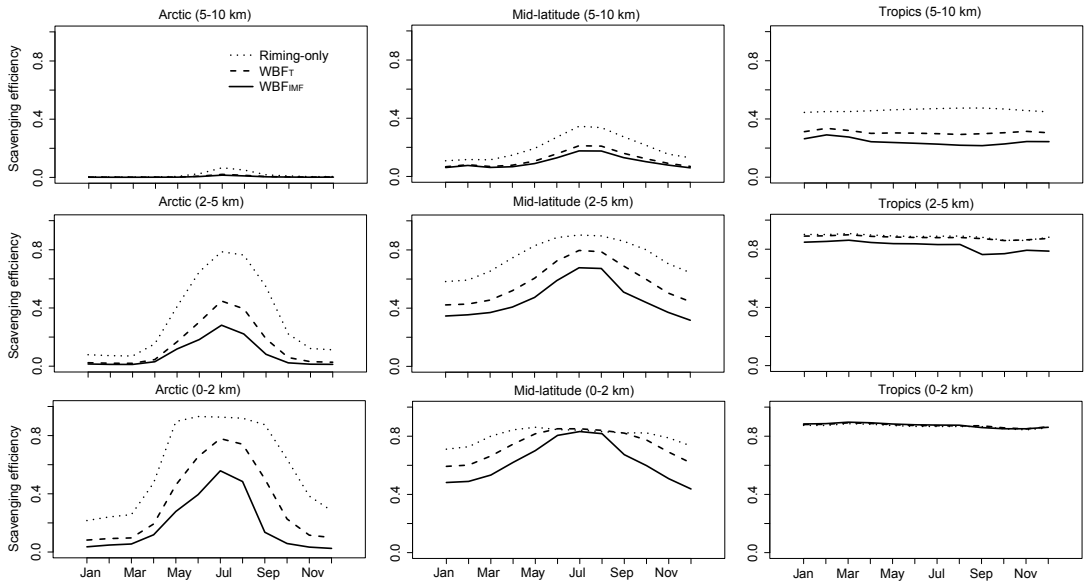

Figure 3.2: GEOS-Chem simulated monthly mean BC scavenging efficiency in the Arctic (60–90°N), mid-latitudes (20–60°N) and the tropics (0–20°N) in the boundary layer (0–2 km), the lower troposphere (2–5 km) and the middle to upper troposphere (5–10 km). Results are averages for 2007–09.

In the northern mid-latitudes, seasonal cycle of BC scavenging efficiency is weaker than that in the Arctic–the value in winter is much higher (0.4–0.6) in the mid-latitudes as a result of higher temperature and lower frequency of pure ice clouds (Zhang et al., 2010). WBF reduces BC scavenging efficiency by 17–44% in winter in the troposphere. The effect is relatively weaker than that in the Arctic (63–85% reduction). In addition, the WBF effect increases with increasing altitude (from 0 at surface to 39–50% in the upper troposphere), different from that in the Arctic.

In the tropics, the seasonal cycle of BC scavenging efficiency disappears in the lower troposphere in all three model experiments, for two reasons. First, temperature is high throughout the year and clouds are mostly warm clouds. Second, most of the tropical clouds are convective where strong updrafts suppress WBF by bringing abundant water vapor to the clouds (*Liu et al.*, 2011). However, in the tropical upper troposphere, WBF reduces BC

scavenging efficiency by 33–47% because the frequency of mixed-phase clouds is higher than that in the middle and lower troposphere.

3.4.2 BC concentration in air

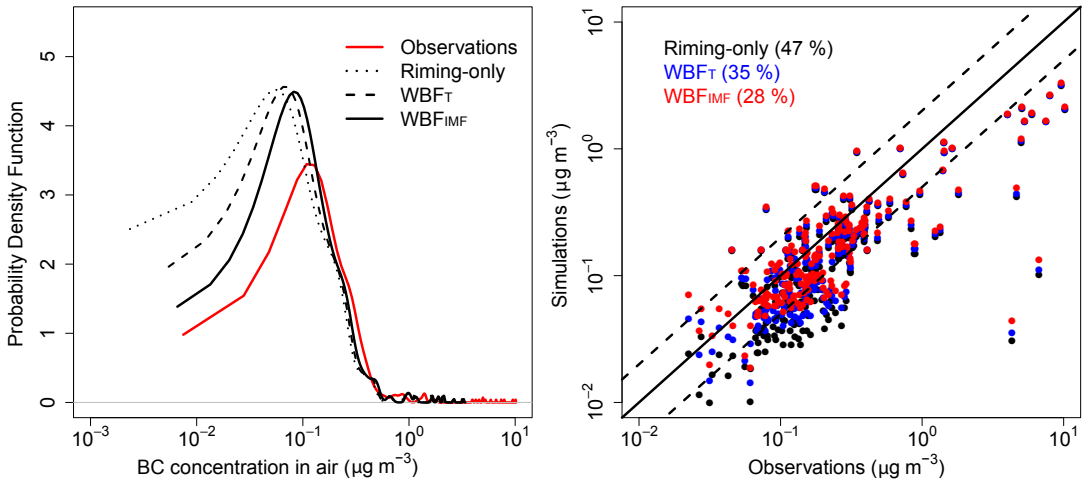

Figure 3.3: (Left panel) Probability density function of observed (red line) and GEOS-Chem simulated (dotted: riming; dashed: WBF_T; solid black: WBF_{IMF}) annual mean BC concentration in air (μg m^{-3}) and (right panel) observed and simulated annual BC concentrations (black: riming; blue: WBF_T; red: WBF_{IMF}; the percentage of annual BC concentrations locate outside the 1:2 and 2:1 lines are in parentheses; Solid line – 1:1 ratio line, dashed lines – 1:2 (or 2:1) ratio lines). Data are for 2007–09. See text for details.

GEOS-Chem captures the probability density function (PDF) of annual BCair at sites from IMPROVE and EMEP and in China and the Arctic (Sect. 3.2.2), but overestimates the frequency of low BC_{air} (Experiment Riming-only) (Fig. 3.3, left panel). WBF releases BC in cloud water droplets back to the interstitial air and thus reduces BC scavenging efficiency and leaves more BC particles in the atmosphere (Sect. 3.4.1). As such, WBF increases BC_{air} and improves the comparison with observations, particularly for the low values (Fig. 3.3, left panel). WBF reduces the fraction of simulated BC_{air} that are underestimated by more than a factor of two (from 47% to 28–35%) (Fig. 3.3, right panel). The largest improvements are

at remote and elevated sites. We use a ratio r to quantify the effect of WBF on BC_{air},

$$r = \frac{[BC]_{\text{WBF}} - [BC]_{\text{riming-only}}}{BC]_{\text{riming-only}}}$$

where r is a fraction that describe the simulated changes in BC_{air} with WBF parameterizations relative to that with riming-only, $[BC]_{WBF}$ and $[BC]_{riming\text{-}only}$ are simulated BC_{air} with and without WBF at the measurement stations (Sect. 3.2.2). The fraction r is much larger in the Arctic (62–140%) than in the northern mid-latitudes (0–40%) (Fig. 3.4, left panel) for several reasons. First, the frequency of mixed-phase clouds is higher in the Arctic (41–90% from spring to fall) than in the mid-latitudes (∼20%) (*Pinto*, 1998; *Shupe et al.*, 2006; *Zhang et al.*, 2010; *Morrison et al.*, 2012). Second, lower temperature and higher IMF in the Arctic result in a stronger WBF effect. Third, WBF increases BC_{air} in the mid-latitudes and consequently the polar-ward transport of BC. In addition, WBF increases BC_{air} substantially in winter and spring and hence delays the transition of high BC_{air} in winter to low BC_{air} in summer (Qi et al., 2016).

We find that r increases with increasing altitude from surface (6–12%) to ∼4 km (45–95%) (Fig. 3.4, right panel). This is because as altitude increases, temperature decreases and IMF increases, resulting in a stronger WBF effect and thus larger reductions of BC scavenging efficiency in the mid-latitudes (Fig. 3.2). As a result, less BC is scavenged and more BC particles remain in the atmosphere. Fig. 3.5 shows IMPROVE and GEOS-Chem simulated monthly mean BC_{air}. In summer, model underestimates BC_{air} by 46–72%. WBF increases BC_{air} and reduces the discrepancy to 35–58% (by 5–55%) from the surface to ∼4 km. The relative change of BC_{air} increases from surface (6–22%) to above 3 km (21–78%). The largest discrepancy (54–58%) is at 1.5–3 km, where the influence of fire emissions is significantly underestimated (*Mao et al.*, 2011, 2014). BC_{air} is strongly underestimated in winter as well and the discrepancy increases monotonically with increasing altitude from

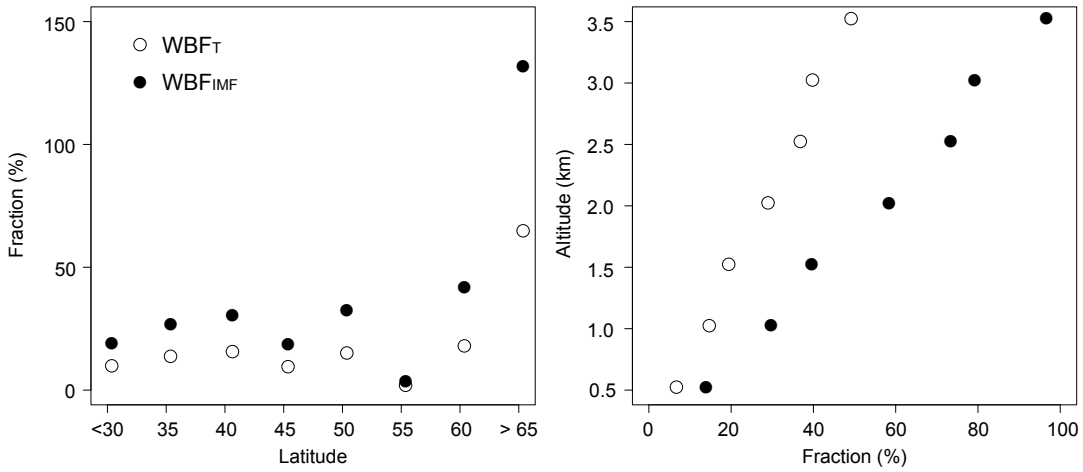

Figure 3.4: GESO-Chem simulated fractional change to BC concentration, relative to riming-only, as a result of WBF, ($[BC]_{WBF}$ - $[BC]_{riming}$) / $[BC]_{riming}$ that varies with (left panel) altitude and (right panel) latitude, averaged for 2007–09.

∼10% at the surface to ∼70% above 2.5 km in winter. WBF increases BC_{air} monotonically from 5% at the surface to 80–156% above 2.5 km, reducing the discrepancy to within 30%, particularly at higher altitudes. Above 2.5 km, the discrepancy of BC_{air} decreases from 67–70% to 15–20%. Cloud observations show not much riming or graupel snow particles and simulations over Montana and Nebraska in October–November suggest that rate of WBF is significantly larger than that of riming (*Smith et al.*, 2009; *Niu et al.*, 2008). WBF has little effect on BC_{air} at sites in the lower troposphere in East Asia and Europe, where temperature is high and mixed-phase clouds rarely occur.

3.4.3 BC wet deposition fluxes

Table 3.3 shows observed and GEOS-Chem simulated annual BC wet deposition fluxes. GEOS-Chem captures the high deposition flux at Cape Hedo in East China Sea (52.5 mg m^{-2} yr^{-1}) and the low deposition flux (5.0 mg m^{-2} yr^{-1}) at Azores (within 40%). Cape Hedo receives outflow of East Asia (*Mori et al.*, 2014), while Azores is mainly affected by clean marine air (*Cerqueira et al.*, 2010). Wet deposition fluxes at Schauinsland and Sonnblick

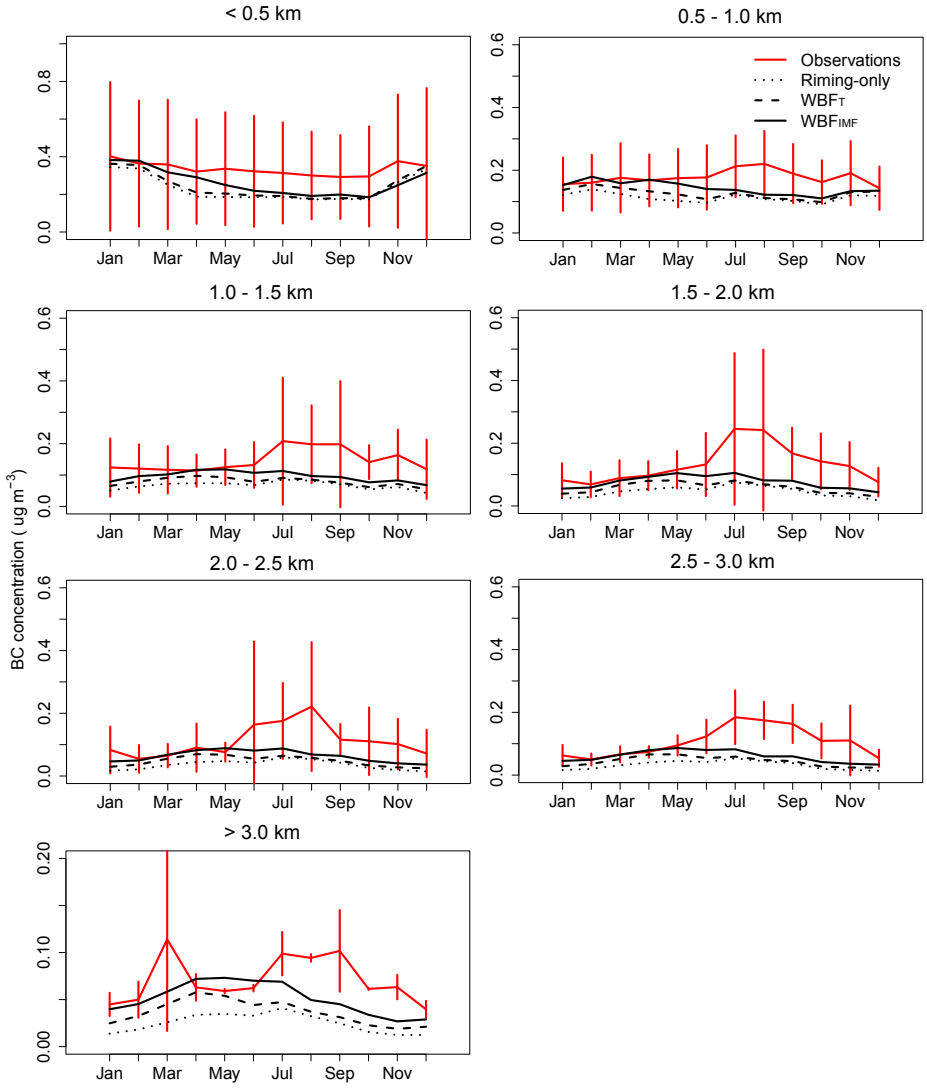

Figure 3.5: IMPROVE observed (red solid line) and GEOS-Chem simulated (dotted: riming-only; dashed: WBF_T; solid black: WBF_{IMF}) seasonal variation of monthly mean BC concentrations (μg m^{-3}) for 2007–09. Also shown are standard deviations of observations (error bars).

are underestimated by ∼50%. One possible reason is the underestimated precipitation at the two sites. In contrast, at K-puszta and Sakaerat, BC wet deposition fluxes are overestimated by a factor of 2–5. At K-puszta, BC in precipitation is overestimated, while BC_{air} is underestimated (Sect. 3.4.4), indicating that wet scavenging is too strong during transit to the site. At Sakaerat, wet deposition is overestimated by a factor of five.

WBF has opposite effects on BC wet deposition fluxes near source regions over land and in remote regions over ocean. Over land, WBF reduces annual wet deposition fluxes by ∼15% at Schauinsland, Sonnblick and K-puszta. This is because of reduced BC scavenging efficiency (5–45%). The largest effect of WBF is at Mt. Changbai, where WBF reduces BC wet deposition flux (November–April) by 45–66% (from 53.8 to 18.1–29.7 mg m^{-2}), reducing the discrepancy from +84% to -40–0%. In contrast, WBF increases wet deposition fluxes at oceanic sites Cape Hedo and Azores and costal site Aveiro by 8–50%, even with a lower local scavenging efficiency (7–20% reduction at the oceanic sites). We find that the increase of wet deposition fluxes is mainly from enhanced outflow from polluted land regions as a result of WBF. In the tropics, WBF has minimal effect on wet deposition flux ($< 1\%$), for example, at Sakaerat, because temperature at the site is above freezing throughout the year and mixed-phase clouds are very rare.

3.4.4 BC concentration in snow

Fig. 3.6 (left panel) presents the PDF of observed and GEOS-Chem simulated BC_{snow} in the Northern Hemisphere (Sect. 3.2.3). Observed BCsnow shows a lognormal distribution and varies by three orders of magnitude from a minimum of 1.8 ng g^{-1} in the Arctic to a maximum of 4758 ng g^{-1} in Northern China. The model (Experiment Riming-only) underestimates the frequency of BC_{snow} at 8–80 ng g^{-1}, while overestimates the frequency outside the range. More importantly, the observations have a single maximum but the model shows a bimodal structure. WBF significantly improves the agreement between observed and simulated distribution by increasing the frequency of BC_{snow} at 8–80 ng g^{-1}, resulting in a single

Table 3.3: Observed and simulated precipitation (cm) and BC wet deposition fluxes (mg m^{-2} yr^{-1}).

		Precipitation (cm)		BC wet deposition fluxes (mg m^{-2} yr^{-1})			
					Model		
		Observations	GEOS-5	Observations	Riming-only	WBF_T	WBF_{IMF}
Continental	Schauinsland (47.9°N, 7.9°E, 1.20 km)	157.4	81	38	21.2	20.4	18.3
	Sonnblick (47°N, 13.4°E, 3.11 km)	208.2	104.1	10	6.1	5.5	5.1
	K-puszta (47°N, 19.5°E, 0.12 km)	59.5	43.8	9.5	31.1	29.5	26.1
	Changbai (42.5°N, 128.5°E, 0.74 km)	10.4	17.7	29.3	53.8	29.7	18.1
Costal & oceanic	Cape Hedo (26.9°N, 128.3°E, 0.06 km)	198.5	138.2	52.5	59.1	61.2	64.1
	Azores (38.5°N, 27.3°W, 0 km)	113.2	57.6	5	4.6	5.7	7
	Aveiro (40.5°N, 8.6°W, 0.05 km)	72.9	51.3	7.5	9.8	10.5	11.2
Tropics	Sakaerat (14.5°N, 101.9°E, 0.04 km)	119.4	226.7	17.7	87.1	87	86.9

maximum. WBF decreases median BC_{snow} by ∼15% (from 25.7 ng g^{-1} to 22.4–22.7 ng g^{-1}) and improves the comparison with observations (median: 19.1 ng g^{-1}).

Fig. 3.6 (right panel) shows observed and simulated medians of BC_{snow} in the nine sub-regions as defined in Sect. 3.2.3. Overall, GEOS-Chem captures the spatial distribution of BC_{snow} from lowest in the Arctic to highest in the Northeast industrial region in Northern China, but overestimates BC_{snow} in the mid-latitudes (by up to a factor of three) and underestimates BC_{snow} in the Arctic (by 27%). WBF reduces BC_{snow} by 16–33% in the mid-latitudes (discrepancy reduced to within a factor of two), while increases BC_{snow} by ∼30% in the Arctic (discrepancy reduced to within 15%). The improvements are due to the redistribution of BC deposition as a result of WBF. WBF reduces BC deposition fluxes (by 12–34%) in North America, Northern China, and Xinjiang, China, while increases the flux in remote Arctic by (7–21%) (Table 3.4). In the mid-latitudes, WBF reduces BC wet deposition fluxes (by 37–63%), while increases dry deposition fluxes (by 3–16%). This is

Table 3.4: GEOS-Chem simulated BC deposition fluxes (mg m^{-2} mon^{-1}) in the Arctic (Sep.–Apr.), North America (Nov.–Feb.), Northern China (Nov.–Feb.) and Western China (Nov.–Feb.), averaged for 2007–09.

	Region	Riming-only	WBF_T	WBF_{IMF}
Total Deposition	**Arctic**	0.14 (0.12–0.18*)	0.15 (0.13–0.17*, +7%+)	0.17 (0.16–0.20*, +21%+)
	N. America	0.75 (0.72–0.80)	0.66 (0.63–0.71, -12%)	0.61 (0.56–0.65, -19%)
	N. China	3.83 (3.80–3.88)	3.02 (2.83–3.25, -21%)	2.92 (2.61–3.24, -24%)
	Xinjiang, China	1.22 (1.07–1.43)	0.95 (0.87–1.00, -25%)	0.84 (0.83–0.85, -34%)
Wet deposition	**Arctic**	0.10 (0.08–0.13)	0.08 (0.06–0.10, -22%)	0.07 (0.06–0.09, -29%)
	N. America	0.35 (0.31–0.38)	0.22 (0.20–0.24, -37%)	0.16 (0.14–0.18, -54%)
	N. China	1.52 (0.83–1.96)	0.68 (0.41–0.89, -52%)	0.52 (0.34–0.65, -63%)
	Xinjiang, China	0.67 (0.47–0.88)	0.36 (0.27–0.46, -46%)	0.22 (0.17–0.25, -57%)
Dry deposition	**Arctic**	0.04 (0.03–0.04)	0.07 (0.06–0.08, +81%)	0.10 (0.09–0.11, +159%)
	N. America	0.39 (0.38–0.42)	0.42 (0.41–0.45, +7%)	0.46 (0.43–0.48, +16%)
	N. China	2.31 (2.10–2.55)	2.37 (2.15–2.61, +3%)	2.42 (2.20–2.65, +5%)
	Xinjiang, China	0.52 (0.47–0.57)	0.56 (0.51–0.61, +8%)	0.59 (0.55–0.64, +15%)

*The minimum and maximum deposition fluxes.
+The deposition flux difference (WBF – Riming_only) relative to that from the Riming-only simulation.

because BC_{air} in boundary layer is increased with the WBF effect (Sect. 3.4.2). The higher dry deposition flux partly offsets the lower wet deposition, resulting in a reduction of 12–34% in the total BC deposition flux. In the Arctic, BC wet deposition flux decreases by 21–29%, while dry deposition flux increases substantially by 81–159%, much larger than that in the mid-latitude regions. As a result, the total deposition flux in the Arctic increases by ∼20%.

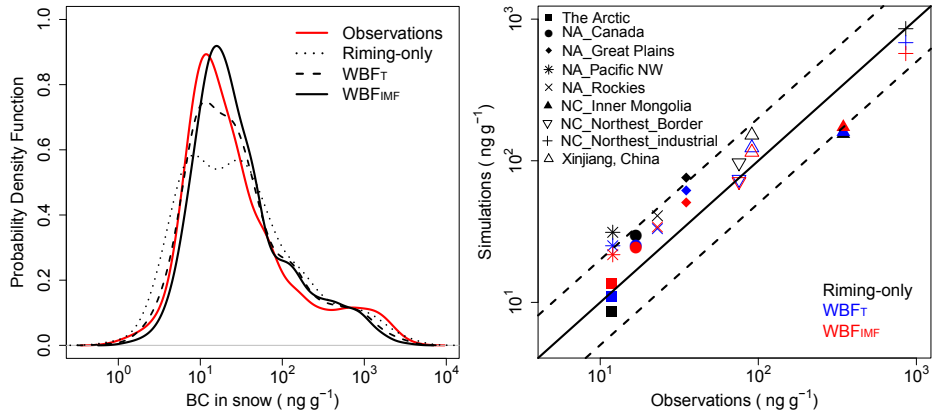

Figure 3.6: (Left panel) Probability density function of observed (solid red line) and GEOS-Chem simulated (dotted: riming-only, dashed: WBF_T, solid black: WBF_{IMF}) BC in snow (ng g^{-1}) and (right panel) medians of observed and simulated BC in snow (ng g^{-1}) in the Arctic, North America (Canada, the Great Plains, the Pacific Northwest, and the Rockies, as defined by Doherty et al. (2014)), Northern China (Inner Mongolia, Northeast Border and Northeast industrial, as defined by Wang et al. (2013)), and Xinjiang, China. The regions are symbol-coded and the simulations are color-coded (see text for details). Solid line – 1:1 ratio line, dashed lines – 1:2 (or 2:1) ratio lines.

Even with the WBF effect, BC_{snow} are still overestimated across much of the mid-latitudes. This indicates that BC scavenging over East Asia and North America is likely overestimated in the model during snow season. The exception is in Inner Mongolia and the Northern industrial region in China. In Inner Mongolia, snow samples were mixed with local soil and the measurements of BC_{snow} were associated with very large uncertainties (*Wang et al.*, 2013). In addition, most of the snow samples in this region were taken from thick

drifted snow layers, therefore BC_{snow} does not correspond to BC deposition. In the Northern industrial region (median: 856 ng g^{-1}, significantly larger than the global median of 19 ng g^{-1}), BC deposition is strongly affected by emissions from local sources and dry deposition flux. At Mt. Changbai, for instance, WBF significantly improves the simulation of wet deposition flux (discrepancy lowered from +80% to -40–0%, Table 3.3). However, dry deposition flux at the site is underestimated by a factor of five. Thus the underestimate of BC_{snow} (by 34%) in the region is likely because of the excessively low BC dry deposition.

3.4.5 Washout ratio of BC

Hegg et al. (2011) reported that now particles mostly showed rimed structures at Zeppelin, resulting in high washout ratios (∼770, Table 3.2). Model simulated washout ratio with riming-only (Experiment Riming-only) is in agreement with observations to within a factor of two at Zeppelin. When snow particles are pristine crystal formed mainly from WBF, for example, at Abisko (*Noone and Clarke*, 1988), the observed washout ratios tend to be significantly lower (94 at Abisko and 145 at Mt. Changbai, Table 3.2). WBF reduces the washout ratio by a factor of five (from 482 to 96) and significantly lowers the discrepancy (from a factor of four to 2%) at Abisko. WBF also drastically reduces the discrepancies at LAVO (from factors of 3–5 to 2).

Fig. 3.7 shows observed and GEOS-Chem simulated monthly mean BC washout ratios, $BC_{rain/snow}$ and BC_{air} at four mountainous sites in Europe and at Cape Hedo. We use only simulations when daily mean precipitation is above the monthly median to compute monthly means, because samples of BC in rain/snow were collected during major rain/snow events (*Cerqueira et al.*, 2010). At Sonnblick (3.1 km), a site that is constantly in the free troposphere, washout ratios are overestimated by orders of magnitude. This is because $BC_{rain/snow}$ is overestimated while BC_{air} is underestimated. WBF significantly reduces the discrepancy of washout ratios, particularly in winter (discrepancy lowered from factors of 4–16 to less that 4). The improvements are because WBF reduces $BC_{rain/snow}$ (discrepancy

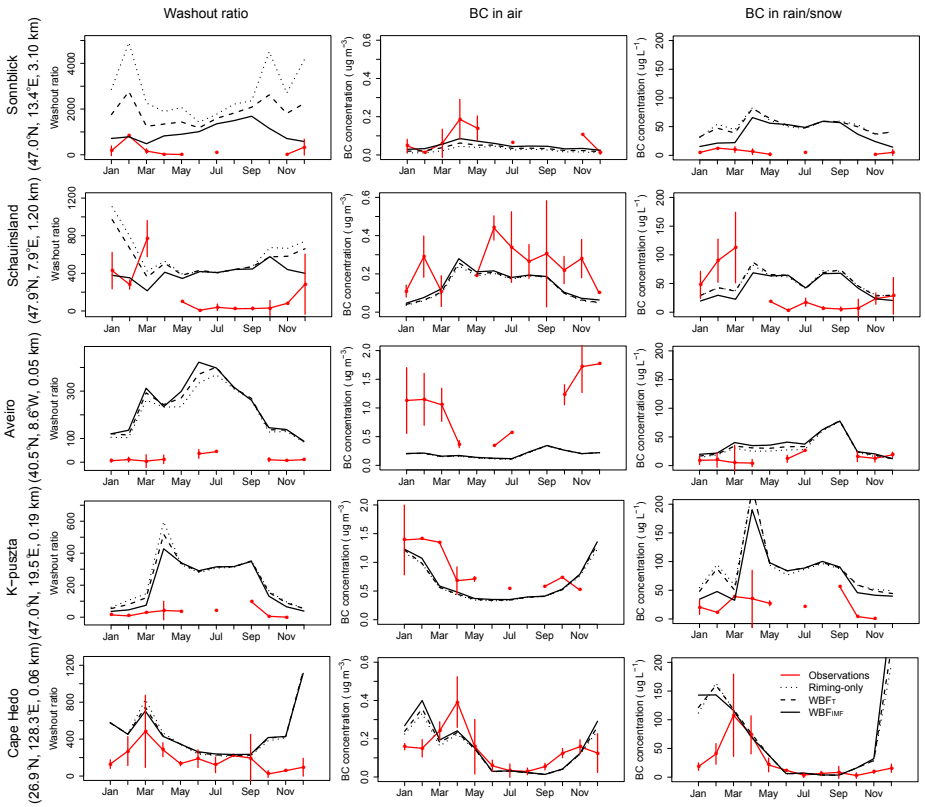

Figure 3.7: Observed and simulated BC washout ratio, BC concentration in surface air and in snow at Cape Hedo in East China Sea, Aveiro and K-puszta (rural sites), and Schauinsland and Sonnblick (elevated sites).

reduced from a factor of seven to a factor of four) and increases BC_{air} (discrepancy decreases from -77% to -51%). Remarkable improvement of washout ratio simulation is also seen at Schauinsland (1.2 km). WBF lowers the discrepancy of washout ratio in winter and spring from a factor of two to ∼20%. However, this improvement is because of decreased BC in snow, which degrades the comparison with observations. WBF does not affect washout ratios at the three sea-level sites Aveiro (0.47 km), K-puszta (0.19 km), and Cape Hedo (0.06 km). That is because cloud processes have rather limited effect on BC at the surface (Sect. 3.4.2). Even with the WBF effect, BC washout ratios are still largely overestimated, because BC_{air} is underestimated and $BC_{rain/snow}$ is overestimated, particularly in summer.

These overestimates suggest that wet deposition is likely too strong over Europe.

3.5 Global BC budget

Compared to AERONET observations of BC AAOD mainly over land, AeroCom models (I and II) underestimate BC loading by 60–160% (in South and Southeast Asia it is a factor of three and four) (*Bond et al.*, 2013). *Bond et al.* (2013) attributed the low bias to insufficient BC emissions. They then scaled BC emissions up according to the discrepancy of modeled versus observed BC AAOD and obtained a total global BC emission of 17 Tg yr^{-1}, twice the median value used in the AeroCom models. They reported BC loading of ∼0.50 mg m^{-2} after scaling (Table 3.5). Our results suggest that the discrepancy can be partially explained by WBF not being accounted for in the AeroCom models. WBF increases global BC loading by 0.07–0.13 mg m^{-2} (by 32–60%), depending on the WBF parameterizations used (based upon either temperature or IMF) (Table 3.5). Such increases are comparable to the median global BC loading from the AeroCom II models (*Myhre et al.*, 2013). With WBF, our results show global BC loadings of 0.29–0.35 mg m^{-2}, which are in remarkable agreement with the AERONET-based estimates (with scaled-up BC AAOD) as reported by *Bond et al.* (2013).

However, we find that even with WBF, model results still have large biases over land, with BC_{air} biased low (Figs. 3.3 and 3.5), BC_{snow} biased high (Fig. 3.6), and washout ratios too large (Fig. 3.7). These remaining discrepancies likely point toward excessive wet scavenging over land in the model. In North America, for instance, model simulated BC_{snow} is too high by ∼50% (Fig. 3.6) and BC_{air} in winter (IMPROVE, Fig. 3.5) is low by up to ∼30%. Additionally, model simulated washout ratio at LAVO, CA is twice the observed value. In Europe, model simulated washout ratios, particularly in summer, are excessively high, a result of overly high $BC_{rain/snow}$ and too low BC_{air} predicted by the model (Fig. 3.7).

In contrast, compared to HIPPO over remote Pacific, AeroCom models overestimate BC_{air} by a factor of two to five (*Schwarz et al.*, 2010). To narrow the gap between model

Table 3.5: Global annual budget of BC.

Model		Emissions (Tg yr^{-1})	Deposition (Tg yr^{-1})		Mass loading		Lifetime (day)	References
			Dry	Wet	Total (mg m^{-2})	> 5 km (%)		
GOES-Chem	Riming-only	8.5	1.5	6.9	0.22	21	5.7	This study
	WBF_T	8.5	1.6	6.8	0.29	25	6.9	
	WBF_{IMF}	8.5	1.7	6.7	0.35	27	8.0	
WB_T	248–273K	8.5	1.6	6.8	0.30	27	7.0	
	258–268K	8.5	1.6	6.9	0.30	25	6.7	
WBF_{IMF}	248–273K	8.5	1.7	6.7	0.36	29	8.0	
	258–268K	8.5	1.6	6.8	0.32	26	7.0	
AeroCom I		6.3			0.25 (0.16–0.38*)	21 (18–41)	7.3 (4.9–11.4)	Schulz *et al.* (2006)
AeroCom II		6.6–10.6			0.14 (0.07–0.31)			Myhre *et al.* (2013)
AeroCom (median)		17			~0.50		6.1	Bond *et al.* (2013)
GEOS-Chem		6.5			0.08	9	4.2	Q. Wang *et al.* (2014)
GEOS-Chem		6.9			0.16	12	4.4	X. Wang *et al.* (2014)
GEOS-Chem		10.8			0.25	7	4.2	He et al. (2016)

*Ranges given in parentheses.

results and HIPPO observations, previous studies resorted to either enhancing wet scavenging or accelerating BC aging near source regions. For example, *Wang et al.* (2014b) included scavenging of hydrophobic BC in convective updrafts and hydrophilic BC in cold clouds (< 258 K) by homogeneous freezing of solution droplets, neither of which was accounted for previously (*Wang et al.*, 2014b). *Wang et al.* (2014c) and *He et al.* (2015) used faster BC aging schemes, which led to stronger wet scavenging close to source regions and consequently weaker outflow from these regions. The BC loadings were estimated to be 0.08 mg m^{-2} (*Wang et al.*, 2014b), 0.16 mg m^{-2} (*Wang et al.*, 2014c) and 0.25 mg m^{-2} *He et al.* (2015) , much lower than those constrained from AERONET measurements (~0.50 mg m^{-2}, *Bond et al.*, 2013).

However, even with a faster aging scheme and stronger wet deposition, simulated BC_{air}

is still biased high by a factor of 2–3 relative to HIPPO observations over the remote Pacific. The remaining high bias is likely a result of either excessive Asian outflow of BC or insufficient scavenging of BC over the Pacific. At Cape Hedo in East China Sea (directly downwind of major sources in Eastern China), model simulated BC_{rain} is an order of magnitude too high while BC_{air} is 50% too large in October–January (Fig. 3.7). This overestimate of wintertime outflow of BC from the region is likely the reason for the overestimate of BC_{air} over the Pacific in winter. Outside of winter, simulated BC_{air} and BC_{rain} at the site both agree with observations (within 50%, Fig. 3.7). This suggests that the overestimate of BC_{air} over the Pacific is likely the result of insufficient removal over Pacific.

WBF results in more BC particles in the upper troposphere (Table 3.5). As a result, there is a significantly higher fraction of BC loading above 5 km altitude (from 21% to 25–29%). This larger fraction, as expected, enhances the top-of-atmosphere absorption forcing efficiencies (forcing per aerosol absorption optical depth, *Bond et al.*, 2013) because of larger solar fluxes at higher altitudes (*Bond et al.*, 2013; *Samset and Myhre*, 2011). The aforementioned fraction (25–29%) falls in the range of AeroCom I model results (*Schulz et al.*, 2006), but is three times higher than those constrained by HIPPO observations (9–12%) (*Wang et al.*, 2014b,c). Moreover, WBF increases BC lifetime from 5.7 days to 6.9–8.0 days, an increase of up to 40%. These longer lifetimes fall within the range of the AeroCom I model results (4.9–11.4 days) but at the higher end (*Schulz et al.*, 2006). However, these lifetimes are nearly twice as long as those constrained by HIPPO observations (*Wang et al.*, 2014b,c).

The temperature threshold for mixed-phase clouds and ice clouds is very uncertain and controlled by processes such as the shattering of isolated drops during freezing and the ice splinter production during riming (*Gayet et al.*, 2009; *Browse et al.*, 2012) that are not explicitly accounted for in GEOS-Chem. To examine the sensitivity of BC distribution to various threshold temperatures, we conduct additional simulations. In the standard simulation, clouds are assumed to be mixed-phase at 258–273 K. In the sensitivity studies, we vary the threshold between 268 and 248 K. The results are summarized in Table 3.5. The

resulting BC deposition, loading, and lifetime are within 15% of the standard simulation. This suggests that our results are rather insensitive to the threshold temperature.

3.6 Conclusions and implications

We used GEOS-Chem (version 9-01-03) driven by GEOS-5 assimilated meteorological fields to investigate the effect of WBF on global BC distribution. Specifically we evaluated model simulations against observations of BC scavenging efficiencies, BC_{air}, BC deposition fluxes, $BC_{rain/snow}$, and BC washout ratios. We distinguished riming- from WBF-dominated conditions in mixed-phase clouds based upon temperature and liquid water content following *Fukuta and Takahashi* (1999). We then parameterized the WBF effect based on either temperature or ice mass fraction following *Cozic et al.* (2007).

The model reproduced the observed low scavenging efficiencies of BC near source regions and high scavenging efficiencies in remote regions. WBF lowered BC scavenging efficiencies at all altitudes and significantly improved the simulations at higher altitudes (such as Jungfraujoch, 3.85 km and Puy de Dme,1.47 km). On average, in northern mid-latitudes, WBF reduced BC scavenging efficiency by 17–44% in winter, depending on the WBF parameterizations used. In summer, the effect increased with increasing altitude (from 0 at surface to 39–50% in the upper troposphere). Across the Arctic, WBF reduced BC scavenging efficiency by 22–69% in summer and 63–85% in winter in the lower and middle troposphere. As a result, WBF increased BC_{air} (< 4 km) globally and halved the discrepancy (from -65% to -30%). The improvements were larger for sites at higher altitudes and latitudes.

The model captured the observed large BC wet deposition flux (52.5 mg m^{-2} yr^{-1}) at Cape Hedo in East China Sea and comparatively low value (5.0 mg m^{-2} yr^{-1}) at Azores in the central Atlantic. WBF resulted in lower wet deposition fluxes near source regions over land (by $\sim$15%) but higher wet deposition fluxes over remote oceans (by $\sim$30%). In addition, WBF lowered BC deposition fluxes (by 12–34%) at mid-latitudes while enhanced

the fluxes (by 2–19%) in the Arctic. The former was because of the strong reduction of BC wet deposition fluxes (by 37–63%) and the latter was from the strong enhancement of dry deposition fluxes (by 81–159%). Thus, BC_{snow} decreased (by 15%) in mid-latitudes and increased (by 26%) in the Arctic as a result of the WBF effect. Overall, WBF lowered the discrepancy of BC_{snow} from 35% to 17%, indicating that WBF explained a large fraction of the high bias of the model results. In addition, WBF significantly lowered the discrepancies of washout ratios of BC in winter from a factor of 16 to 4. In summer, washout ratios were overestimated by orders of magnitudes. WBF corrected a fraction of the biases. Reasons of the large overestimate warrant further investigation.

WBF increased global BC loading by 60% (from 0.22 mg m^{-2} yr^{-1} to 0.35 mg m^{-2} yr^{-1}) and partially explained the low biases of AAOD from the AeroCom models (*Bond et al.*, 2013). In addition, WBF increased the fraction of BC loading above 5 km (from 21% to 25–29%) and hence a larger absorption forcing efficiency of BC. BC lifetime is longer by 40% (from 5.7 to 8.0 days) from the WBF effect.

On average, model simulations of BC scavenging efficiencies, BC_{air}, deposition fluxes, $BC_{rain/snow}$, and washout ratios improved significantly. However, the comparisons degraded at riming-dominated sites, for example, Zeppelin. These results suggest that more observations are needed to better differentiate WBF- versus riming-dominated scavenging of BC. In addition, measurements of BC scavenging efficiencies in mixed-phase clouds at different latitudes and altitudes should be conducted, especially over the oceans where there are scarce measurements of BC scavenging efficiency.

Acknowledgements. This study was funded by NASA grant NNX14AF11G from the Atmospheric Chemistry Modeling and Analysis Program (ACMAP). The authors thank J. P. Schwarz, B. Craft, and H. Liu for helpful discussions.

CHAPTER 4

Sources of Springtime Surface Black Carbon in the Arctic: An Adjoint Analysis

Abstract

We quantify source contributions to springtime (April 2008) surface BC in the Arctic by interpreting surface observations of BC at five receptor sites (Denali and Barrow in Alaska, Alert in Canada, Zeppelin in Norway, and Summit in Greenland) GEOS-Chem and its adjoint. Contributions to BC at Barrow, Alert, and Zeppelin are dominated by Asian anthropogenic sources (40–43%) before April 18 and by Siberian open biomass burning emissions (29–41%) afterward. In contrast, Summit, a mostly free tropospheric site, has predominantly an Asian anthropogenic source contribution (24–68% with an average of 45%). We compute the adjoint sensitivity of BC concentrations at the five sites during a pollution episode (April 20–25) to global emissions from March 1 to April 25. The associated contributions are the combined results of these sensitivities and BC emissions. Local and regional anthropogenic sources in Alaska are the largest anthropogenic sources of BC at Denali (63%), and natural gas flaring emissions in the Western Extreme North of Russia (WENR) are the largest anthropogenic sources of BC at Zeppelin (26%) and Alert (13%). We find that long-range transport of emissions from Beijing-Tianjin-Hebei (also known as Jing-Jin-Ji), the biggest urbanized region in Northern China, contribute significantly (∼10%) to surface BC across the Arctic. On average it takes ∼12 days for Asian anthropogenic emissions and Siberian biomass burning emissions to reach Arctic lower troposphere, supporting earlier studies. Natural gas flaring emissions from the WENR reach Zeppelin in about a week. We find that

episodic, direct transport events dominate BC at Denali (87%), a site outside the Arctic front, a strong transport barrier. The relative contribution of direct transport to surface BC within the Arctic front is much smaller (∼50% at Barrow and Zeppelin and ∼10% at Alert). The large contributions from Asian anthropogenic sources are predominately in the form of 'chronic' pollution (∼40% at Barrow and 65% at Alert and 57% at Zeppelin) on 1–2 month timescales. As such, it is likely that previous studies using 5- or 10-day trajectory analyses strongly underestimated the contribution from Asia to surface BC in the Arctic. Both finer temporal resolution of biomass burning emissions and accounting for the WBF process in wet scavenging improve the source attribution estimates.

4.1 Introduction

The Arctic, one of the most sensitive regions to climate change, warms at a rate twice as rapid as the global average (*Quinn et al.*, 2011). Climate modeling studies indicate that Arctic surface warms from global BC, which absorbs solar radiation in the atmosphere (*Bond et al.*, 2013, and references therein). Specifically, atmospheric BC at lower latitudes warms the Arctic surface due to polar-ward transport of heat absorbed by BC (*Shindell and Faluvegi*, 2009; *Flanner*, 2013; *Sand et al.*, 2013, 2015). Although the total effect of BC in the Arctic troposphere is warming the surface, BC at different altitudes have different climate effects on surface Arctic (*Shindell and Faluvegi*, 2009; *Flanner*, 2013). BC in the upper tropospheric Arctic slightly cools (-0.03 ± 0.02 K (Gg yr)$^{-1}$) the Arctic surface due to surface dimming, while surface atmospheric BC exerts a strong surface warming effect (0.11 ± 0.02 K (Gg yr)$^{-1}$, *Flanner*, 2013). In addition, this climate effect has a strong seasonal variation with the largest mass-normalized Arctic warming in spring, when the high insolation and surface albedo strongly facilitate a large radiative forcing of BC and the associated surface warming (*Quinn et al.*, 2008; *Flanner*, 2013). It is thus imperative to improve our understanding of the distribution of BC in springtime in the Arctic and identify the sources both in the troposphere and at surface.

Numerous studies have analyzed BC vertical profiles and identified sources of springtime BC in the troposphere in the Arctic (*Liu et al.*, 2015, and references therein), particularly during polar year 2008. They found that dense haze layer with maximum BC concentration is usually observed in the middle troposphere (*Warneke et al.*, 2009, 2010; *Wang et al.*, 2011; *Brock et al.*, 2011; *Marelle et al.*, 2015) and their sources are largely diverse. *Stohl et al.* (2007) found that agricultural fires in Eastern Europe strongly enhanced BC concentration in the European Arctic in spring 2006. Studies based on aircraft observations from Arctic Research of the Composition of the Troposphere from Aircraft and Satellites (ARCTAS, *Jacob et al.*, 2010), and Aerosol, Radiation, and Cloud Processes affecting Arctic Climate (ARCPAC, *Brock et al.*, 2011) found that agricultural as well as boreal forest fires in south Siberia dominated BC concentrations (up to 80%) in a large part of the Arctic troposphere (particularly in North American sector) in spring 2008 (*Warneke et al.*, 2009, 2010; *Wang et al.*, 2011; *Brock et al.*, 2011). Given that an increasing trend of frequency of boreal forest fires has been predicted due to global warming, the contribution of these fires to Arctic BC is likely to increase in the future (*Soja et al.*, 2007; *Flannigan et al.*, 2009; *Wotton et al.*, 2010; *Liu et al.*, 2012). With the rapid increase of anthropogenic emissions in Eastern and Northern Asia, recent studies have shown that this region may become an important source (up to 90%) of Arctic BC in late winter and early spring, particularly in the free troposphere (*Shaw et al.*, 2010; *Frossard et al.*, 2011; *Liu et al.*, 2015). Other studies suggest otherwise because strong scavenging during uplift processes in warm conveyer belts can significantly decrease the BC transport efficiency and the resulting contribution from this source (*Stohl*, 2006; *Matsui et al.*, 2011).

The Arctic surface is isolated from the free troposphere by a strong transport barrier, the so-called 'Arctic front', which is a closed dome formed by surfaces of constant potential temperature (*Stohl*, 2006, and references therein). As such, the Arctic front strongly reduces the influence from episodic pollution entering the Arctic in the middle and upper troposphere and limits their impact on surface BC concentrations (*Stohl*, 2006; *Brock et al.*, 2011). In

addition, emissions in the Arctic front are trapped in the lower troposphere and enhance surface concentration. The Arctic front extends further south (40°N) over Europe and Russia in winter and early spring (*Stohl*, 2006). Thus, sources of Arctic surface BC have been repeatedly identified as emissions from the two regions. A large fraction of the 5- or 10-day back trajectories ends in the industrial regions in Russia and Europe (*Polissar et al.*, 2001; *Sharma et al.*, 2006; *Huang et al.*, 2010b; *Dutkiewicz et al.*, 2014). In addition, long-term observations (decades) at surface sites Barrow (*Polissar et al.*, 2001; *Sharma et al.*, 2006; *Hirdman et al.*, 2010b), Alert (*Sharma et al.*, 2004, 2006; *Huang et al.*, 2010b; *Hirdman et al.*, 2010b), Zeppelin (*Eleftheriadis et al.*, 2009; *Hirdman et al.*, 2010b), and Kevo (*Dutkiewicz et al.*, 2014) showed that BC concentration has been steadily declined since 1980. They relate these declining trends with declining emissions in the former Soviet Union. Asian contributions to surface BC were considered not to be significant due to two reasons. First, very few back trajectories end in this region (*Polissar et al.*, 2001; *Sharma et al.*, 2006; *Huang et al.*, 2010b; *Dutkiewicz et al.*, 2014). Second, observed atmospheric surface BC concentrations at Alert, Barrow and Zeppelin did not increase with increasing BC emissions in East Asia since 2000 (*Sharma et al.*, 2013). In addition, most of these studies were focused on the long-term averaged sources and contrasted sources in winter and in summer. Few studies have identified sources of BC in springtime surface Arctic, which efficiently warms the Arctic surface (*Flanner*, 2013).

Previous studies on BC source apportionment have used either statistical analysis of trajectories (*Polissar et al.*, 2001; *Sharma et al.*, 2004; *Eleftheriadis et al.*, 2009; *Stohl*, 2006; *Hirdman et al.*, 2010b; *Harrigan et al.*, 2011; *Dutkiewicz et al.*, 2014), tag tracer technique (*Wang et al.*, 2011, 2014a) or sensitivity simulation with perturbed emissions (*Koch and Hansen*, 2005; *Shindell et al.*, 2008; *Huang et al.*, 2010b; *Bourgeois and Bey*, 2011; *Sharma et al.*, 2013; *Ma et al.*, 2013). Trajectory analysis efficiently identifies transport pathways, but the model integration error increases when modeling time exceeds 5–6 days. This error introduces large uncertainties to the back trajectory paths, thereby sources can only be

reliably assigned on continental scales (*Liu et al.*, 2015). In addition, the assumption of the trajectory method is that the tracer is inert and not affected by chemical or other removal processes, which introduce large uncertainties to source apportionment (*Liu et al.*, 2015). Tagged tracer and sensitivity simulations include chemical and physical processing of BC but are computationally limited in the spatial and temporal resolution of the source regions that can be considered (*Wang et al.*, 2014a). The Chemical Transport Model (CTM) adjoint not only explicitly simulates chemical and physical processes of aerosols but also offers a far more computationally efficient approach for a receptor-oriented source attribution (*Henze et al.*, 2007; *Hakami et al.*, 2007). A single run of the adjoint model can compute the sensitivity of BC concentrations at a given location (or an average over a spatial domain) and time (or an average in a time interval) to global emissions over the spatial and temporal resolution of the model (*Zhang et al.*, 2009a). The method has been applied previously to examine transpacific (*Zhang et al.*, 2009a) and Arctic (*Walker et al.*, 2012) transport of ozone, source apportionment of aerosol pollution episodes (*Nester and Panitz*, 2006; *Zhang et al.*, 2015a) and BC radiative forcing in the Himalayas and Tibetan Plateau (*Kopacz et al.*, 2011).

Based on the improved simulation of BC distribution in the Arctic (Chapter 2), we use here the tagged tracer technique in a global 3D chemical transport model, GEOS-Chem, to identify sources of BC at Arctic surface sites (Denali, Barrow, Alert, Zeppelin and Summit) resolved at continental scales in April, 2008 (Sect. 4.4.1). We then use the GEOS-Chem adjoint to refine our estimated source contributions to BC at the five sites to sources resolved at the 2° latitude × 2.5° longitude horizontal scale and hourly temporal resolution during a pollution event (April 20–25, Sect. 4.4.2).

4.2 Surface BC Observations

In-situ measurements of BC in April 2008 are available at five sites within the Arctic Circle (Fig. 4.1): Denali, AL (63.7°N, 149.0°W, 0.66 km a.s.l.) in the low Arctic, three sites in the high Arctic, Barrow, AL (71.3°N, 156.6°W, 0.01 km a.s.l.), Alert, Canada (82.3°N, 62.3°W, 0.21 km a.s.l.), and Zeppelin, Norway (79°N, 12°E, 0.47 km a.s.l.), and a free tropospheric site at Summit, Greenland (72.6°N, 38.5°W, 3.22 km a.s.l.). Denali, outside the Arctic front (∼66°N), receives pollution transported to the Arctic via 'Aleution Storm Track' displaced to the central and north Alaska in April 2008 (*Fuelberg et al.*, 2010). Barrow and Alert are within the Arctic front and experience regular temperature inversion (*Sharma et al.*, 2013). This inversion strongly suppresses the vertical transport from above and traps emissions in the Arctic front in the lower troposphere (*Stohl*, 2006; *Brock et al.*, 2011). Barrow is on the Northern land tip of Alaska, 8 km northeast of the town Barrow. It is influenced by both marine and continental air (*Hirdman et al.*, 2010b). Alert is located at the furthest north of all the five sites and is most isolated from continental sources (*Hirdman et al.*, 2010b). The Zeppelin observatory is on a mountain ridge on the Svalbard archipelago. Because of the relatively high elevation (478 m), Zeppelin is not always in a stable inversion layer (*Sharma et al.*, 2013). Summit, on the top of the Greenland glacial ice sheet, is always in the Arctic free troposphere (*Hirdman et al.*, 2010b). Measurement methods and their associated uncertainties are summarized in Chapter 2.

4.3 GEOS-Chem and its adjoint

4.3.1 GEOS-Chem simulation of BC

GEOS-Chem is a global chemical transport model driven with assimilated meteorology from the Goddard Earth Observing System (GEOS) of the NASA Global Modeling and Assimilation Office (GMAO). We use GEOS-5 meteorological data set to drive model simulation at

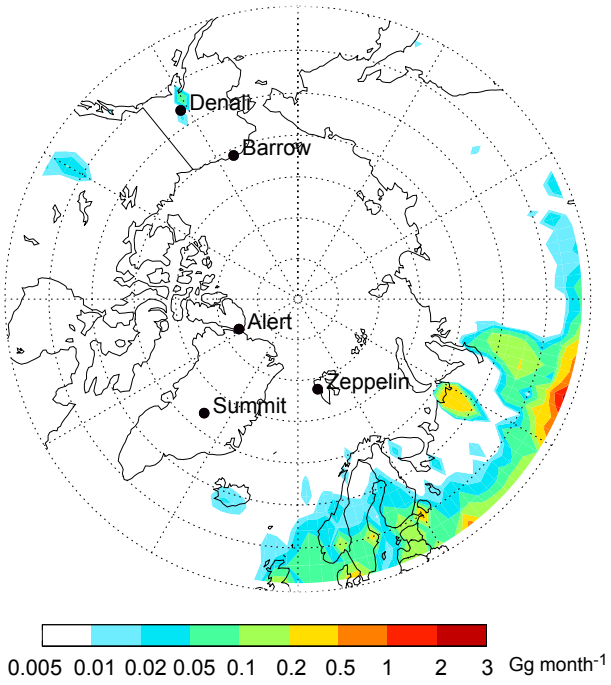

Figure 4.1: BC emissions (Gg month^{-1}) in the Arctic for April. Solid circles are surface sites: Denali, AL (63.7°N, 149.0°W, 0.66 km a.s.l.), Barrow, AL (71.3°N, 156.6°W, 0.01 km a.s.l.), Alert, Canada (82.3°N, 62.3°W, 0.21 km a.s.l.), Summit, Greenland (72.6°N, 38.5°W, 3.22 km a.s.l.), and Zeppelin, Norway (79°N, 12°E, 0.47 km a.s.l.). Data from *Bond et al.* (2007) and natural gas flaring emissions from *Stohl et al.* (2013).

2° latitude × 2.5° longitude resolution and 47 vertical layers from the surface to 0.01 hPa. The lowest model levels are centered at approximately 60, 200, 300, 450, 600, 700, 850, 1000, 1150, 1300, 1450, 1600, 1800 m above sea level. Tracer advection, moist convection, deep convection and shallow convection schemes are summarized in *Qi et al.* (2016a).

Northern hemispheric BC emissions in April are shown in Fig.4.2. Anthropogenic emissions of BC are from *Bond et al.* (2007) with Asian emissions from *Zhang et al.* (2009b). We applied seasonal variation for domestic heating emissions, which are concentrated in winter at high latitude, based on the heating degree day concept (*Stohl et al.*, 2013). Open Biomass burning emissions are available from the Global Fire Emissions Database version

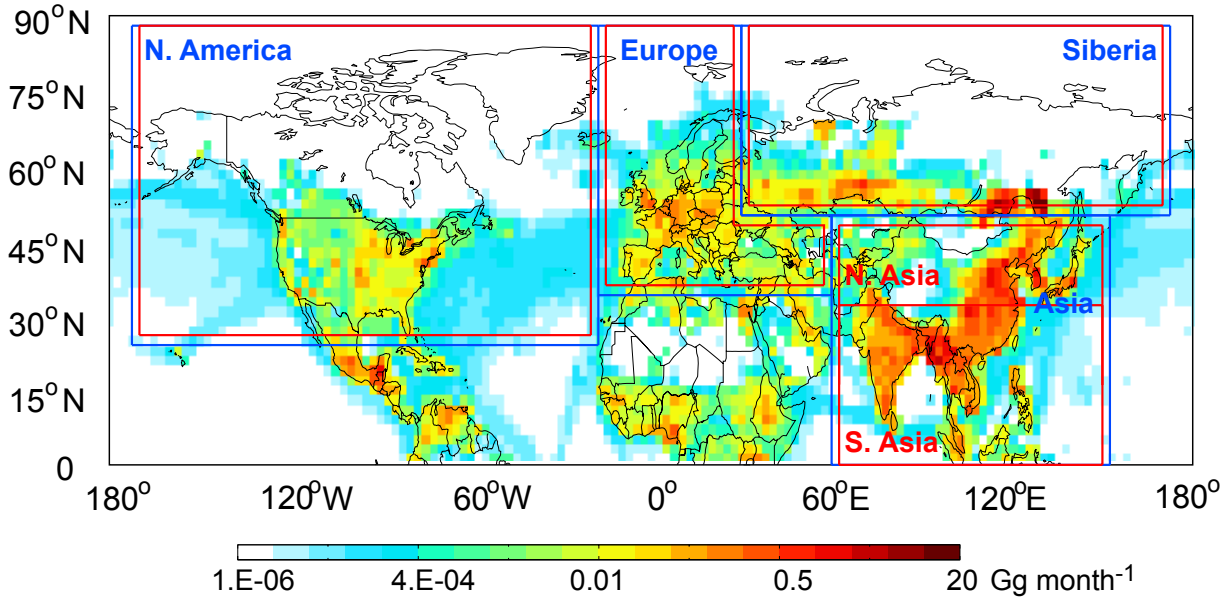

Figure 4.2: Northern hemispheric BC emissions for April (Gg month^{-1}). BC tracers are tagged by four anthropogenic (blue rectangles) and five biomass burning sources (red rectangles): North America (172.5–17.5°W, 24–88°N) – both anthropogenic and biomass burning, Europe (17.5°W–30°E, 33–88°N and 30–60°E, 33–50°N) – both, Siberia (30–172.5°E, 50–88°N) – both, Asia – anthropogenic (60–152.5°E, 0–50°N), Northern China (60–152.5°E, 30–50°N) – biomass burning sources, South Asia and Southern China (60–152.5°E, 0–30°N) – biomass burning.

3.1 (GFEDv3) with updates for small fire emissions (*Randerson et al.*, 2012). We use the GFED inventory with two temporal resolutions, the standard monthly inventory and a 3-hourly inventory. We use the monthly inventory for the standard simulation and the 3-hourly inventory for the uncertainty simulation To derive the 3-hourly inventory, daily emissions are first re-sampled temporally from the monthly inventory according to Moderate Resolution Imaging Spectroradiometer (MODIS) daily active fire counts (*Giglio et al.*, 2003). Then a diurnal cycle with a 3-hourly time step based on the active fire observations (*Prins et al.*, 1998) is applied to the daily inventory. The resulting 3-hourly inventory has the same overall emissions as the monthly inventory but with a much finer temporal distribution. We also

include emissions from gas flares in the oil and natural gas industry (*Stohl et al.*, 2013). It is suggested that the total emissions of gas flaring only account for 3% of global total BC emissions but they account for 42% of total BC emissions in the Arctic (*Stohl et al.*, 2013). They are significant contributors to both BC deposition (∼20%) and ambient BC concentrations during snow season (Sep. – Apr.) in the Arctic (*Qi et al.*, 2016a). BC emissions in the Arctic are shown in Fig. 4.1.

We assume 80% of the freshly emitted BC particles are hydrophobic and are converted to hydrophilic with an e-folding time of 1.15 days, which reproduces the Asian outflow (*Park et al.*, 2003, 2005). We estimates dry deposition velocity of BC over snow and ice using resistance-in-series method (*Wesely*, 1989; *Zhang et al.*, 2001), validated by recent measurements of aerosol deposition velocity over snow and ice (*Qi et al.*, 2016a). Wet scavenging of BC follows *Wang et al.* (2011) with updates for BC scavenging efficiency in mixed-phase clouds (*Qi et al.*, 2016b). We parameterize BC scavenging efficiency in mixed-phase clouds accounting for the effects of WBF process (*Qi et al.*, 2016b). WBF occurs when environmental vapor pressure is above the saturation vapor pressure of ice crystals and below that of cold water drops. Ice crystals grow and cold water drops evaporate, releasing BC particles in the cold water drops back into interstitial air. This process strongly reduces BC scavenging efficiency globally, slow down wet scavenging and increases atmospheric BC concentration. Including WBF significantly improves the simulation of BC distribution in air and in snow globally as shown in Chapter 3.

We identify sources of BC in spring Arctic using the tagged tracer technique, which is a physically consistent and computationally efficient approach to attribute sources resolved at continental scales (*Wang et al.*, 2011, 2014a). BC emitted from different source types (anthropogenic versus open biomass burning emissions) and source regions (Europe, Russia, Asia and North America) are tagged with no overlap among these geographical regions (Fig. 4.2). BC emitted in these tagged regions are explicitly tracked in the model and are treated the same way (transport, chemical and physical processes) as the original BC, allowing for

direct estimate of the contributions from individual tagged source types and source regions.

4.3.2 GEOS-Chem adjoint simulation of BC

Compared with the tagged tracer technique, the adjoint modeling approach computes source-receptor sensitivities for individual receptor locations more efficiently and can be done at a much finer temporal and spatial resolution. We use GEOS-Chem adjoint (*Henze et al.*, 2007) model version 8-02-01 with updated emissions, dry deposition velocity and wet scavenging as described in Sect. 4.3.1. The adjoint model has previously been used to constrain emissions of CO (*Kopacz et al.*, 2009, 2010), BC (*Mao et al.*, 2015; *Zhang et al.*, 2015b) and other aerosols (*Henze et al.*, 2009) and to identify sources of ozone (*Zhang et al.*, 2009a), BC (*Kopacz et al.*, 2011) and other aerosols (*Zhang et al.*, 2015a). In addition, the adjoint has also been used to estimate the sensitivity of direct radiative forcing to aerosol emissions (*Henze et al.*, 2012).

In this study, we use the adjoint to compute the sensitivity of BC concentrations ($[\mathrm{BC}]_\mathrm{s}$) at the five receptor sites in the Arctic to global BC emissions ($\boldsymbol{e}$) at 2° latitude × 2.5° longitude horizontal resolution over the history of air parcels reaching the sites (March 1–April 25). This sensitivity is denoted as $\boldsymbol{k}$,

$$[BC]_\mathrm{s} = \boldsymbol{e} \times \boldsymbol{k}$$

As horizontal advection in GEOS-Chem is approximately linear, and the rest of the chemical and physical process are entirely linear, multiplication of the sensitivity ($\boldsymbol{k}$) by emissions ($\boldsymbol{e}$) yields an estimate of how much BC emissions from each grid cell contribute to BC concentrations at a receptor site ($[\mathrm{BC}]_\mathrm{s}$) (*Henze et al.*, 2007; *Kopacz et al.*, 2011). In this study, $[\mathrm{BC}]_\mathrm{s}$ is the mean BC concentration at each receptor site (Fig. 4.1) during April 20–

25, 2008. The sensitivity is propogated backwards in time from April 25 to March 1. Then, hourly contributions from each grid cell can be estimated by multiplying these sensitivities with emissions at that time. Integrating these contributions from March 1 to April 25 gives the contributions of each grid cell to $[BC]_s$ at the receptor sites. Further integrating these contributions globally approximates the mean $[BC]_s$ during April 20–25 at each site.

We validate GEOS-Chem adjoint via comparison of adjoint gradients to forward model sensitivities, Λ, calculated using the finite difference approximation,

$$\Lambda = \frac{J(\sigma + \delta\sigma) - J(\sigma)}{\delta\sigma}$$

where J is the cost function, defined as the mean $[BC]_s$ at the receptor sites, σ the scaling factor for BC emissions ($\sigma = 1$ for the sensitivity simulation). We use $\delta\sigma = 0.1$ for all tests in this study. We compare the sensitivities of mean [BC] in April 20–25 at each receptor site to anthropogenic and biomass burning emissions in March 1–April 25 estimated by finite difference and adjoint method. This evaluation is quite time consuming to perform at each grid cell throughout the globe owing to the expense of the finite difference calculations (144 $\times$ 91 runs). Hence, we selected 10 model grid cells with the largest anthropogenic and open biomass burning sources for the validation, because the absolute difference between the two methods is more substantial for larger values (*Henze et al.*, 2007).

Fig. 4.3 shows the adjoint validation results. The simulation is for March 1–April 25 and the cost function J is evaluated at the end of each simulation. The agreements between finite difference sensitivities and the adjoint gradients are within $\sim$15% (slopes vary from 0.84 to 1.15, except for biomass burning contribution at Summit), largely within the uncertainty that arises from deriving the adjoint of the advection using the continuous approach despite their being nonlinearities in the discrete treatment of advection in the forward model (*Henze et al.*, 2007). To quantify the discrepancy, we compare the sensitivities estimated by finite

difference and the adjoint method at one grid cell in biomass burning regions in Siberia, with advection turned on and off. Without advection, finite difference sensitivities agree with adjoint gradients to within 1%. However, with advection turned on, the difference increases to ∼15%. Long-range transport from source regions to receptor sites in the Arctic does not exaggerate the disagreement. In addition, simulation lengths of 1, 5, 10, 20 and 50 days are not found to substantially alter the overall comparison either, indicating that this error does not accumulate in time. In addition, the adjoint gradients estimated by the continuous advection scheme are likely smoother and more physically meaningful than the finite difference sensitivities estimated by the discrete advection scheme (*Henze et al.*, 2007; *Liu and Sandu*, 2008; *Gou and Sandu*, 2011). For example, a negative value of finite difference sensitivity is shown for anthropogenic sources for Denali and an abnormally low finite difference sensitivity value is also shown for anthropogenic sources for Barrow, because of the discrete advection scheme used in the forward model (*Thuburn and Haine*, 2001; *Henze et al.*, 2007; *Hakami et al.*, 2007).

4.4 Results and Discussion

4.4.1 Sources of Arctic BC in April 2008

4.4.1.1 Sources contributing to BC at selected surface sites

Fig. 4.4 (left panels) shows measured and GEOS-Chem simulated daily mean BC concentrations at the five sites for April 2008. At Denali, model reproduces both monthly mean (within 26%) and day-to-day variation (correlation coefficient $r = 0.96$). At Barrow and Alert, simulated monthly mean BC concentrations agree with observations to within 10%. At Zeppelin, monthly mean BC is overestimated by 80%. These discrepancies are likely because GEOS-Chem does not differentiate WBF- vs. riming-dominated in-cloud scavenging in mixed-phase clouds properly (*Qi et al.*, 2016a). At Summit, a free tropospheric site, monthly mean BC concentration is overestimated by 60%.

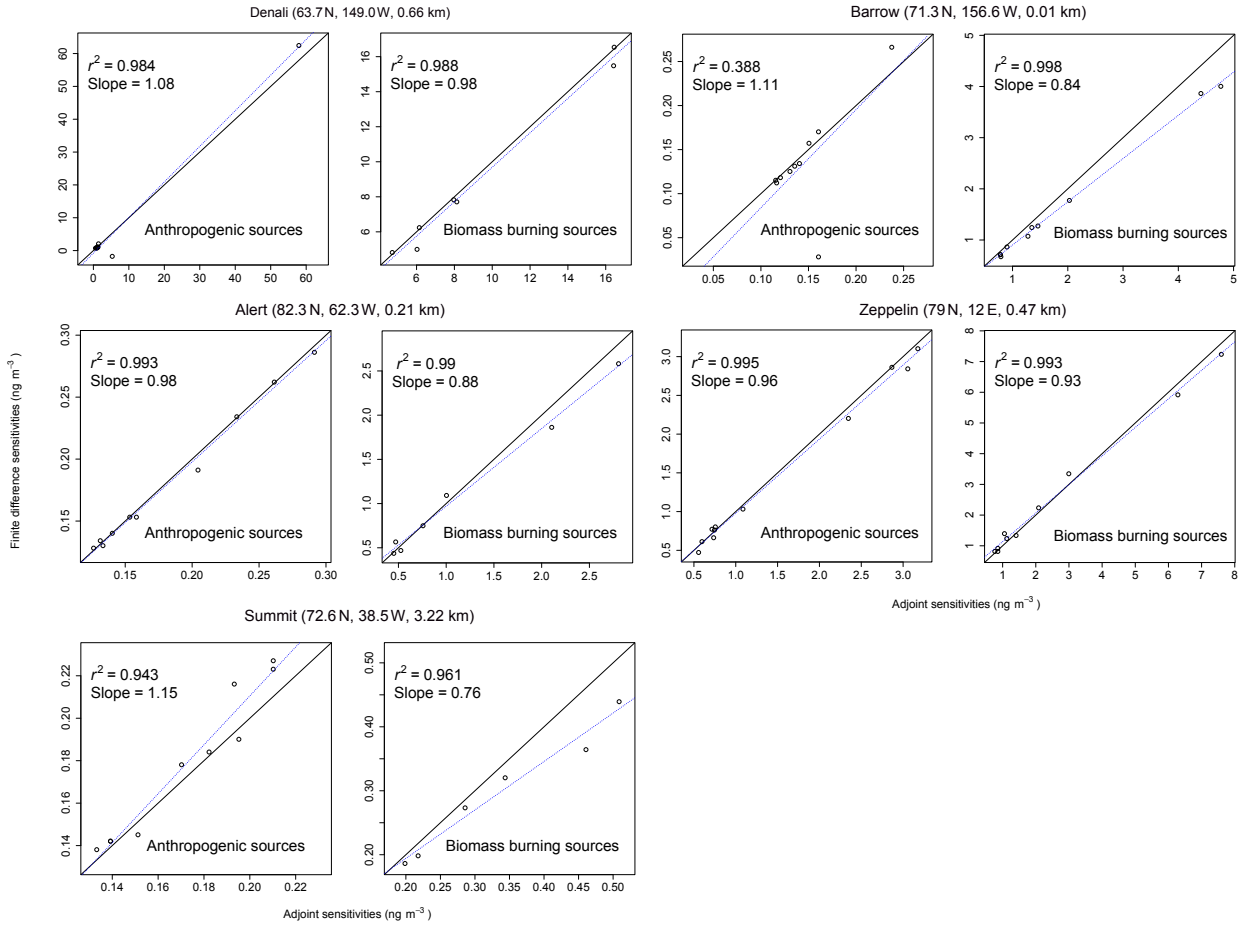

Figure 4.3: GEOS-Chem adjoint versus finite difference gradients of BC concentration for 10 model gridcells with largest anthropogenic BC contributions and 10 gridcells with largest biomass burning BC contributions at Denali, Barrow, Alert, Zeppelin, and Summit (see Fig. 4.1). Values are for March 1–April 25, 2008. Regression lines, slopes and r^2 values are shown.

Using tagged tracers, we compute the contribution from major source regions at continental scale (Fig. 4.2) to surface BC in the Arctic (Fig. 4.4, right panels). Asian anthropogenic sources represent the largest contribution to surface BC (e.g. 32–35% at Barrow, Alert and Zeppelin) and free tropospheric BC (45% at Summit) in the Arctic. Other large anthropogenic sources are from North America (for BC at Barrow) and Siberia (for BC at Zeppelin) because of their close proximity. Anthropogenic contributions from Europe, Siberia and North America to BC at Alert are comparable.

We also find that Asian anthropogenic contribution sharply increase (double or triple) from January–March (not shown) to April across the five sites, although BC emissions in Asia are much lower in April than in the previous three months (by 25%) due to less energy consumption from domestic heating. In contrast, contributions from European, North American, and Siberian anthropogenic sources are relatively flat from January–March to April. Such distinct contrast indicates that the polar-ward transport of Asian emissions in April is enhanced so much so that it offsets the relatively lower emissions in that month. Given that Asian pollution is likely to continue to rise over the coming years (*Qin and Xie*, 2012), it is likely that their contribution to springtime BC in the Arctic will likewise increase.

Observations show a strong enhancement of BC concentration at Denali (up to ∼400 ng m^{-3}) during April 18–30 (Fig. 4.4, top left). GEOS-Chem reproduces this strong transport event (to within 20%). This enhancement is from a strong increase of contribution from North American anthropogenic sources (up to ∼200 ng m^{-3}) and Siberian biomass burning emissions (up to ∼200 ng m^{-3}) (Fig. 4.4, top right). The Siberian biomass burning emissions are from forest fires in southern Siberia-Lake Baikal area and agricultural burning in Kazakhstan-southern Russia (*Warneke et al.*, 2009, 2010; *Wang et al.*, 2011). These biomass burning emissions also enhance BC concentrations at the other sites, although with much smaller magnitudes (up to ∼60 ng m^{-3}) and at different times. At Denali, contribution of Siberian biomass burning reaches its maximum in April 18–25. At Barrow, two maxima appear at April 18 and 24. At Alert and Summit, the Siberian biomass burning contributions are

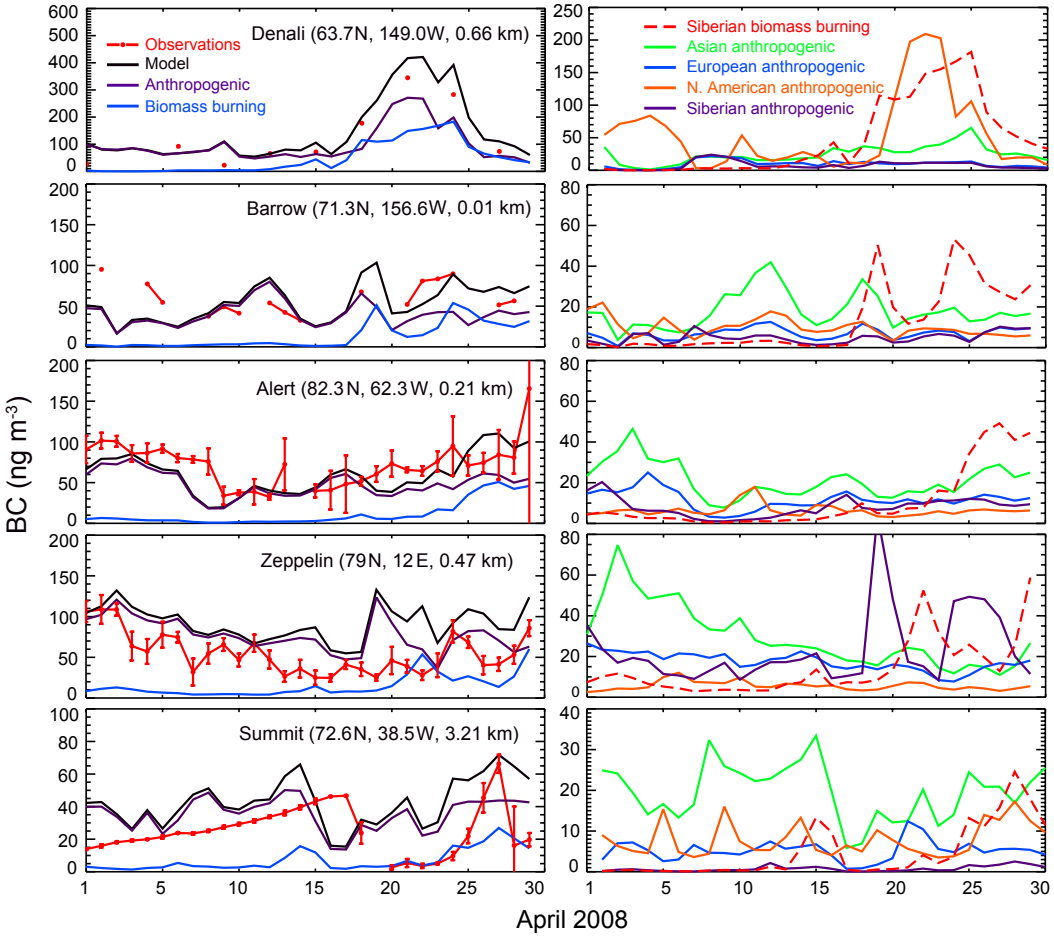

Figure 4.4: (left panels) Observed (red lines) and GEOS-Chem simulated (black lines) daily mean BC concentrations at Denali, Barrow, Alert, Zeppelin and Summit (see Fig. 4.1) for April 2008. Bars are standard deviations of observations. Modeled BC concentrations are decomposed into contributions from anthropogenic (purple lines) and biomass burning emissions (blue lines). (right panels) major contributions: Siberian biomass burning (red dashed line), Asian anthropogenic (green solid line), European anthropogenic (blue solid line), North American anthropogenic (orange solid line), and Siberian anthropogenic (purple solid line) sources.

the largest during April 25–30. At Zeppelin, the two peaks are at April 22 and 30. The relative contributions from biomass burning to BC at the five sites reach up to 46–64%, exceeding the contribution from anthropogenic sources during the pollution event. *Yttri et al.* (2014) derived BC concentration from biomass burning at Zeppelin based on the ratio of Levoglucosan and BC in 2008. They found that the lower and upper estimates of biomass burning contributed BC at Zeppelin were 4.3–13.3% and 31–45%. This estimate is broadly consistent with the range from this study (5.2–55.1% with a mean of 17.6%). It indicates that ways to mitigate open biomass burning can be effective at reducing springtime surface BC in the Arctic and thus lessen the BC snow albedo effect (*Flanner*, 2013).

4.4.1.2 Atmospheric lifetimes of Arctic BC

Using tagged tracers (Sect. 4.3.1), we show GEOS-Chem simulated transport pathways of Arctic BC in April 2008 from major sources (Fig. 4.2) in Figs. S1 and S2. These transport pathways are in broad agreements with previously identified pathways of BC reaching the Arctic surface (*Hirdman et al.*, 2010b; *Dutkiewicz et al.*, 2014) and the troposphere (e.g. *Klonecki et al.*, 2003; *Stohl*, 2006; *Wang et al.*, 2014a). For instance, anthropogenic emissions from Siberia and Europe are transported to the Arctic through low-level transport (*Klonecki et al.*, 2003; *Stohl*, 2006; *Harrigan et al.*, 2011; *Marelle et al.*, 2015), while anthropogenic emissions from Asia and biomass burning emissions from South Asia are uplifted in source regions and enter the Arctic through the middle and upper troposphere (*Matsui et al.*, 2011; *Wang et al.*, 2014a; *Liu et al.*, 2015). These transport pathways result in considerably different lifetimes of Arctic BC against deposition (Table 4.1). For example, BC from Europe and Siberia enters the Arctic through the lower troposphere where it experiences relatively fast dry and wet deposition (*Bourgeois and Bey*, 2011; *Wang et al.*, 2014a). Consequently, the lifetimes are relatively short (7–9 days annually, 10–16 days for March–April). In contrast, BC from Asian anthropogenic and South Asian biomass burning emissions is transported into the Arctic middle and upper troposphere where deposition is relatively weak. As ex-

pected, the resulting lifetimes are much longer (∼1.5–3 months annually and ∼2–4 months for March–April). The lifetimes of BC from North American anthropogenic sources and Siberian biomass burning sources fall somewhere in between (2–3 weeks annually and ∼1 month for March–April). *Stohl* (2006) estimated that the Arctic age of particles against transport decrease with increasing height (surface: up to 2 weeks; 3–5 km: ∼5 days; 5–8 km: ∼3 days). Thus, BC lifetime in the Arctic is determined by deposition and transport at surface and is dominated by transport in the middle and upper troposphere. If both deposition and transport were considered, BC particles in the middle troposphere might have the longest lifetime in the Arctic.

Table 4.1: Atmospheric lifetimes of Arctic BC (2008) from major sources and source regions (days).

		Annual	March-April
Anthropogenic	North America	22	36
	Europe	9	16
	Siberia	7	10
	Asia	47	71
Biomass Burning	Siberia	16	30
	South Asia	98	141

4.4.2 Adjoint source attribution of Arctic BC during a pollution episode

Tagged tracers can identify sources of BC efficiently at large geographical (e.g. continental) scales (see Sect. 4.4.1). However, for episodic transport, source attribution at much finer spatial and temporal resolutions is often needed. In this section, we focus our analysis on

the strong pollution event during April 20–25 most notably at Denali (Fig. 4.4). We use GEOS-Chem adjoint to estimate sources of BC at all five sites at 2° latitude × 2.5° longitude horizontal and hourly temporal resolution.

4.4.2.1 Sensitivity of surface Arctic BC to global emissions

Fig. 4.5 shows the sensitivity of mean BC in April 20–25 at the five surface sites to emissions in Northern Hemisphere during the last 5, 10 and 25 days (dates back from April 25) of transport. The sensitivities are computed per model grid cell using results from the adjoint simulations (Sect. 4.3.2) and averaged for the given time periods (5, 10 or 25 days). BC at Denali and Barrow is most sensitive to ship emissions over the North Pacific Ocean within 5 to 10 days prior to reaching the two sites. Thus, ship emissions over the North Pacific Ocean can strongly influence BC concentration in Alaska in April. When averaged over the 25 days prior to arrival, the two sites are then exposed to anthropogenic BC emissions from North America, Asia and Russia. Denali is more sensitive to BC emissions over Asia than Barrow is, whereas Barrow is more sensitive to BC emissions over Russia and North America. BC at Alert and Zeppelin is sensitive to emissions in the Arctic Circle (60°N). More specifically, BC at Alert is most sensitive to emissions in Northern Canada and the Arctic Ocean in the North American sector within 5 and 10 days of transport. The sensitivity extends to Eurasia in 25 days. BC at Zeppelin is most sensitive to emissions in the European and Russian sectors of the Arctic. Our estimates are consistent with sensitivity patterns of the transport climatologies (2000-07) in winter (*Hirdman et al.*, 2010b) for Alert and Zeppelin, but not for Barrow. They found that in winter the highest sensitivities of Barrow were in the Arctic Circle and extended to Northern Eurasia while in summer the sensitivities were confined to the Arctic Ocean basin and sharply decreased near the continental coasts. The apparent inconsistency at Barrow is partially explained by anomalous meteorological conditions over the Pacific Ocean in April 2008 (*Fuelberg et al.*, 2010). The central pressure of the sub-tropical anticyclone is ∼5 hPa higher than normal and extends farther north than

usual, pushing the 'Aleutian Storm Track' north of its typical position. These meteorological conditions facilitate the transport of air parcels from the Pacific Ocean to Alaska.

Table 4.2: Model simulated relative contributions to surface BC concentration (ng m^{-3}) at selected Arctic sites (Fig. 4.1) for April 20–25*, 2008.

		Anthropogenic				Biomass burning		Total	Adjoint / Forward
		Asia	Siberia	Europe	N.A.	Siberia	S. Asia		
Denali	Forward	41.9	10.4	11.1	142.4	142.4	0.33	352.1	
	Adjoint	38.3	9.5	10.0	146.0	137.8	0.26	341.9	97%
Barrow	Forward	15.0	4.4	5.9	7.6	27.8	0.15	60.1	
	Adjoint	13.6	4.3	5.5	7.4	30.4	0.11	61.8	103%
Alert	Forward	16.6	10.1	10.8	4.7	14.3	0.25	58.5	
	Adjoint	13.8	9.5	9.3	4.5	14.3	0.15	51.8	89%
Zeppelin	Forward	21.0	32.8	14.6	5.7	39.3	0.35	116.5	
	Adjoint	17.8	32.4	13.4	5.3	39.3	0.23	108.8	93%
Summit	Forward	17.2	0.8	7.5	6.1	5.9	1.15	42.0	
	Adjoint	14.3	0.7	7.1	7.2	4.8	1.13	38.0	90%

*Values are averages for April 20–25. 'Forward' and 'Adjoint' are from 'tagged tracer' and from adjoint simulations. See text for details.

Sensitivity of BC at Summit is distinctly different from the other four low-level surface sites. BC at Summit in the free troposphere is more sensitive to emissions at lower than at higher latitudes, consistent with a previous study (*Hirdman et al.*, 2010b). Because of its higher altitude, Summit (3.2 km), more than the other four Arctic surface sites, is frequently exposed to air parcels from warmer low-latitudes that rise isentropically and transported northwards (*Hirdman et al.*, 2010b). In addition, Summit is relatively less sensitive to Eurasia emissions than the other four surface sites. The difference of sensitivities for Summit between this study and *Hirdman et al.* (2010b) is that this study does not show a strong sensitivity to emissions over Greenland, where is the highest sensitivity shown in *Hirdman et al.* (2010b). This difference is probably resulted from different seasons and years simulated in the two

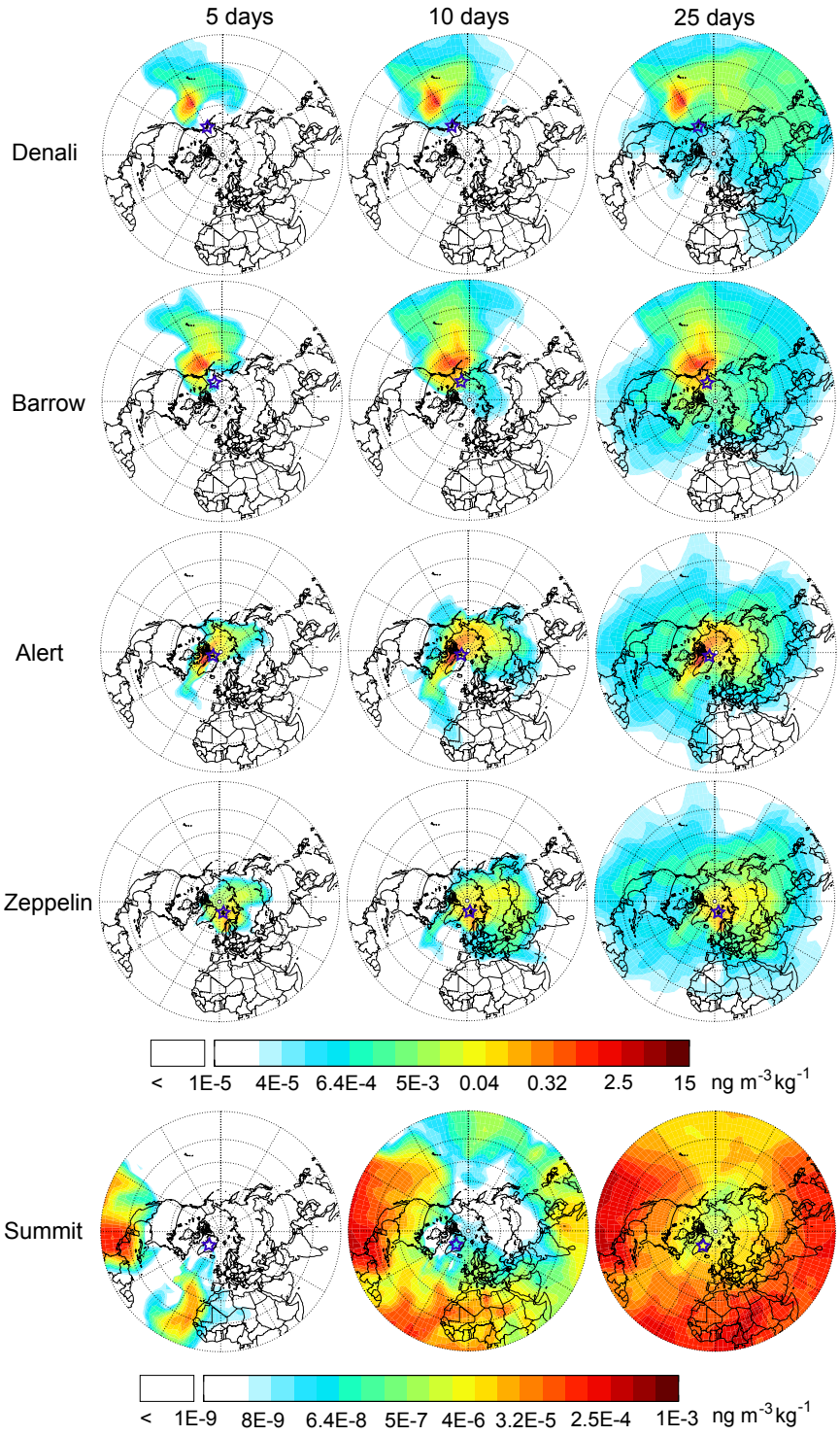

Figure 4.5: Sensitivity of mean BC concentration (averages for April 20–25, 2008) at Denali, Barrow, Alert, Zeppelin, and Summit (see Fig. 4.1) to Northern Hemispheric BC emissions from during the 5, 10 and 25 days prior to April 25. See text for details.

studies (this study: April 20–25, 2008; *Hirdman et al.*, 2010b, : climatology (2000–07) in winter and summer).

4.4.2.2 Source attribution of surface Arctic BC based on adjoint sensitivity

Fig. 4.6 shows contributions from global BC emissions during March 1–April 25 to BC concentrations during April 20–25 at Denali, Barrow, Alert, Zeppelin and Summit as computed from the GEOS-Chem adjoint simulations (Sect. 4.3.2). The left panels show the contributions integrated from March 1 to April 25. The right panels are hourly contributions from major source regions (as defined in Fig. 4.2) during March 1–April 25. The left panels are BC concentrations originated from each model grid cell subsequently transported to the receptor sites. Summing these values up globally approximates (within 15%, see Sect. 4.3.2) the mean BC concentrations in April 20–25 at the receptor sites. Summing up these values in a specific region (e.g. regions defined in Fig. 4.2), i.e., integrating the area underneath an individual curve (Fig. 4.6, right panels), gives the overall contribution from BC emitted in that source region during March 1–April 25. The results are summarized in Table 4.2. The difference between this adjoint attribution and the tagged tracer method is within 15% (Table 4.2). Such difference is largely explained by the choices of discrete (in the forward simulation) vs. continuous (in the adjoint simulation) advection schemes (Sect. 4.3.2). Transport timescales to the five sites can also be inferred from the spectra in the right panels.

Previous studies found that boreal forest fires in the southern Siberia-Lake Baikal area (40–60°N, 100–140°E) and grass/crops burning in Kazakhstan-southern Russia (40–60°N, 30–90°E) were the major sources of BC sampled along the ARCPAC and ARCTAS flights in April 2008 based on MODIS fire detection (*Warneke et al.*, 2009, 2010). We aggregate separately the contributions from forest fires and grass/crops burning to BC at the five receptor sites. The resulting adjoint sensitivity-based estimates show that Siberian biomass burning contributions at the five sites are predominantly ($> 90\%$) from forest fires in the

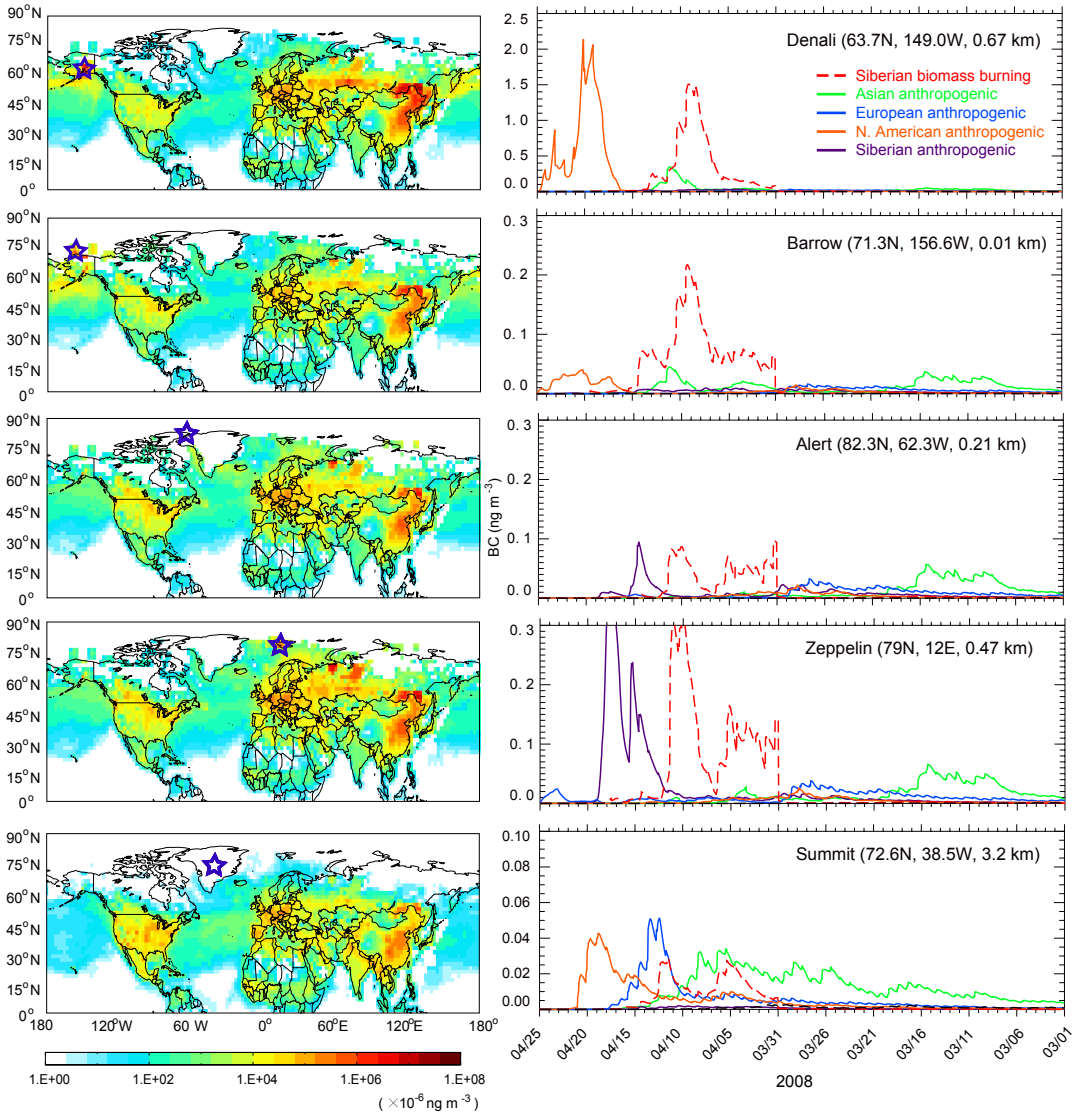

Figure 4.6: GEOS-Chem simulated contributions to BC concentrations, averaged over April 20–25, 2008, at (stars, left panels) Denali, AL (63.7°N, 149.0°W, 0.66 km a.s.l.), Barrow, AL (71.3°N, 156.6°W, 0.01 km a.s.l.), Alert, Canada (82.3°N, 62.3°W, 0.21 km a.s.l.), Zeppelin, Norway (79°N, 12°E, 0.47 km a.s.l.), and Summit, Greenland (72.6°N, 38.5°W, 3.22 km a.s.l.) from global emissions as computed from adjoint simulations (see Sect. 4.3.2 for details): (left panels) Cumulative contributions from March 1–April 25 and (right panels) time-dependent contributions from Siberian biomass burning (red dashed line), Asian anthropogenic (solid green line), European anthropogenic (solid blue), North American anthropogenic (solid orange), and Siberian anthropogenic sources (solid purple). Source regions are as defined in Fig. 4.2.

southern Siberia-Lake Baikal area. Forest fires in that region during April 1–14 have large influences on BC at the two Alaskan sites Denali and Barrow, reaching these two sites after 11–25 days of transport (Fig. 4.6). The contribution from those forest fires, when integrated during April 1–14, is four times larger at Denali (137.8 ng m^{-3}) than at Barrow (30.4 ng m^{-3}). Note the different y-axis ranges (Fig. 4.6, right panels). The contributions at Alert and Zeppelin show similar temporal distributions, with relatively large influences from emissions during April 1–6 and 7–12, but different intensities. The contribution is a factor of three higher at Zeppelin (39.3 ng m^{-3}) than at Alert (14.3 ng m^{-3}).

In contrast, global anthropogenic contributions are considerably more scattered. At Denali, for instance, local and regional emissions – power plants (such as North Pole, US EIA, 2010) and petroleum refinery industries near Fairbanks (US EIA, 2016) account for 63% of total global anthropogenic contribution to BC at Denali. Additionally, we find that the two sites are influenced by long-range transport of emissions from Northeast China, particularly residential emissions from Heilongjiang province. BC emissions from natural gas flares in WENR are significant sources of BC in the Arctic(*Stohl et al.*, 2013; *Qi et al.*, 2016a). These flares are the largest sources to BC at Alert (13% of the global anthropogenic contributions) and Zeppelin (26% of global anthropogenic contributions). Global contributions to BC at Summit are distributed more evenly geographically compared to the other four sites. An interesting feature of the anthropogenic contributions is that industrial and residential BC emissions from the Jing-jin-ji cluster of megacities and Shandong province in East China (together they encompass six model grid cells) are common important sources (7–10% of global contributions) of BC at all five sites.

At Denali, and to a much lesser degree at Barrow, significant contributions are seen from Asian anthropogenic emissions of BC emitted during April 8–15, with a maximum contribution from emissions on April 11. These emissions arrived at the sites after 12–17 days of transport. This episode results from 'direct' transport from Asia to the two sites (*Brock et al.*, 2011, and references therein). The transport time scales are broadly

consistent with previous estimates. For example, using a trajectory model coupled with tracer emissions, *Stohl* (2006) showed that, of the air parcels from Asia transported to the Arctic in winter, 25% arrived in less than 14 days and 50% in more than 20 days. *Harrigan et al.* (2011) attributed BC sampled along an April 12, 2008 DC-8 flight during the ARCTAS field campaign (*Jacob et al.*, 2010) to Asian emissions 10–15 days prior to sampling times. At Denali, Barrow, Alert, and Zeppelin, all four low-level sites, model results show persistent influences from Asian anthropogenic emissions of BC, emitted as far back as March 6–16, after journeys of 40–50 days of transport, presumably after being transported to the Arctic circle and entrained by and became part of the circumpolar transport around and within the Arctic circle (*Ma et al.*, 2013). These transport time scales are born out by the ∼2-month lifetime of Asian anthropogenic emissions of BC against deposition in the Arctic (Table 4.1). Direct, episodic transport of Asian emissions during April 8–15 account for 66% of the total Asian contribution (from emissions during March 1–April 25) to BC at Denali and 37% at Barrow. In contrast, Asian emissions during March 6–16 and subsequently circumpolar transport (hence 'chronic' pollution, *Brock et al.*, 2011) accounts for 39% of the total Asian contribution to BC at Barrow, 65% at Alert and 57% at Zeppelin. These results suggest that both direct, episodic events and chronic Asian anthropogenic pollution, on time scales of 1–2 months, play comparable roles in enhancing springtime Arctic surface BC. Previous studies identifying sources of Arctic surface BC used 5- or 10-day back trajectory analyses (*Polissar et al.*, 2001; *Sharma et al.*, 2004; *Eleftheriadis et al.*, 2009; *Huang et al.*, 2010b; *Matsui et al.*, 2011; *Dutkiewicz et al.*, 2014). As such, the relatively short time scales used in those studies likely result in significant underestimates of long-range transport of BC from Asia to the Arctic.

At Denali, North American emissions have nearly an immediate impact, on a timescale of 0–9 days, because of the proximity to regional sources (power plants and petroleum refinery industries) in Alaska. These episodic transport events are the major parts of North American contributions at Denali (98%) and to a much lesser degree at Barrow (64%). There are

secondary maxima in the North American anthropogenic contributions during March 16–31 (a time lag of 20–30 days) at Denali, Barrow. These maxima reflect circumpolar transport of North American sources from Canada and the lower 48 states, hence the longer time lags. At Alert and Zeppelin, no direct transport events from North American anthropogenic sources are seen. Instead, circumpolar transport dominates the contribution from North American anthropogenic sources, which account for ∼9% of total BC at Alert and ∼5% at Zeppelin. At Denali, Barrow, Alert and Zeppelin, there is no direct transport from European anthropogenic emissions during this period. Rather, a long tail in March (more than 25 days of time lag) is seen at each of the four sites, most evident at Barrow, Alert and Zeppelin. These are European anthropogenic emissions that had been circulating the Arctic troposphere. Their relative contributions are 10% at Barrow, 18% at Alert and 13% at Zeppelin. Siberian anthropogenic contributions, mostly from natural gas flares (42% at Alert and 62% at Zeppelin) in the WENR (*Stohl et al.*, 2013; *Qi et al.*, 2016a), have large impacts on BC at Alert and Zeppelin after 6–15 days of transport. Gas flaring contributions are relatively small at Denali (∼3%) and Barrow (∼7%) and negligible at Summit (∼1%) because of the weak sensitivities (Sect. 4.4.2.1).

Overall, episodic, direct transport dominates anthropogenic contributions at Denali (out of Arctic front, 87%), while chronic, circumpolar transport dominates anthropogenic contributions at Alert (furthest North in the Arctic of the five sites, 89%). The two types of contributions are comparable at Barrow (direct: 42%) and Zeppelin (direct: 52%). BC concentration from direct transport events at Barrow (12.9 ng m^{-3}) is more than one order of magnitude lower than that at Denali (177.4 ng m^{-3}). This difference is largely explained by the strong transport barrier, 'Arctic front' at ∼66°N (*Stohl*, 2006, and references therein), which lies between and separates Denali (63.7°N) and Barrow (71.3°N). BC concentration at 750 hPa, above the Arctic front, over Barrow is more than a factor of three larger than that at the surface during April 20–25 (Fig. 4.7). Contributions from both Asian anthropogenic sources and Siberian biomass burning emissions to BC at 750 hPa Barrow (Asian anthro-

pogenic: 57.0 ng m^{-3}; Siberian biomass burning: 119.8 ng m^{-3}) are four times larger than those at the surface Barrow (Asian anthropogenic: 13.6 ng m^{-3}; Siberian biomass burning: 30.4 ng m^{-3}) and are comparable to their contributions to Denali (Asian anthropogenic: 38.3 ng m^{-3}; Siberian biomass burning: 137.8 ng m^{-3}). The Arctic front also traps BC emitted the front to within the Arctic lower troposphere. This trapping is evident at Barrow – North American anthropogenic emissions are significant sources for BC at the surface (13%) but negligible at 750 hPa (1%). Zeppelin is strongly influenced by direct transport of natural gas flaring emissions in the WENR and European anthropogenic emissions. BC at Alert is also enhanced by direct transport from these flaring emissions, but to a much less extent (a factor of five lower) compared with Zeppelin. In contrast, almost all biomass burning contributions (> 97%) are from direct transport events in April at the four sites.

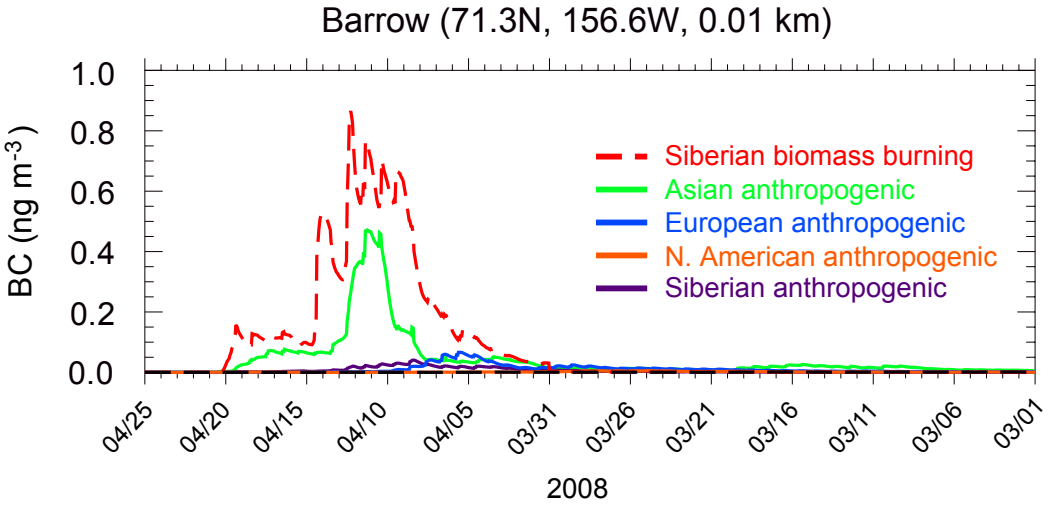

Figure 4.7: Same as Fig. 4.6 (right panels) but for BC at 750 hPa above Barrow.

BC at Summit shows remarkably different signatures of source types and source regions than that at the other four sites. This free tropospheric site experiences a large and persistent contribution from anthropogenic sources of BC emitted during March 1–April 15 in Asia, spanning time scales of 10–50 days. North American anthropogenic emissions take as short as four days (4–16 days) to impact BC at Summit because of the close proxim-

ity. Somewhat surprisingly Summit sees comparable influences from European and North American anthropogenic emissions (∼20%). Anthropogenic BC emitted during April 8–15 in Europe arrive at the site after 10–17 days of transport.

4.4.3 Uncertainty analysis

4.4.3.1 Uncertainty associated with the temporal resolution of biomass burning emissions

Open biomass burning emissions are known to have large day-to-day and diurnal variations (*Giglio*, 2007). It is conceivable that the temporal resolution of biomass burning emissions used in the model may introduce significant uncertainty in our source attribution. Here we examine the sensitivity of BC at the five sites to temporal variation of Siberian biomass burning emissions and explore the implications of these variations on atmospheric transport of BC to the Arctic. Specifically, we use both a monthly and a 3-hourly biomass burning emission inventories (Sect. 4.3.1) to assess the abovementioned uncertainty. Fig. 4.8 (left panels) show both monthly and 3-hourly BC biomass burning emissions in Siberia in March–April 2008. Also overlaid is the adjoint sensitivity of Arctic surface BC (at the five sites) to the emissions. Biomass burning contributions to Arctic surface BC are thus the combined results of the spatiotemporal distribution of the emissions and the sensitivities (Sect. 4.3.2). Fig. 4.8 (right panels) show the resulting contributions from Siberian biomass burning to mean BC concentrations on April 20–25 at the five sites. The 3-hourly inventory results in more significant day-to-day and diurnal variations, as expected, and more acute episodic contributions (e.g. at Barrow from emissions on April 9–10 and 13–15). In contrast, the monthly inventory leads to more broad and persistent contributions from emissions on April 1–15, with more mesoscale variations. The temporal variation of contributions in April estimated from the monthly inventory generally follows the variation of sensitivities. Contribution maxima correspond to sensitivity maxima, such as the contribution peaks on April 7–10 at Barrow and on April 8–11 at Alert. Contributions estimated using 3-hourly

inventory also peak on the same days. Contributions in March are negligible because of very low biomass burning emissions. Overall, the 3-hourly inventory leads to weaker polar-ward transport of BC. For instance, the contribution is 50% lower at Denali, 31–39% lower at Barrow, Alert and Zeppelin, and 6% lower at Summit. The lower contributions are likely because the temporal variation of the 3-hourly inventory is out of phase of the sensitivities at all sites (Fig. 4.8 left panels).

4.4.3.2 Uncertainty associated with wet scavenging

We examine here the role of wet scavenging, a determining factor of BC loading in the Arctic (*Huang et al.*, 2010a; *Vignati et al.*, 2010; *Liu et al.*, 2011; *Browse et al.*, 2012; *Qi et al.*, 2016a), on polar-ward transport of BC. A critical process that affects the wet scavenging of BC particles is WBF (*Cozic et al.*, 2007; *Henning et al.*, 2004). In a previous study, we have shown that WBF releases BC particles incorporated in cloud water drops back into interstitial air in mixed-phase clouds, thereby strongly reduces BC scavenging efficiency and slows down subsequent wet scavenging (*Qi et al.*, 2016b). Conversely, the absence of WBF leads to lower mean BC concentrations in surface air. To examine the effect of WBF on Arctic surface BC, we conduct a simulation whereby WBF is turned off. A direct consequence of the absence of WBF is weaker sensitivities of Arctic BC to global emissions. Fig. 4.9 shows the reductions of these sensitivities relative to the standard simulation (which includes WBF). In the absence of WBF, the sensitivities are lower by 10–90% for most regions. The resulting BC concentrations in surface air at the five sites are lower by 35–52%.

The absence of WBF results in inhomogeneous reduction of sensitivities. For Denali, Barrow, Alert and Zeppelin, the reductions of sensitivities are larger in far field source regions and smaller to near field emissions. The resulting relative contributions are higher from near field, but lower from far field. At Denali for example, the WBF effect results in significantly larger reductions of sensitivities to emissions from Europe (50–70%) than to those from the North American sector in the Arctic and the North Pacific (20–40%). Consequently, the

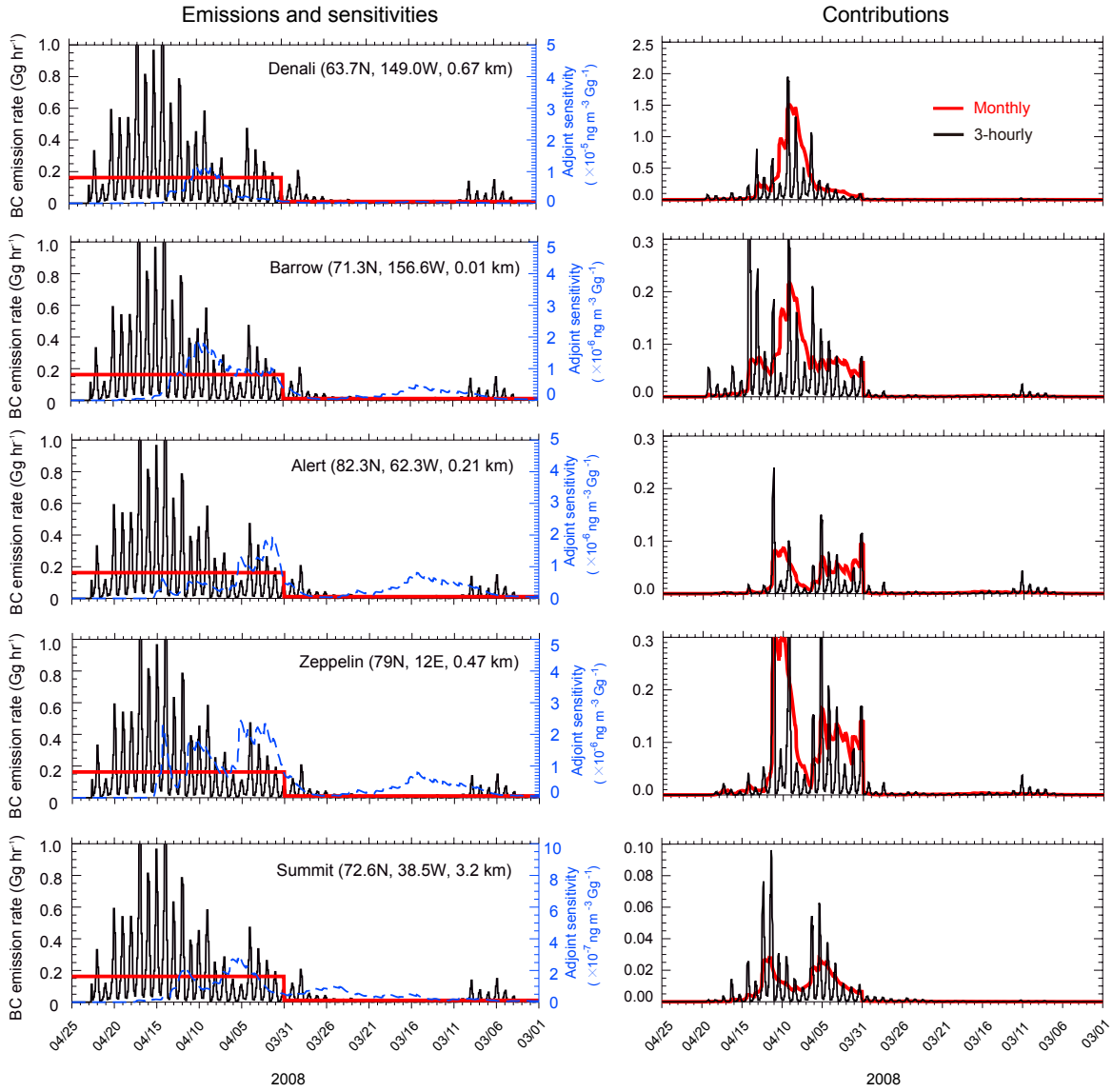

Figure 4.8: (left) Biomass burning BC emission rates (Gg hr^{-1}, red – monthly, black – 3-hourly) in Siberia (see Fig. 4.2) for April 2008 and (right) contributions to BC at the five sites from Siberian biomass burning emissions (red – monthly, black – 3-hourly) during March 1–April 25. Emission data is from the Global Fire Emissions Database version 3 (GFEDv3) inventory (*Randerson et al.*, 2012). Adjoint sensitivities of mean BC during April 20–25, 2008 at the five sites (see Fig. 4.1) to Siberia biomass burning emissions are also shown (left panel, dashed blue).

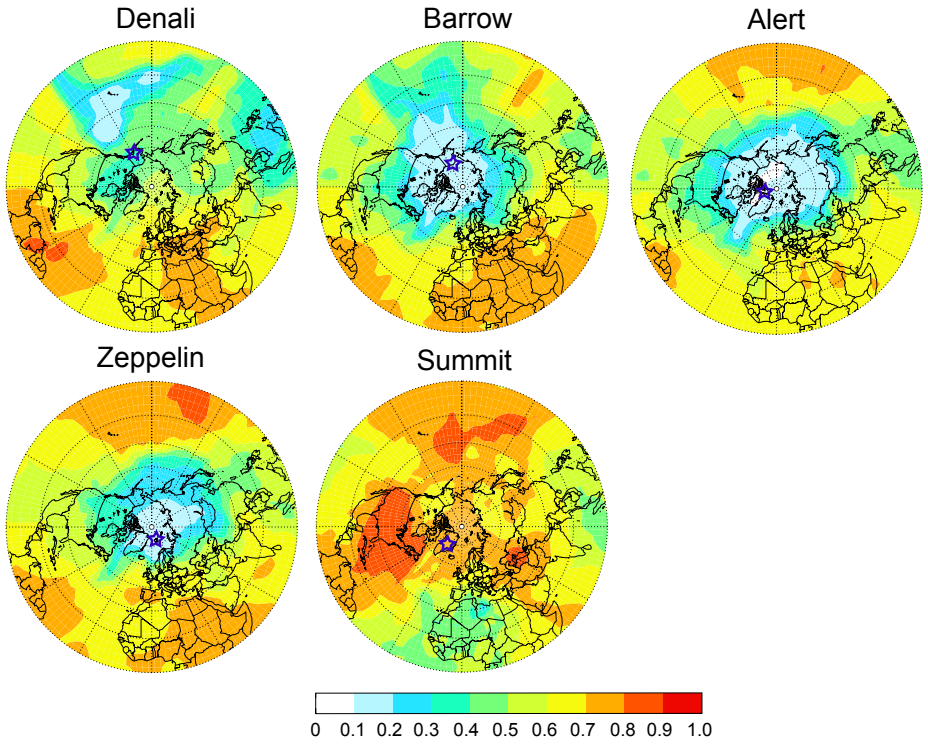

Figure 4.9: Reduction of adjoint sensitivities of BC concentration at selected Arctic sites (Fig. 4.1) to global emissions in the absence of WBF relative to standard simulation, averaged for the whole simulation period in March 1–April 25, 2008.

resulting relative contribution from North America are larger in the absence of WBF (50%) than that with WBF included (43%). Similarly, for Barrow the relative contribution increases from 12% to 17% for North American emissions and from 49% to 51% for Siberian emissions in the absence of WBF, while the relative contributions decrease for other sources. For Alert and Zeppelin, the relative contributions from proximate source region Siberia increase from 46% to 53% at Alert and from 66% to 72% at Zeppelin. This indicates that WBF strongly increases the polar-ward transport of BC from far field regions. For Summit, the reduction of sensitivity without WBF is more evenly distributed than other surface sites and the resulting relative contributions from different sources change marginally.

4.5 Summary and conclusions

This study identified sources of BC at surface sites in the low Arctic (Denali), the high Arctic (Barrow, Alert and Zeppelin) in the Arctic free troposphere (Summit) using a 3D global chemical transport model GEOS-Chem with concentrations tagged by emission source regions at the continental scale in April 2008. We also identified sources and temporal variations of BC during a pollution episode at these five sites at 2° latitude × 2.5° longitude horizontal and hourly temporal resolution using the GEOS-Chem adjoint model.

The tagger tracer technique showed that the largest sources of BC in April 2008 were Asian anthropogenic sources (35–45%) and Siberian biomass burning emissions (46–64%). Adjoint sensitivity showed that during a transport episode in April 20–25, BC at Denali and Barrow in Alaska was most sensitive to emissions in the Pacific ocean while BC at Alert and Zeppelin was most sensitive to emissions in the Arctic Circle and Eurasia. At Summit in the free troposphere, BC was more sensitive to emissions at lower than higher altitudes.

The fine horizontal resolution of adjoint helps identify forest fires in southern Siberia-Lake Baikal area as the largest sources of biomass burning, accounting for more than 90% of total global biomass burning contributions. The largest anthropogenic sources of BC at Denali and Barrow were local and regional emissions in Alaska. In addition, residential emissions from Heilongjiang province in Northeast China was a large anthropogenic source for Denali. For Alert and Zeppelin, the largest anthropogenic sources were gas flares in WENR. Anthropogenic sources (industrial and residential) in Jing-jin-ji megacities and Shandong province in China were large sources (∼10%) of BC at Barrow, Alert and Zeppelin in high Arctic.

The transport time scales can be inferred from the temporal contribution spectra. Except for the immediate impact of local sources in Alaska to Denali and Barrow, other sources took more than 5 days to reach the surface sites. It took six days for Siberian anthropogenic emissions to reach Zeppelin and Alert. Biomass burning emissions in South Siberia and

Asian anthropogenic emissions took more than 10 days of transport to influence BC concentration at surface Arctic. The fine temporal resolution of contribution differentiated the contributions of episodic, direct transport from that of chronic, circumpolar transport. Our results suggested that even during this strong pollution episode, direct transport accounted for half of the contribution at most (42% at Barrow, 52% at Zeppelin and 11% at Alert). The chronic, circumpolar transport of BC is the largest contributor to BC at surface. A large fraction of the Asian contribution was from the chronic circumpolar transport (∼60% at Barrow and ∼100% at Alert and Zeppelin). The long direct transport time scale (>12 days) and the chronic transport dominated contribution suggested that contribution from Asia was strongly underestimated by previous studies that were based on 5- or 10-day trajectory analysis.

Source attribution of Arctic surface BC using the adjoint method was associated with uncertainties from all processes, including emissions, transport, aging, and deposition. We found that using a 3-hourly temporal resolution of biomass burning emissions reduced BC concentration strongly at Denali (∼50%), moderately (∼30%) at Barrow, Alert and Zeppelin and marginally (6%) at Summit. Finer resolution did not affect global sensitivity. The decrease of contribution resulted from the emissions and sensitivities being out of phase. BC concentrations at the five sites were lower by 35–52% without WBF, resulting from a reduction of sensitivities to global emissions. Without WBF, the sensitivity decreased more in the far field sources faraway than near field sources for Denali, Barrow, Alert and Zeppelin. Thus, the relative contribution from proximate sources increased in the absence of WBF. This indicates that WBF strongly increases the polar-ward transport from far field regions. For Summit, the change of the relative contribution from different regions without WBF was negligible.

Acknowledgements. This study was funded by NASA grant NNX14AF11G from the Atmospheric Chemistry Modeling and Analysis Program (ACMAP). We would also like to thank the Global Monitoring Division at NOAA Earth System Research Laboratory, the

Atmospheric Science and Technology Directorate at Environment Canada and SFT Norway for providing data. The Swedish Environmental Protection Agency and the Swedish Research Council have sponsored BC measurements at Zeppelin.

CHAPTER 5

Conclusions and Implications

This dissertation sought to understand the capability of GEOS-Chem in simulating BC distribution in the Arctic and the controlling factors of this distribution, including flaring emissions, dry deposition velocity over snow and ice, and WBF in mixed-phase clouds. As an extension, we also investigated the effect of WBF on global BC distribution. Based on the improved simulation of BC distribution, we identified sources of BC in the Arctic in springtime, when the radiative forcing is the largest.

We examined the role of gas flaring emissions, dry deposition velocity, the WBF effect, and precipitation on BC distribution in the Arctic. We first included BC emissions from a missing source in current emission inventories–natural gas flares. We then implied resistance-in-series method to estimate dry deposition velocity of BC over snow and ice to replace the uniform constant dry deposition velocity of 0.03 cm s^{-1} over snow and ice. We also parameterized the effects of WBF process on BC scavenging efficiency in mixed-phase clouds. WBF was stronger at lower temperature and higher ice mass fraction. We evaluated the model simulation against process specific observations, BC_{snow} measurements across the Arctic and long-term in-situ measurements of surface BC_{air} at Denali in lower Arctic, Barrow, Alert and Zeppelin in higher Arctic, and Summit in the free troposphere.

With all these improvements, the discrepancy of BC_{snow} across the whole Arctic decreased substantially (from -40% to -10%). In the eight sub-regions, the simulated BC_{snow} agreed with observations within a factor of two. Including flaring emissions significantly improved the simulation of BC_{snow} with a strong reduction of discrepancy (from -40% to -20%) and

an increase of correlation coefficient with observations (from 0.15 to 0.24). WBF further reduced the discrepancy of BC_{snow} to within -10%, with the largest improvement in the North American section in the Arctic. Simulation of BC_{snow} with the abovementioned improvements was among the best of AeroCom models evaluated by *Jiao et al.* (2014). The resulting BC_{air} agreed with observations within a factor of two, also among the best simulations in a recent assessment study (*Eckhardt et al.*, 2015). In addition to these physical processes, we also tested the sensitivity of BC_{snow} to precipitation in the Arctic, which is poorly constrained due to the sparse observation network. The difference of precipitation rate in the region among GEOS-5, GPCP and CMAP was up to a factor of ten. Our model results suggested that the negative (positive) bias introduced by doubling (halving) precipitation rate in the Arctic was similar to the combined effects of flaring emissions and WBF. Although this effect might be exaggerated because our method of estimating BC_{snow} strongly depends on precipitation flux, it is worthwhile to notice the importance of precipitation on BC_{snow} simulation.

We distinguished riming- from WBF-dominated conditions in mixed-phase clouds based upon temperature and liquid water content following *Fukuta and Takahashi* (1999). We then parameterized the WBF effect on BC scavenging efficiency based on either temperature or ice mass fraction following *Cozic et al.* (2007). To examine the effects of WBF on global BC distribution, we evaluated model simulations against observations of BC scavenging efficiencies, BC_{air} , BC deposition fluxes, $BC_{rain/snow}$, and BC washout ratios. Overall, model simulations of BC scavenging efficiencies, BC_{air}, deposition fluxes, $BC_{rain/snow}$, and washout ratios improved significantly. However, the comparisons degraded at riming-dominated sites, for example, Zeppelin. Specifically, the model reproduced the observed low scavenging efficiencies of BC near source regions and high scavenging efficiencies in remote regions. WBF lowered BC scavenging efficiencies at all altitudes and significantly improved the simulations at higher altitudes (such as Jungfraujoch, 3.85 km and Puy de *Dôme*,1.47 km). On average, in mid-latitudes, WBF reduced BC scavenging efficiency by 17–44% in winter, depending on the WBF parameterizations used. In summer, the effect increased with increasing al-

titude (from 0 at surface to 39–50% in the upper troposphere). Across the Arctic, WBF reduced BC scavenging efficiency by 22–69% in summer and 63–85% in winter in the lower and middle troposphere. As a result, WBF increased BC_{air} (< 4 km) globally and halved the discrepancy (from -65% to -30%). The improvements were larger for sites at higher altitudes and latitudes. WBF increased global BC loading by 60% (from 0.22 mg m^{-2} yr^{-1} to 0.35 mg m^{-2} yr^{-1}) and partially explained the low biases of AAOD from the AeroCom models (*Bond et al.*, 2013). In addition, WBF increased the fraction of BC loading above 5 km (from 21% to 25–29%) and hence a larger absorption forcing efficiency of BC. BC lifetime is longer by 40% (from 5.7 to 8.0 days) from the WBF effect.

The model captured the observed large BC wet deposition flux (52.5 mg m^{-2} yr^{-1}) at Cape Hedo in East China Sea and comparatively low value (5.0 mg m^{-2} yr^{-1}) at Azores in the central Atlantic. WBF resulted in lower wet deposition fluxes near source regions over land (by ∼15%) but higher wet deposition fluxes over remote oceans (by ∼30%). In addition, WBF lowered BC deposition fluxes (by 12–34%) at mid-latitudes while enhanced the fluxes (by 2–19%) in the Arctic. The former was because of the strong reduction of BC wet deposition fluxes (by 37–63%) and the latter was from the strong enhancement of dry deposition fluxes (by 81–159%). Thus, BC_{snow} decreased (by 15%) in mid-latitudes and increased (by 26%) in the Arctic as a result of the WBF effect. Overall, WBF lowered the discrepancy of BC_{snow} from 35% to 17%, indicating that WBF explained a large fraction of the high bias of the model results in mid-latitudes. In addition, WBF significantly lowered the discrepancies of washout ratios of BC in winter from a factor of 16 to 4. In summer, washout ratios were overestimated by orders of magnitudes. WBF corrected a fraction of the biases. Reasons of the large overestimate warrant further investigation.

Based on the improved simulation of BC distribution in the Arctic, we identified sources of BC at Denali in low Arctic, Barrow, Alert and Zeppelin in high Arctic and Summit in the free troposphere with BC tracer tagged by emission source regions at continental scale in April 2008. We also identified sources of BC during a pollution episode at the five sites at

2° latitude × 2.5° longitude horizontal and hourly temporal resolution using GEOS-Chem adjoint.

Tagger tracer technique showed that the largest sources of BC in April 2008 were Asian anthropogenic sources (35–45%) and Siberian biomass burning emissions (46–64%). The fine horizontal resolution of adjoint helped identify forest fires in southern Siberia-Lake Baikal area as the largest sources of biomass burning, accounting for more than 90% of total global biomass burning contributions. The largest anthropogenic sources of BC at Denali and Barrow were local and regional emissions in Alaska. In addition, residential emissions from Heilongjiang province in Northeast China was a large anthropogenic source for Denali. For Alert and Zeppelin, the largest anthropogenic sources were gas flares in the Western Extreme North of Russia. Anthropogenic sources (industrial and residential) in Jing-jin-ji megacities and Shandong province in China were large sources (∼10%) of BC at Barrow, Alert and Zeppelin in high Arctic.

The transport time scales can be inferred from the temporal contribution spectra. Except for the immediate impact of local sources in Alaska to Denali and Barrow, other sources took more than 5 days to reach the surface sites. It took six days for Siberian anthropogenic emissions to reach Zeppelin and Alert. Biomass burning emissions in South Siberia and Asian anthropogenic emissions took more than 10 days of transport to influence BC concentration at surface Arctic. The fine temporal resolution of contribution differentiated the contributions of episodic, direct transport from that of chronic, circumpolar transport. Our results suggested that even during this strong pollution episode, direct transport accounted for half of the contribution at most (42% at Barrow, 52% at Zeppelin and 11% at Alert). The chronic, circumpolar transport of BC is the largest contributor to BC at surface. A large fraction of the Asian contribution was from the chronic circumpolar transport (∼60% at Barrow and ∼100% at Alert and Zeppelin). The long direct transport time scale (>12 days) and the chronic transport dominated contribution suggested that contribution from Asia was strongly underestimated by previous studies based on 5- or 10-day trajectory analysis.

There remain large uncertainties in flaring emission factors, spatial and temporal variation of flaring emissions, dry deposition velocities of BC and BC scavenging efficiencies in clouds. Process-specific measurements, particularly in the Arctic, are useful to better understand BC distribution and sources in the region. For example, we need direct measurements of emission factors of gas flares in the Western Extreme North of Russia, including their spatial and temporal variations. In addition, dry deposition velocity measurements specific to BC particles over snow and ice covered land surfaces should be made in winter. Our analysis also suggest that more observations are needed to better differentiate WBF- versus riming-dominated scavenging of BC. In addition, measurements of BC scavenging efficiencies in mixed-phase clouds at different latitudes and altitudes should be conducted, especially over the oceans where there are scarce measurements of BC scavenging efficiency. Moreover, more observations of precipitation in the Arctic are needed to better constrain this process. We also need more ^{14}C measurements to differentiate fossil fuel combustion from biomass burning and to further constrain the model simulations of BC.

Bibliography

Allen, D. J., P. Kasibhatla, A. M. Thompson, R. B. Rood, B. G. Doddridge, K. E. Pickering, R. D. Hudson, and S.-J. Lin (1996a), Transport-induced interannual variability of carbon monoxide determined using a chemistry and transport model, *Journal of Geophysical Research: Atmospheres*, *101*(D22), 28,655–28,669.

Allen, D. J., R. B. Rood, A. M. Thompson, and R. D. Hudson (1996b), Three-dimensional radon 222 calculations using assimilated meteorological data and a convective mixing algorithm, *Journal of Geophysical Research: All Series*, *101*, 6871–6881.

Anderson, J. L., V. Balaji, A. J. Broccoli, W. F. Cooke, et al. (2004), The new gfdl global atmosphere and land model am2-lm2: Evaluation with prescribed sst simulations, *Journal of Climate*, *17*(24), 4641.

Andreae, M., and D. Rosenfeld (2008), Aerosol–cloud–precipitation interactions. part 1. the nature and sources of cloud-active aerosols, *Earth-Science Reviews*, *89*(1), 13–41.

Arakawa, A., and W. H. Schubert (1974), Interaction of a cumulus cloud ensemble with the large-scale environment, part i, *Journal of the Atmospheric Sciences*, *31*(3), 674–701.

Barahona, D., A. Molod, J. Bacmeister, A. Nenes, A. Gettelman, H. Morrison, V. Phillips, and A. Eichmann (2014), Development of two-moment cloud microphysics for liquid and ice within the nasa goddard earth observing system model (geos-5), *Geoscientific Model Development*, *7*(4), 1733–1766.

Barrie, L. A. (1986), Arctic air pollution: an overview of current knowledge, *Atmospheric Environment (1967)*, *20*(4), 643–663.

Bergin, M., J. Jaffrezo, C. Davidson, J. E. Dibb, S. Pandis, R. Hillamo, W. Maenhaut, H. Kuhns, and T. Makela (1995), The contributions of snow, fog, and dry deposition

to the summer flux of anions and cations at summit, greenland, *Journal of Geophysical Research*.

Bond, T. C., and R. W. Bergstrom (2006), Light absorption by carbonaceous particles: An investigative review, *Aerosol science and technology*, *40*(1), 27–67.

Bond, T. C., T. L. Anderson, and D. Campbell (1999), Calibration and intercomparison of filter-based measurements of visible light absorption by aerosols, *Aerosol Science & Technology*, *30*(6), 582–600.

Bond, T. C., E. Bhardwaj, R. Dong, R. Jogani, S. Jung, C. Roden, D. G. Streets, and N. M. Trautmann (2007), Historical emissions of black and organic carbon aerosol from energy-related combustion, 1850–2000, *Global Biogeochemical Cycles*, *21*(2).

Bond, T. C., S. J. Doherty, D. Fahey, P. Forster, T. Berntsen, B. DeAngelo, M. Flanner, S. Ghan, B. Kärcher, D. Koch, et al. (2013), Bounding the role of black carbon in the climate system: A scientific assessment, *Journal of Geophysical Research: Atmospheres*, *118*(11), 5380–5552.

Bourgeois, Q., and I. Bey (2011), Pollution transport efficiency toward the arctic: Sensitivity to aerosol scavenging and source regions, *Journal of Geophysical Research: Atmospheres*, *116*(D8).

Bradbury, J., Z. Clement, and A. Down (2015), Greenhouse gas emissions and fuel use within the natural gas supply chain–sankey diagram methodology.

Brock, C. A., J. Cozic, R. Bahreini, K. D. Froyd, A. M. Middlebrook, A. McComiskey, J. Brioude, O. Cooper, A. Stohl, K. Aikin, et al. (2011), Characteristics, sources, and transport of aerosols measured in spring 2008 during the aerosol, radiation, and cloud processes affecting arctic climate (arcpac) project, *Atmospheric Chemistry and Physics*, *11*(6), 2423–2453.

Browse, J., K. Carslaw, S. Arnold, K. Pringle, and O. Boucher (2012), The scavenging processes controlling the seasonal cycle in arctic sulphate and black carbon aerosol, *Atmos. Chem. Phys.*, *12*, 6775–6798.

Castro, L., C. Pio, R. M. Harrison, and D. Smith (1999), Carbonaceous aerosol in urban and rural european atmospheres: estimation of secondary organic carbon concentrations, *Atmospheric Environment*, *33*(17), 2771–2781.

Cerqueira, M., C. Pio, M. Legrand, H. Puxbaum, A. Kasper-Giebl, J. Afonso, S. Preunkert, A. Gelencsér, and P. Fialho (2010), Particulate carbon in precipitation at european background sites, *Journal of Aerosol Science*, *41*(1), 51–61.

Chen, Y., Q. Li, J. Randerson, E. Lyons, R. Kahn, D. Nelson, and D. Diner (2009), The sensitivity of co and aerosol transport to the temporal and vertical distribution of north american boreal fire emissions, *Atmospheric Chemistry and Physics*, *9*(17), 6559–6580.

Chow, J. C., J. G. Watson, L. C. Pritchett, W. R. Pierson, C. A. Frazier, and R. G. Purcell (1993), The dri thermal/optical reflectance carbon analysis system: description, evaluation and applications in us air quality studies, *Atmospheric Environment. Part A. General Topics*, *27*(8), 1185–1201.

Chow, J. C., J. G. Watson, L.-W. A. Chen, W. P. Arnott, H. Moosmüller, and K. Fung (2004), Equivalence of elemental carbon by thermal/optical reflectance and transmittance with different temperature protocols, *Environmental science & technology*, *38*(16), 4414–4422.

Clarke, A. D., and K. J. Noone (1985), Soot in the arctic snowpack: A cause for perturbations in radiative transfer, *Atmospheric Environment (1967)*, *19*(12), 2045–2053.

Clarke, A. D., K. J. Noone, J. Heintzenberg, S. G. Warren, and D. S. Covert (1987), Aerosol light absorption measurement techniques: Analysis and intercomparisons, *Atmospheric Environment (1987)*, *21*(6), 1455–1465.

Cooke, W., C. Liousse, H. Cachier, and J. Feichter (1999), Construction of a 1× 1 fossil fuel emission data set for carbonaceous aerosol and implementation and radiative impact in the echam4 model, *Journal of Geophysical Research: Atmospheres*, *104*(D18), 22,137–22,162.

Cozic, J., B. Verheggen, S. Mertes, P. Connolly, K. Bower, A. Petzold, U. Baltensperger, and E. Weingartner (2007), Scavenging of black carbon in mixed phase clouds at the high alpine site jungfraujoch, *Atmospheric Chemistry and Physics*, *7*(7), 1797–1807.

Delene, D. J., and J. A. Ogren (2002), Variability of aerosol optical properties at four north american surface monitoring sites, *Journal of the Atmospheric Sciences*, *59*(6), 1135–1150.

Di Liberto, L., F. Angelini, I. Pietroni, F. Cairo, G. Di Donfrancesco, A. Viola, S. Argentini, F. Fierli, G. Gobbi, M. Maturilli, et al. (2012), Estimate of the arctic convective boundary layer height from lidar observations: a case study, *Advances in Meteorology*, *2012*.

Doherty, S., S. Warren, T. Grenfell, A. Clarke, and R. Brandt (2010), Light-absorbing impurities in arctic snow, *Atmospheric Chemistry and Physics*, *10*(23), 11,647–11,680.

Doherty, S., C. Bitz, and M. Flanner (2014a), Biases in modeled surface snow bc mixing ratios in prescribed-aerosol climate model runs, *Atmospheric Chemistry and Physics*, *14*(21), 11,697–11,709.

Doherty, S. J., T. C. Grenfell, S. Forsström, D. L. Hegg, R. E. Brandt, and S. G. Warren (2013), Observed vertical redistribution of black carbon and other insoluble light-absorbing particles in melting snow, *Journal of Geophysical Research: Atmospheres*, *118*(11), 5553–5569.

Doherty, S. J., C. Dang, D. A. Hegg, R. Zhang, and S. G. Warren (2014b), Black carbon and other light-absorbing particles in snow of central north america, *Journal of Geophysical Research: Atmospheres*, *119*(22).

Dusek, U., G. Reischl, and R. Hitzenberger (2006), Ccn activation of pure and coated carbon black particles, *Environmental science & technology*, *40*(4), 1223–1230.

Dutkiewicz, V. A., A. M. DeJulio, T. Ahmed, J. Laing, P. K. Hopke, R. B. Skeie, Y. Viisanen, J. Paatero, and L. Husain (2014), Forty-seven years of weekly atmospheric black carbon measurements in the finnish arctic: Decrease in black carbon with declining emissions, *Journal of Geophysical Research: Atmospheres*, *119*(12), 7667–7683.

Eckhardt, S., B. Quennehen, D. J. L. Oliviè, T. K. Berntsen, R. Cherian, J. H. Christensen, W. Collins, S. Crepinsek, N. Daskalakis, M. Flanner, et al. (2015), Current model capabilities for simulating black carbon and sulfate concentrations in the arctic atmosphere: a multi-model evaluation using a comprehensive measurement data set, *Atmospheric Chemistry and Physics*, *15*(16), 9413–9433.

Eleftheriadis, K., S. Vratolis, and S. Nyeki (2009), Aerosol black carbon in the european arctic: Measurements at zeppelin station, ny-ålesund, svalbard from 1998–2007, *Geophysical Research Letters*, *36*(2).

Elvidge, C. D., D. Ziskin, K. E. Baugh, B. T. Tuttle, T. Ghosh, D. W. Pack, E. H. Erwin, and M. Zhizhin (2009), A fifteen year record of global natural gas flaring derived from satellite data, *Energies*, *2*(3), 595–622.

Elvidge, C. D., M. Zhizhin, K. Baugh, F.-C. Hsu, and T. Ghosh (2015), Methods for global survey of natural gas flaring from visible infrared imaging radiometer suite data, *Energies*, *9*(1), 14.

Elvidge, C. D. B., Z. Kimberly E., A. Daniel, and T. Sharolyn, Ghosh (2011), Estimation of gas flaring volumes using nasa modis fire detection products.

Fan, J., S. Ghan, M. Ovchinnikov, X. Liu, P. J. Rasch, and A. Korolev (2011), Representation of arctic mixed-phase clouds and the wegener-bergeron-findeisen process in climate models: Perspectives from a cloud-resolving study, *Journal of Geophysical Research: Atmospheres*, *116*(D1).

Fisher, J. A., D. J. Jacob, Q. Wang, R. Bahreini, C. C. Carouge, M. J. Cubison, J. E. Dibb, T. Diehl, J. L. Jimenez, E. M. Leibensperger, et al. (2011), Sources, distribution, and acidity of sulfate–ammonium aerosol in the arctic in winter–spring, *Atmospheric Environment*, *45*(39), 7301–7318.

Flanner, M., X. Liu, C. Zhou, J. E. Penner, and C. Jiao (2012), Enhanced solar energy absorption by internally-mixed black carbon in snow grains, *Atmospheric Chemistry and Physics*, *12*(10), 4699–4721.

Flanner, M. G. (2013), Arctic climate sensitivity to local black carbon, *Journal of Geophysical Research: Atmospheres*, *118*(4), 1840–1851.

Flanner, M. G., C. S. Zender, J. T. Randerson, and P. J. Rasch (2007), Present-day climate forcing and response from black carbon in snow, *Journal of Geophysical Research: Atmospheres*, *112*(D11).

Flanner, M. G., C. S. Zender, P. Hess, N. M. Mahowald, T. H. Painter, V. Ramanathan, and P. Rasch (2009), Springtime warming and reduced snow cover from carbonaceous particles, *Atmospheric Chemistry and Physics*, *9*(7), 2481–2497.

Flannigan, M. D., M. A. Krawchuk, W. J. de Groot, B. M. Wotton, and L. M. Gowman (2009), Implications of changing climate for global wildland fire, *International journal of wildland fire*, *18*(5), 483–507.

Forsström, S., E. Isaksson, R. Skeie, J. Ström, C. Pedersen, S. Hudson, T. Berntsen, H. Lihavainen, F. Godtliebsen, and S. Gerland (2013), Elemental carbon measurements in european arctic snow packs, *Journal of Geophysical Research: Atmospheres*, *118*(24).

Frossard, A. A., P. M. Shaw, L. M. Russell, J. H. Kroll, M. R. Canagaratna, D. R. Worsnop, P. K. Quinn, and T. S. Bates (2011), Springtime arctic haze contributions of submicron organic particles from european and asian combustion sources, *Journal of Geophysical Research: Atmospheres*, *116*(D5).

Fuelberg, H. E., D. L. Harrigan, and W. Sessions (2010), A meteorological overview of the arctas 2008 mission, *Atmospheric Chemistry and Physics*, *10*(2), 817–842.

Fukuta, N., and T. Takahashi (1999), The growth of atmospheric ice crystals: A summary of findings in vertical supercooled cloud tunnel studies, *Journal of the atmospheric sciences*, *56*(12), 1963–1979.

Gallagher, M., E. Nemitz, J. Dorsey, D. Fowler, M. Sutton, M. Flynn, and J. Duyzer (2002), Measurements and parameterizations of small aerosol deposition velocities to grassland, arable crops, and forest: Influence of surface roughness length on deposition, *Journal of Geophysical Research: Atmospheres*, *107*(D12).

Garrett, T. J., C. Zhao, and P. C. Novelli (2010), Assessing the relative contributions of transport efficiency and scavenging to seasonal variability in arctic aerosol, *Tellus B*, *62*(3), 190–196.

Garrett, T. J., S. Brattström, S. Sharma, D. E. Worthy, and P. Novelli (2011), The role of scavenging in the seasonal transport of black carbon and sulfate to the arctic, *Geophysical Research Letters*, *38*(16).

Gayet, J.-F., R. Treffeisen, A. Helbig, J. Bareiss, A. Matsuki, A. Herber, and A. Schwarzenboeck (2009), On the onset of the ice phase in boundary layer arctic clouds, *Journal of Geophysical Research: Atmospheres*, *114*(D19).

Ghan, S. J., H. Abdul-Razzak, A. Nenes, Y. Ming, X. Liu, M. Ovchinnikov, B. Shipway, N. Meskhidze, J. Xu, and X. Shi (2011), Droplet nucleation: Physically-based parameterizations and comparative evaluation, *Journal of Advances in Modeling Earth Systems*, *3*(4).

Gieray, R., P. Wieser, T. Engelhardt, E. Swietlicki, H.-C. Hansson, B. Mentes, D. Orsini, B. Martinsson, B. Svenningsson, K. Noone, et al. (1997), Phase partitioning of aerosol

constituents in cloud based on single-particle and bulk analysis, *Atmospheric Environment*, *31*(16), 2491–2502.

Giglio, L. (2007), Characterization of the tropical diurnal fire cycle using virs and modis observations, *Remote Sensing of Environment*, *108*(4), 407–421.

Giglio, L., J. Kendall, and R. Mack (2003), A multi-year active fire dataset for the tropics derived from the trmm virs, *International Journal of Remote Sensing*, *24*(22), 4505–4525.

Gilardoni, S., P. Massoli, L. Giulianelli, M. Rinaldi, M. Paglione, F. Pollini, C. Lanconelli, V. Poluzzi, S. Carbone, R. Hillamo, et al. (2014), Fog scavenging of organic and inorganic aerosol in the po valley, *Atmospheric Chemistry and Physics*, *14*(13), 6967–6981.

Giorgi, F., and W. L. Chameides (1986), Rainout lifetimes of highly soluble aerosols and gases as inferred from simulations with a general circulation model, *Journal of Geophysical Research: Atmospheres*, *91*(D13), 14,367–14,376.

Goldenson, N., S. Doherty, C. Bitz, M. Holland, B. Light, and A. Conley (2012), Arctic climate response to forcing from light-absorbing particles in snow and sea ice in cesm, *Atmospheric Chemistry and Physics*, *12*(17), 7903–7920.

Gou, T., and A. Sandu (2011), Continuous versus discrete advection adjoints in chemical data assimilation with cmaq, *Atmospheric environment*, *45*(28), 4868–4881.

Hack, J. J. (1994), Parameterization of moist convection in the national center for atmospheric research community climate model (ccm2), *Journal of Geophysical Research: Atmospheres*, *99*(D3), 5551–5568.

Hadley, O., C. Corrigan, T. Kirchstetter, S. Cliff, and V. Ramanathan (2010), Measured black carbon deposition on the sierra nevada snow pack and implication for snow pack retreat, *Atmospheric Chemistry and Physics*, *10*(15), 7505–7513.

Hadley, O. L., C. E. Corrigan, and T. W. Kirchstetter (2008), Modified thermal-optical analysis using spectral absorption selectivity to distinguish black carbon from pyrolized organic carbon, *Environmental science & technology*, *42*(22), 8459–8464.

Hagler, G. S., M. H. Bergin, E. A. Smith, and J. E. Dibb (2007), A summer time series of particulate carbon in the air and snow at summit, greenland, *Journal of Geophysical Research: Atmospheres*, *112*(D21).

Hakami, A., D. K. Henze, J. H. Seinfeld, K. Singh, A. Sandu, S. Kim, D. Byun, and Q. Li (2007), The adjoint of cmaq, *Environmental science & technology*, *41*(22), 7807–7817.

Hallberg, A., J. Ogren, K. Noone, J. Heintzenberg, A. Berner, I. Solly, C. Kruisz, G. Reischl, S. Fuzzi, M. Facchini, et al. (1992), Phase partitioning for different aerosol species in fog, *Tellus B*, *44*(5), 545–555.

Hallberg, A., K. Noone, J. Ogren, I. Svenningsson, A. Flossmann, A. Wiedensohler, H.-C. Hansson, J. Heintzenberg, T. Anderson, B. Arends, et al. (1994), Phase partitioning of aerosol particles in clouds at kleiner feldberg, *Journal of atmospheric chemistry*, *19*(1-2), 107–127.

Hansen, J., and L. Nazarenko (2004), Soot climate forcing via snow and ice albedos, *Proceedings of the National Academy of Sciences of the United States of America*, *101*(2), 423–428.

Harrigan, D., H. Fuelberg, I. Simpson, D. Blake, G. Carmichael, and G. Diskin (2011), Anthropogenic emissions during arctas-a: mean transport characteristics and regional case studies, *Atmospheric Chemistry and Physics*, *11*(16).

He, C., Q. Li, K.-N. Liou, Y. Takano, Y. Gu, L. Qi, Y. Mao, and L. R. Leung (2014a), Black carbon radiative forcing over the tibetan plateau, *Geophysical Research Letters*, *41*(22), 7806–7813.

He, C., Q. Li, K. Liou, J. Zhang, L. Qi, Y. Mao, M. Gao, Z. Lu, D. Streets, Q. Zhang, et al. (2014b), A global 3-d ctm evaluation of black carbon in the tibetan plateau, *Atmospheric Chemistry and Physics*, *14*(13), 7091–7112.

He, C., Q. Li, K. Liou, L. Qi, S. Tao, and J. Schwarz (2015), Microphysics-based black carbon aging in a global ctm: constraints from hippo observations and implications for global black carbon budget., *Atmospheric Chemistry & Physics Discussions*, *15*(22).

Hegg, D. A., A. D. Clarke, S. J. Doherty, and J. Ström (2011), Measurements of black carbon aerosol washout ratio on svalbard, *Tellus B*, *63*(5), 891–900.

Heintzenberg, J., and C. Leck (1994), Seasonal variation of the atmospheric aerosol near the top of the marine boundary layer over spitsbergen related to the arctic sulphur cycle, *Tellus B*, *46*(1), 52–67.

Held, A., I. Brooks, C. Leck, and M. Tjernstrom (2011), On the potential contribution of open lead particle emissions to the central arctic aerosol concentration, *Atmospheric Chemistry and Physics*, *11*(7), 3093–3105.

Henning, S., S. Bojinski, K. Diehl, S. Ghan, S. Nyeki, E. Weingartner, S. Wurzler, and U. Baltensperger (2004), Aerosol partitioning in natural mixed-phase clouds, *Geophysical research letters*, *31*(6).

Henze, D., J. Seinfeld, and D. Shindell (2009), Inverse modeling and mapping us air quality influences of inorganic pm 2.5 precursor emissions using the adjoint of geos-chem, *Atmospheric Chemistry and Physics*, *9*(16), 5877–5903.

Henze, D. K., A. Hakami, and J. H. Seinfeld (2007), Development of the adjoint of geos-chem, *Atmospheric Chemistry and Physics*, *7*(9), 2413–2433, doi:10.5194/acp-7-2413-2007.

Henze, D. K., D. T. Shindell, F. Akhtar, R. J. Spurr, R. W. Pinder, D. Loughlin, M. Kopacz, K. Singh, and C. Shim (2012), Spatially refined aerosol direct radiative forcing efficiencies, *Environmental science & technology*, *46*(17), 9511–9518.

Hirdman, D., J. F. Burkhart, H. Sodemann, S. Eckhardt, A. Jefferson, P. K. Quinn, S. Sharma, J. Ström, and A. Stohl (2010a), Long-term trends of black carbon and sulphate aerosol in the arctic: changes in atmospheric transport and source region emissions, *Atmospheric Chemistry and Physics*, *10*(19), 9351–9368.

Hirdman, D., H. Sodemann, S. Eckhardt, J. F. Burkhart, A. Jefferson, T. Mefford, P. K. Quinn, S. Sharma, J. Ström, and A. Stohl (2010b), Source identification of short-lived air pollutants in the arctic using statistical analysis of measurement data and particle dispersion model output, *Atmos. Chem. Phys*, *10*(2), 669–693.

Hitzenberger, R., A. Berner, R. Kromp, A. Kasper-Giebl, A. Limbeck, W. Tscherwenka, and H. Puxbaum (2000), Black carbon and other species at a high-elevation european site (mount sonnblick, 3106 m, austria): Concentrations and scavenging efficiencies, *Journal of Geophysical Research: Atmospheres*, *105*(D20), 24,637–24,645.

Hitzenberger, R., A. Berner, H. Giebl, K. Drobesch, A. Kasper-Giebl, M. Loeflund, H. Urban, and H. Puxbaum (2001), Black carbon (bc) in alpine aerosols and cloud water?concentrations and scavenging efficiencies, *Atmospheric Environment*, *35*(30), 5135–5141.

Huang, J., Q. Fu, W. Zhang, X. Wang, R. Zhang, H. Ye, and S. G. Warren (2011), Dust and black carbon in seasonal snow across northern china, *Bulletin of the American Meteorological Society*, *92*(2), 175.

Huang, K., J. S. Fu, V. Y. Prikhodko, J. M. Storey, A. Romanov, E. L. Hodson, J. Cresko, I. Morozova, Y. Ignatieva, and J. Cabaniss (2015), Russian anthropogenic black carbon: Emission reconstruction and arctic black carbon simulation, *Journal of Geophysical Research: Atmospheres*, *120*(21).

Huang, L., S. Gong, C. Jia, and D. Lavoué (2010a), Importance of deposition processes

in simulating the seasonality of the arctic black carbon aerosol, *Journal of Geophysical Research: Atmospheres*, *115*(D17).

Huang, L., S. Gong, C. Jia, and D. Lavoué (2010b), Relative contributions of anthropogenic emissions to black carbon aerosol in the arctic, *Journal of Geophysical Research: Atmospheres*, *115*(D19).

Huffman, G. J., R. F. Adler, M. M. Morrissey, D. T. Bolvin, S. Curtis, R. Joyce, B. McGavock, and J. Susskind (2001), Global precipitation at one-degree daily resolution from multisatellite observations, *Journal of Hydrometeorology*, *2*(1), 36–50.

Jacob, D. J., J. Crawford, H. Maring, A. Clarke, J. E. Dibb, L. Emmons, R. Ferrare, C. Hostetler, P. Russell, H. Singh, et al. (2010), The arctic research of the composition of the troposphere from aircraft and satellites (arctas) mission: design, execution, and first results, *Atmospheric Chemistry and Physics*, *10*(11), 5191–5212.

Jacobson, M. Z. (2004), Climate response of fossil fuel and biofuel soot, accounting for soot's feedback to snow and sea ice albedo and emissivity, *Journal of Geophysical Research: Atmospheres*, *109*(D21).

Jiao, C., M. Flanner, Y. Balkanski, S. Bauer, N. Bellouin, T. Berntsen, H. Bian, K. Carslaw, M. Chin, N. De Luca, et al. (2014), An aerocom assessment of black carbon in arctic snow and sea ice, *Atmospheric Chemistry and Physics*, *14*(5), 2399–2417.

Kasper-Giebl, A., A. Koch, R. Hitzenberger, and H. Puxbaum (2000), Scavenging efficiency of ?aerosol carbon?and sulfate in supercooled clouds at mt. sonnblick (3106 m asl, austria), *Journal of atmospheric chemistry*, *35*(1), 33–46.

Keegan, K. M., M. R. Albert, J. R. McConnell, and I. Baker (2014), Climate change and forest fires synergistically drive widespread melt events of the greenland ice sheet, *Proceedings of the National Academy of Sciences*, *111*(22), 7964–7967.

Klonecki, A., P. Hess, L. Emmons, L. Smith, J. Orlando, and D. Blake (2003), Seasonal changes in the transport of pollutants into the arctic troposphere-model study, *Journal of Geophysical Research: Atmospheres*, *108*(D4).

Koch, D., and J. Hansen (2005), Distant origins of arctic black carbon: a goddard institute for space studies modele experiment, *Journal of Geophysical Research: Atmospheres*, *110*(D4).

Koch, D., S. Menon, A. Del Genio, R. Ruedy, I. Alienov, and G. A. Schmidt (2009), Distinguishing aerosol impacts on climate over the past century, *Journal of Climate*, *22*(10), 2659–2677.

Koehler, K. A., P. J. DeMott, S. M. Kreidenweis, O. B. Popovicheva, M. D. Petters, C. M. Carrico, E. D. Kireeva, T. D. Khokhlova, and N. K. Shonija (2009), Cloud condensation nuclei and ice nucleation activity of hydrophobic and hydrophilic soot particles, *Physical Chemistry Chemical Physics*, *11*(36), 7906–7920.

Kopacz, M., D. J. Jacob, D. K. Henze, C. L. Heald, D. G. Streets, and Q. Zhang (2009), Comparison of adjoint and analytical bayesian inversion methods for constraining asian sources of carbon monoxide using satellite (mopitt) measurements of co columns, *Journal of Geophysical Research: Atmospheres*, *114*(D4).

Kopacz, M., D. J. Jacob, J. Fisher, J. A. Logan, L. Zhang, I. A. Megretskaia, R. M. Yantosca, K. Singh, D. Henze, J. Burrows, et al. (2010), Global estimates of co sources with high resolution by adjoint inversion of multiple satellite datasets (mopitt, airs, sciamachy, tes), *Atmospheric Chemistry and Physics*, *10*(3), 855–876.

Kopacz, M., D. Mauzerall, J. Wang, E. Leibensperger, D. Henze, and K. Singh (2011), Origin and radiative forcing of black carbon transported to the himalayas and tibetan plateau, *Atmospheric Chemistry and Physics*, *11*(6), 2837–2852.

Ladd, M. J., and K. Gajewski (2010), The north american summer arctic front during 1948–2007, *International Journal of Climatology*, *30*(6), 874–883.

Lammel, G., and T. Novakov (1995), Water nucleation properties of carbon black and diesel soot particles, *Atmospheric Environment*, *29*(7), 813–823.

Li, J.-L., D. Waliser, W.-T. Chen, B. Guan, T. Kubar, G. Stephens, H.-Y. Ma, M. Deng, L. Donner, C. Seman, et al. (2012), An observationally based evaluation of cloud ice water in cmip3 and cmip5 gcms and contemporary reanalyses using contemporary satellite data, *Journal of Geophysical Research: Atmospheres*, *117*(D16).

Lin, S.-J., and R. B. Rood (1996), Multidimensional flux-form semi-lagrangian transport schemes, *Monthly Weather Review*, *124*(9), 2046–2070.

Liou, K., Y. Takano, C. He, P. Yang, L. Leung, Y. Gu, and W. Lee (2014), Stochastic parameterization for light absorption by internally mixed bc/dust in snow grains for application to climate models, *Journal of Geophysical Research: Atmospheres*, *119*(12), 7616–7632.

Liston, G., and M. Sturm (2004), The role of winter sublimation in the arctic moisture budget, *Hydrology Research*, *35*(4-5), 325–334.

Liu, D., B. Quennehen, E. Darbyshire, J. D. Allan, P. I. Williams, J. W. Taylor, S.-B. Bauguitte, M. J. Flynn, D. Lowe, M. Gallagher, et al. (2015), The importance of asia as a source of black carbon to the european arctic during springtime 2013, *Atmospheric Chemistry and Physics*, *15*(20), 11,537–11,555.

Liu, H., D. J. Jacob, I. Bey, and R. M. Yantosca (2001), Constraints from 210pb and 7be on wet deposition and transport in a global three-dimensional chemical tracer model driven by assimilated meteorological fields, *Journal of Geophysical Research: Atmospheres*, *106*(D11), 12,109–12,128.

Liu, J., S. Fan, L. W. Horowitz, and H. Levy (2011), Evaluation of factors controlling long-range transport of black carbon to the arctic, *Journal of Geophysical Research: Atmospheres*, *116*(D4).

Liu, Z., and A. Sandu (2008), On the properties of discrete adjoints of numerical methods for the advection equation, *International journal for numerical methods in fluids*, *56*(7), 769–803.

Liu, Z., J. Yang, Y. Chang, P. J. Weisberg, and H. S. He (2012), Spatial patterns and drivers of fire occurrence and its future trend under climate change in a boreal forest of northeast china, *Global Change Biology*, *18*(6), 2041–2056.

Ma, P.-L., P. J. Rasch, H. Wang, K. Zhang, R. C. Easter, S. Tilmes, J. D. Fast, X. Liu, J.-H. Yoon, and J.-F. Lamarque (2013), The role of circulation features on black carbon transport into the arctic in the community atmosphere model version 5 (cam5), *Journal of Geophysical Research: Atmospheres*, *118*(10), 4657–4669.

Malm, W. C., J. F. Sisler, D. Huffman, R. A. Eldred, and T. A. Cahill (1994), Spatial and seasonal trends in particle concentration and optical extinction in the united states, *Journal of Geophysical Research: Atmospheres*, *99*(D1), 1347–1370.

Mann, G., K. Carslaw, D. Spracklen, D. Ridley, P. Manktelow, M. Chipperfield, S. Pickering, and C. Johnson (2010), Description and evaluation of glomap-mode: a modal global aerosol microphysics model for the ukca composition-climate model, *Geoscientific Model Development*, *3*(2), 519–551.

Mao, Y., Q. Li, L. Zhang, Y. Chen, J. Randerson, D. Chen, and K. Liou (2011), Biomass burning contribution to black carbon in the western united states mountain ranges, *Atmospheric Chemistry and Physics*, *11*(21), 11,253–11,266.

Mao, Y., Q. Li, D. Chen, L. Zhang, W.-M. Hao, and K.-N. Liou (2014), Top-down estimates

of biomass burning emissions of black carbon in the western united states, *Atmospheric Chemistry and Physics*, *14*(14), 7195–7211.

Mao, Y., Q. Li, D. Henze, Z. Jiang, D. Jones, M. Kopacz, C. He, L. Qi, M. Gao, W. Hao, et al. (2015), Estimates of black carbon emissions in the western united states using the geos-chem adjoint model, *Atmos. Chem. Phys*, *15*, 7685–7702.

Marelle, L., J.-C. Raut, J. L. Thomas, K. S. Law, B. Quennehen, G. Ancellet, J. Pelon, A. Schwarzenboeck, and J. D. Fast (2015), Transport of anthropogenic and biomass burning aerosols from europe to the arctic during spring 2008, *Atmospheric Chemistry and Physics*, *15*(7), 3831–3850.

Marks, A., and M. King (2013), The effects of additional black carbon on the albedo of arctic sea ice: variation with sea ice type and snow cover, *The Cryosphere*, *7*(4), 1193–1204.

Matsui, H., Y. Kondo, N. Moteki, N. Takegawa, L. Sahu, Y. Zhao, H. Fuelberg, W. Sessions, G. Diskin, D. Blake, et al. (2011), Seasonal variation of the transport of black carbon aerosol from the asian continent to the arctic during the arctas aircraft campaign, *Journal of Geophysical Research: Atmospheres*, *116*(D5).

McEwen, J. D., and M. R. Johnson (2012), Black carbon particulate matter emission factors for buoyancy-driven associated gas flares, *Journal of the Air & Waste Management Association*, *62*(3), 307–321.

McMeeking, G., N. Good, M. Petters, G. McFiggans, and H. Coe (2011), Influences on the fraction of hydrophobic and hydrophilic black carbon in the atmosphere, *Atmospheric Chemistry and Physics*, *11*(10), 5099–5112.

McNaughton, C., A. Clarke, S. Freitag, V. Kapustin, Y. Kondo, N. Moteki, L. Sahu, N. Takegawa, J. Schwarz, J. Spackman, et al. (2011), Absorbing aerosol in the troposphere of the western arctic during the 2008 arctas/arcpac airborne field campaigns, *Atmospheric Chemistry and Physics*, *11*(15), 7561–7582.

Moorthi, S., and M. J. Suarez (1992), Relaxed arakawa-schubert. a parameterization of moist convection for general circulation models, *Monthly Weather Review*, *120*(6), 978–1002.

Mori, T., Y. Kondo, S. Ohata, N. Moteki, H. Matsui, N. Oshima, and A. Iwasaki (2014), Wet deposition of black carbon at a remote site in the east china sea, *Journal of Geophysical Research: Atmospheres*, *119*(17), 10,485–10,498.

Morrison, H., G. de Boer, G. Feingold, J. Harrington, M. D. Shupe, and K. Sulia (2012), Resilience of persistent arctic mixed-phase clouds, *Nature Geoscience*, *5*(1), 11–17.

Moteki, N., Y. Kondo, N. Oshima, N. Takegawa, M. Koike, K. Kita, H. Matsui, and M. Kajino (2012), Size dependence of wet removal of black carbon aerosols during transport from the boundary layer to the free troposphere, *Geophysical Research Letters*, *39*(13).

Myhre, G., B. Samset, M. Schulz, Y. Balkanski, S. Bauer, T. Berntsen, H. Bian, N. Bellouin, M. Chin, T. Diehl, et al. (2013), Radiative forcing of the direct aerosol effect from aerocom phase ii simulations, *Atmospheric Chemistry and Physics*, *13*(4), 1853.

Namazi, M., K. v. Salzen, and J. N. Cole (2015), Simulation of black carbon in snow and its climate impact in the canadian global climate model, *Atmospheric Chemistry and Physics*, *15*(18), 10,887–10,904.

Nester, K., and H.-J. Panitz (2006), Sensitivity analysis by the adjoint chemistry transport model draisfor an episode in the berlin ozone (berlioz) experiment, *Atmospheric Chemistry and Physics*, *6*(8), 2091–2106.

Niu, J., L. D. Carey, P. Yang, and T. H. V. Haar (2008), Optical properties of a vertically inhomogeneous mid-latitude mid-level mixed-phase altocumulus in the infrared region, *Atmospheric Research*, *88*(3), 234–242.

Noone, K. J., and A. D. Clarke (1988), Soot scavenging measurements in arctic snowfall, *Atmospheric Environment (1967)*, *22*(12), 2773–2778.

Ogren, J. A., J. Heintzenberg, and R. J. Charlson (1985), In-situ sampling of clouds with a droplet to aerosol converter, *Geophysical Research Letters*, *12*(3), 121–124.

Overland, J. E., and P. Turet (1994), Variability of the atmospheric energy flux across 70 n computed from the gfdl data set, *The polar Oceans and Their Role in Shaping the Global Environment*, pp. 313–325.

Park, R. J., D. J. Jacob, M. Chin, and R. V. Martin (2003), Sources of carbonaceous aerosols over the united states and implications for natural visibility, *Journal of Geophysical Research: Atmospheres*, *108*(D12).

Park, R. J., D. J. Jacob, P. I. Palmer, A. D. Clarke, R. J. Weber, M. A. Zondlo, F. L. Eisele, A. R. Bandy, D. C. Thornton, G. W. Sachse, et al. (2005), Export efficiency of black carbon aerosol in continental outflow: Global implications, *Journal of Geophysical Research: Atmospheres*, *110*(D11).

Petzold, A., J. A. Ogren, M. Fiebig, P. Laj, S.-M. Li, U. Baltensperger, T. Holzer-Popp, S. Kinne, G. Pappalardo, N. Sugimoto, et al. (2013), Recommendations for reporting" black carbon" measurements, *Atmospheric Chemistry and Physics*, *13*(16), 8365–8379.

Pinto, J. O. (1998), Autumnal mixed-phase cloudy boundary layers in the arctic, *Journal of the atmospheric sciences*, *55*(11), 2016–2038.

Pio, C., M. Legrand, T. Oliveira, J. Afonso, C. Santos, A. Caseiro, P. Fialho, F. Barata, H. Puxbaum, A. Sanchez-Ochoa, et al. (2007), Climatology of aerosol composition (organic versus inorganic) at nonurban sites on a west-east transect across europe, *Journal of Geophysical Research: Atmospheres*, *112*(D23).

Polissar, A. V., P. K. Hopke, and J. M. Harris (2001), Source regions for atmospheric aerosol measured at barrow, alaska, *Environmental science & technology*, *35*(21), 4214–4226.

Pozzoli, L., I. Bey, S. Rast, M. Schultz, P. Stier, and J. Feichter (2008), Trace gas and aerosol interactions in the fully coupled model of aerosol-chemistry-climate echam5-hammoz: 1.

model description and insights from the spring 2001 trace-p experiment, *Journal of Geophysical Research: Atmospheres*, *113*(D7).

Prins, E. M., J. M. Feltz, W. P. Menzel, and D. E. Ward (1998), An overview of goes-8 diurnal fire and smoke results for scar-b and 1995 fire season in south america, *Journal of Geophysical Research: Atmospheres*, *103*(D24), 31,821–31,835.

Qi, L., Q. Li, Y. Li, and C. He (2016a), Factors controlling black carbon distribution in the arctic, *Atmospheric Chemistry and Physics Discussions*, *2016*, 1–39, doi: 10.5194/acp-2016-707.

Qi, L., Q. Li, C. He, X. Wang, and J. Huang (2016b), Effects of wegener-bergeron-findeisen process on global black carbon distribution, *Atmospheric Chemistry and Physics Discussions*, *2016*, 1–33, doi:10.5194/acp-2016-706.

Qin, Y., and S. Xie (2012), Spatial and temporal variation of anthropogenic black carbon emissions in china for the period 1980–2009, *Atmospheric Chemistry and Physics*, *12*(11), 4825–4841.

Quinn, A., A. Stohl, T. B. Arneth, J. F. Burkhart, J. Christensen, M. Flanner, H. Kupiainen, M. Shepherd, V. Shevchenko, H. Skov, and V. Vestreng (2011), The impact of black carbon on arctic climate, *AMAP Technical Report No. 4*.

Quinn, P., T. Bates, E. Baum, N. Doubleday, A. Fiore, M. Flanner, A. Fridlind, T. J. Garrett, D. Koch, S. Menon, et al. (2008), Short-lived pollutants in the arctic: their climate impact and possible mitigation strategies, *Atmospheric Chemistry and Physics*, *8*(6), 1723–1735.

Ramanathan, V., and G. Carmichael (2008), Global and regional climate changes due to black carbon, *Nature geoscience*, *1*(4), 221–227.

Randerson, J., Y. Chen, G. Werf, B. Rogers, and D. Morton (2012), Global burned area and biomass burning emissions from small fires, *Journal of Geophysical Research: Biogeosciences*, *117*(G4).

Rannik, U. (2001), Turbulent aerosol fluxes over the arctic ocean 1. dry deposition over sea and pack ice, *Journal of Geophysical Research*, *106*(D23), 32–125.

Samset, B. H., and G. Myhre (2011), Vertical dependence of black carbon, sulphate and biomass burning aerosol radiative forcing, *Geophysical Research Letters*, *38*(24).

Sand, M., T. K. Berntsen, J. E. Kay, J. F. Lamarque, Ø. Seland, and A. Kirkevåg (2013), The arctic response to remote and local forcing of black carbon, *Atmospheric Chemistry and Physics*, *13*(1), 211–224, doi:10.5194/acp-13-211-2013.

Sand, M., T. Berntsen, K. von Salzen, M. Flanner, J. Langner, and D. Victor (2015), Response of arctic temperature to changes in emissions of short-lived climate forcers, *Nature Climate Change*.

Schulz, M., C. Textor, S. Kinne, Y. Balkanski, S. Bauer, T. Berntsen, T. Berglen, O. Boucher, F. Dentener, S. Guibert, et al. (2006), Radiative forcing by aerosols as derived from the aerocom present-day and pre-industrial simulations, *Atmospheric Chemistry and Physics*, *6*(12), 5225–5246.

Schutgens, N. A., E. Gryspeerdt, N. Weigum, S. Tsyro, D. Goto, M. Schulz, and P. Stier (2016), Will a perfect model agree with perfect observations? the impact of spatial sampling, *Atmospheric Chemistry and Physics*, *16*(10), 6335–6353.

Schwarz, J., R. Gao, J. Spackman, L. Watts, D. Thomson, D. Fahey, T. Ryerson, J. Peischl, J. Holloway, M. Trainer, et al. (2008), Measurement of the mixing state, mass, and optical size of individual black carbon particles in urban and biomass burning emissions, *Geophysical Research Letters*, *35*(13).

Schwarz, J., J. Spackman, R. Gao, L. Watts, P. Stier, M. Schulz, S. Davis, S. Wofsy, and D. Fahey (2010), Global-scale black carbon profiles observed in the remote atmosphere and compared to models, *Geophysical Research Letters*, *37*(18).

Schwarz, J. P., J. S. Holloway, J. M. Katich, S. McKeen, E. A. Kort, M. L. Smith, T. B. Ryerson, C. Sweeney, and J. Peischl (2015), Black carbon emissions from the bakken oil and gas development region, *Environmental Science & Technology Letters*, *2*(10), 281–285.

Sellegri, K., P. Laj, R. Dupuy, M. Legrand, S. Preunkert, and J.-P. Putaud (2003), Size-dependent scavenging efficiencies of multicomponent atmospheric aerosols in clouds, *Journal of Geophysical Research: Atmospheres*, *108*(D11).

Serreze, M. C., and C. M. Hurst (2000), Representation of mean arctic precipitation from ncep-ncar and era reanalyses, *Journal of Climate*, *13*(1), 182–201.

Serreze, M. C., R. G. Barry, and J. E. Walsh (1995), Atmospheric water vapor characteristics at 70 n, *Journal of Climate*, *8*(4), 719–731.

Sharma, S., D. Lavoué, H. Cachier, L. Barrie, and S. Gong (2004), Long-term trends of the black carbon concentrations in the canadian arctic, *Journal of Geophysical Research: Atmospheres*, *109*(D15).

Sharma, S., E. Andrews, L. Barrie, J. Ogren, and D. Lavoue (2006), Variations and sources of the equivalent black carbon in the high arctic revealed by long-term observations at alert and barrow: 1989–2003, *Journal of Geophysical Research: Atmospheres*, *111*(D14).

Sharma, S., M. Ishizawa, D. Chan, D. Lavoué, E. Andrews, K. Eleftheriadis, and S. Maksyutov (2013), 16-year simulation of arctic black carbon: Transport, source contribution, and sensitivity analysis on deposition, *Journal of Geophysical Research: Atmospheres*, *118*(2), 943–964.

Shaw, P., L. Russell, A. Jefferson, and P. Quinn (2010), Arctic organic aerosol measurements show particles from mixed combustion in spring haze and from frost flowers in winter, *Geophysical Research Letters*, *37*(10).

Shindell, D., and G. Faluvegi (2009), Climate response to regional radiative forcing during the twentieth century, *Nature Geoscience*, *2*(4), 294–300.

Shindell, D., M. Chin, F. Dentener, R. Doherty, G. Faluvegi, A. M. Fiore, P. Hess, D. Koch, I. MacKenzie, M. Sanderson, et al. (2008), A multi-model assessment of pollution transport to the arctic, *Atmospheric Chemistry and Physics*, *8*(17), 5353–5372.

Shupe, M. D., S. Y. Matrosov, and T. Uttal (2006), Arctic mixed-phase cloud properties derived from surface-based sensors at sheba, *Journal of the atmospheric sciences*, *63*(2), 697–711.

Slowik, J. G., E. S. Cross, J.-H. Han, P. Davidovits, T. B. Onasch, J. T. Jayne, L. R. Williams, M. R. Canagaratna, D. R. Worsnop, R. K. Chakrabarty, et al. (2007), An inter-comparison of instruments measuring black carbon content of soot particles, *Aerosol Science and Technology*, *41*(3), 295–314.

Smith, A. J., V. E. Larson, J. Niu, J. A. Kankiewicz, and L. D. Carey (2009), Processes that generate and deplete liquid water and snow in thin midlevel mixed-phase clouds, *Journal of Geophysical Research: Atmospheres*, *114*(D12).

Soja, A. J., N. M. Tchebakova, N. H. French, M. D. Flannigan, H. H. Shugart, B. J. Stocks, A. I. Sukhinin, E. Parfenova, F. S. Chapin, and P. W. Stackhouse (2007), Climate-induced boreal forest change: predictions versus current observations, *Global and Planetary Change*, *56*(3), 274–296.

Stier, P., J. Feichter, S. Kinne, S. Kloster, E. Vignati, J. Wilson, L. Ganzeveld, I. Tegen, M. Werner, Y. Balkanski, et al. (2005), The aerosol-climate model echam5-ham, *Atmospheric Chemistry and Physics*, *5*(4), 1125–1156.

Stohl, A. (2006), Characteristics of atmospheric transport into the arctic troposphere, *Journal of Geophysical Research: Atmospheres*, *111*(D11).

Stohl, A., T. Berg, J. Burkhart, A. Fj?raa, C. Forster, A. Herber, Ø. Hov, C. Lunder, W. McMillan, S. Oltmans, et al. (2007), Arctic smoke–record high air pollution levels in

the european arctic due to agricultural fires in eastern europe in spring 2006, *Atmospheric Chemistry and Physics*, *7*(2), 511–534.

Stohl, A., Z. Klimont, S. Eckhardt, K. Kupiainen, V. Shevchenko, V. Kopeikin, and A. Novigatsky (2013), Black carbon in the arctic: the underestimated role of gas flaring and residential combustion emissions, *Atmospheric Chemistry and Physics*, *13*(17), 8833–8855.

Stroeve, J. C., M. C. Serreze, M. M. Holland, J. E. Kay, J. Malanik, and A. P. Barrett (2012), The arctic?s rapidly shrinking sea ice cover: a research synthesis, *Climatic Change*, *110*(3-4), 1005–1027.

Taylor, J., J. Allan, G. Allen, H. Coe, P. Williams, M. Flynn, M. Le Breton, J. Muller, C. Percival, D. Oram, et al. (2014), Size-dependent wet removal of black carbon in canadian biomass burning plumes, *Atmospheric Chemistry and Physics*, *14*(24), 13,755–13,771.

Tedesco, M., S. Doherty, X. Fettweis, P. Alexander, J. Jeyaratnam, and J. Stroeve (2016), The darkening of the greenland ice sheet: trends, drivers, and projections (1981–2100), *Cryosphere (The)*, *10*, 477–496.

Textor, C., M. Schulz, S. Guibert, S. Kinne, Y. Balkanski, S. Bauer, T. Berntsen, T. Berglen, O. Boucher, M. Chin, et al. (2006), Analysis and quantification of the diversities of aerosol life cycles within aerocom, *Atmospheric Chemistry and Physics*, *6*(7), 1777–1813.

Textor, C., M. Schulz, S. Guibert, S. Kinne, Y. Balkanski, S. Bauer, T. Berntsen, T. Berglen, O. Boucher, M. Chin, et al. (2007), The effect of harmonized emissions on aerosol properties in global models–an aerocom experiment, *Atmospheric Chemistry and Physics*, *7*(17), 4489–4501.

Thuburn, J., and T. W. Haine (2001), Adjoints of nonoscillatory advection schemes, *Journal of Computational Physics*, *171*(2), 616–631.

Van der Werf, G. R., J. T. Randerson, L. Giglio, G. Collatz, M. Mu, P. S. Kasibhatla, D. C. Morton, R. DeFries, Y. v. Jin, and T. T. van Leeuwen (2010), Global fire emissions and

the contribution of deforestation, savanna, forest, agricultural, and peat fires (1997–2009), *Atmospheric Chemistry and Physics*, *10*(23), 11,707–11,735.

Verheggen, B., J. Cozic, E. Weingartner, K. Bower, S. Mertes, P. Connolly, M. Gallagher, M. Flynn, T. Choularton, and U. Baltensperger (2007), Aerosol partitioning between the interstitial and the condensed phase in mixed-phase clouds, *Journal of Geophysical Research: Atmospheres*, *112*(D23).

Vignati, E., M. Karl, M. Krol, J. Wilson, P. Stier, and F. Cavalli (2010), Sources of uncertainties in modelling black carbon at the global scale, *Atmospheric chemistry and physics*, *10*(6), 2595–2611.

Virkkula, A., N. C. Ahlquist, D. S. Covert, W. P. Arnott, P. J. Sheridan, P. K. Quinn, and D. J. Coffman (2005), Modification, calibration and a field test of an instrument for measuring light absorption by particles, *Aerosol Science and Technology*, *39*(1), 68–83.

von Schneidemesser, E., J. J. Schauer, G. S. Hagler, and M. H. Bergin (2009), Concentrations and sources of carbonaceous aerosol in the atmosphere of summit, greenland, *Atmospheric Environment*, *43*(27), 4155–4162.

Walker, T., D. Jones, M. Parrington, D. Henze, L. Murray, J. Bottenheim, K. Anlauf, J. Worden, K. Bowman, C. Shim, et al. (2012), Impacts of midlatitude precursor emissions and local photochemistry on ozone abundances in the arctic, *Journal of Geophysical Research: Atmospheres*, *117*(D1).

Wang, H., P. J. Rasch, R. C. Easter, B. Singh, R. Zhang, P.-L. Ma, Y. Qian, S. J. Ghan, and N. Beagley (2014a), Using an explicit emission tagging method in global modeling of source-receptor relationships for black carbon in the arctic: Variations, sources, and transport pathways, *Journal of Geophysical Research: Atmospheres*, *119*(22).

Wang, Q., D. J. Jacob, J. A. Fisher, J. Mao, E. Leibensperger, C. Carouge, P. L. Sager, Y. Kondo, J. Jimenez, M. Cubison, et al. (2011), Sources of carbonaceous aerosols and

deposited black carbon in the arctic in winter-spring: implications for radiative forcing, *Atmospheric Chemistry and Physics*, *11*(23), 12,453–12,473.

Wang, Q., D. J. Jacob, J. R. Spackman, A. E. Perring, J. P. Schwarz, N. Moteki, E. A. Marais, C. Ge, J. Wang, and S. R. Barrett (2014b), Global budget and radiative forcing of black carbon aerosol: Constraints from pole-to-pole (hippo) observations across the pacific, *Journal of Geophysical Research: Atmospheres*, *119*(1), 195–206.

Wang, X., S. J. Doherty, and J. Huang (2013), Black carbon and other light-absorbing impurities in snow across northern china, *Journal of Geophysical Research: Atmospheres*, *118*(3), 1471–1492.

Wang, X., C. Heald, D. Ridley, J. Schwarz, J. Spackman, A. Perring, H. Coe, D. Liu, and A. Clarke (2014c), Exploiting simultaneous observational constraints on mass and absorption to estimate the global direct radiative forcing of black carbon and brown carbon, *Atmospheric Chemistry and Physics*, *14*(20), 10,989–11,010.

Wang, X., B. Xu, and J. Ming (2014d), An overview of the studies on black carbon and mineral dust deposition in snow and ice cores in east asia, *Journal of Meteorological Research*, *28*, 354–370.

Wang, Z., J. Gallet, C. Pedersen, X. Zhang, J. Ström, and Z. Ci (2014e), Elemental carbon in snow at changbai mountain, northeastern china: concentrations, scavenging ratios, and dry deposition velocities, *Atmospheric Chemistry and Physics*, *14*(2), 629–640.

Warneke, C., R. Bahreini, J. Brioude, C. Brock, J. De Gouw, D. Fahey, K. Froyd, J. Holloway, A. Middlebrook, L. Miller, et al. (2009), Biomass burning in siberia and kazakhstan as an important source for haze over the alaskan arctic in april 2008, *Geophysical Research Letters*, *36*(2).

Warneke, C., K. Froyd, J. Brioude, R. Bahreini, C. Brock, J. Cozic, J. De Gouw, D. Fahey,

R. Ferrare, J. Holloway, et al. (2010), An important contribution to springtime arctic aerosol from biomass burning in russia, *Geophysical Research Letters*, *37*(1).

Warren, S. G., I. G. Rigor, N. Untersteiner, V. F. Radionov, N. N. Bryazgin, Y. I. Aleksandrov, and R. Colony (1999), Snow depth on arctic sea ice, *Journal of Climate*, *12*(6), 1814–1829.

Weingartner, E., H. Burtscher, and U. Baltensperger (1997), Hygroscopic properties of carbon and diesel soot particles, *Atmospheric Environment*, *31*(15), 2311–2327.

Weingartner, E., H. Saathoff, M. Schnaiter, N. Streit, B. Bitnar, and U. Baltensperger (2003), Absorption of light by soot particles: determination of the absorption coefficient by means of aethalometers, *Journal of Aerosol Science*, *34*(10), 1445–1463.

Wesely, M. (1989), Parameterization of surface resistances to gaseous dry deposition in regional-scale numerical models, *Atmospheric Environment (1967)*, *23*(6), 1293–1304.

Weyant, C. L., P. B. Shepson, R. Subramanian, M. O. Cambaliza, A. Heimburger, D. McCabe, E. Baum, B. H. Stirm, and T. C. Bond (2016), Black carbon emissions from associated natural gas flaring, *Environmental science & technology*, *50*(4), 2075–2081.

Wieringa, J. (1980), Representativeness of wind observations at airports, *Bulletin of the American Meteorological Society*, *61*(9), 962–971.

Wotton, B. M., C. A. Nock, and M. D. Flannigan (2010), Forest fire occurrence and climate change in canada, *International Journal of Wildland Fire*, *19*(3), 253–271.

Wyslouzil, B., K. Carleton, D. Sonnenfroh, W. Rawlins, and S. Arnold (1994), Observation of hydration of single, modified carbon aerosols, *Geophysical research letters*, *21*(19), 2107–2110.

Xie, P., and P. A. Arkin (1997), Global precipitation: A 17-year monthly analysis based

on gauge observations, satellite estimates, and numerical model outputs, *Bulletin of the American Meteorological Society*, *78*(11), 2539.

Ye, H., R. Zhang, J. Shi, J. Huang, S. G. Warren, and Q. Fu (2012), Black carbon in seasonal snow across northern xinjiang in northwestern china, *Environmental Research Letters*, *7*(4), 044,002.

Yttri, K. E., C. Lund Myhre, S. Eckhardt, M. Fiebig, C. Dye, D. Hirdman, J. Ström, Z. Klimont, and A. Stohl (2014), Quantifying black carbon from biomass burning by means of levoglucosan–a one-year time series at the arctic observatory zeppelin, *Atmospheric Chemistry and Physics*, *14*(12), 6427–6442.

Zhang, D., Z. Wang, and D. Liu (2010), A global view of midlevel liquid-layer topped stratiform cloud distribution and phase partition from calipso and cloudsat measurements, *Journal of Geophysical Research: Atmospheres*, *115*(D4).

Zhang, L., S. Gong, J. Padro, and L. Barrie (2001), A size-segregated particle dry deposition scheme for an atmospheric aerosol module, *Atmospheric Environment*, *35*(3), 549–560.

Zhang, L., D. J. Jacob, M. Kopacz, D. K. Henze, K. Singh, and D. A. Jaffe (2009a), Intercontinental source attribution of ozone pollution at western us sites using an adjoint method, *Geophysical Research Letters*, *36*(11).

Zhang, L., L. Liu, Y. Zhao, S. Gong, X. Zhang, D. K. Henze, S. L. Capps, T.-M. Fu, Q. Zhang, and Y. Wang (2015a), Source attribution of particulate matter pollution over north china with the adjoint method, *Environmental Research Letters*, *10*(8), 084,011.

Zhang, L., D. K. Henze, G. A. Grell, G. R. Carmichael, N. Bousserez, Q. Zhang, O. Torres, C. Ahn, Z. Lu, J. Cao, and Y. Mao (2015b), Constraining black carbon aerosol over asia using omi aerosol absorption optical depth and the adjoint of geos-chem, *Atmospheric Chemistry and Physics*, *15*(18), 10,281–10,308, doi:10.5194/acp-15-10281-2015.

Zhang, Q., D. G. Streets, G. R. Carmichael, K. He, H. Huo, A. Kannari, Z. Klimont, I. Park, S. Reddy, J. Fu, et al. (2009b), Asian emissions in 2006 for the nasa intex-b mission, *Atmospheric Chemistry and Physics*, *9*(14), 5131–5153.

Zhang, R., A. F. Khalizov, J. Pagels, D. Zhang, H. Xue, and P. H. McMurry (2008a), Variability in morphology, hygroscopicity, and optical properties of soot aerosols during atmospheric processing, *Proceedings of the National Academy of Sciences*, *105*(30), 10,291–10,296.

Zhang, R., D. Hegg, J. Huang, and Q. Fu (2013), Source attribution of insoluble light-absorbing particles in seasonal snow across northern china, *Atmos. Chem. Phys*, *13*(12), 6091–6099.

Zhang, X., Y. Wang, X. Zhang, W. Guo, and S. Gong (2008b), Carbonaceous aerosol composition over various regions of china during 2006, *Journal of Geophysical Research: Atmospheres*, *113*(D14).